Abstract

Title of Document:	THE EFFECT OF SURFACTANTS ON THE BREAKUP OF AN AXISYMMETRIC LAMINAR LIQUID JET
	Justin R. Walker, Doctor of Philosophy, 2012
Directed By:	Professor Richard V. Calabrese Department of Chemical and Biomolecular Engineering

The contacting of multiple liquid phases is a complex process, and one that is difficult to study experimentally. Liquid dispersion studies in stirred tanks and high shear mixers frequently involve the use of surfactants without a strong physical understanding of how the surfactants affect the mechanics of droplet production and breakup. In this study, experiments are performed using the axisymmetric laminar jet system. The breakup of a laminar axisymmetric jet is a well-studied fluid dynamics phenomenon. Despite the extensive literature on jet breakup, the impact of surface active agents on jet breakup has received limited attention.

An extensive series of experiments with water-air and oil-water jet systems with and without surfactants has been performed, varying fluid flow rate, jet diameter, jet bulk viscosity, surfactant type, and surfactant concentration. Surfactants were found to significantly affect the breakup of laminar liquid jets. Significant effects on both the length of jets and the size of resulting droplets are reported. In general, the effect of surfactants is to reduce the interfacial tension of the system in question, which results in longer jet breakup lengths and larger diameter droplets. However, the interfacial tension alone is insufficient to explain the physics of the jet breakup phenomena. Several breakup mechanisms were identified, and the regimes in which each operates vary not only due to jet geometry and velocity, but on the interfacial properties as well. The effect of surfactants on the breakup phenomena differs in each of these distinct breakup regimes.

A mechanistic model for the prediction of breakup length for surfactant laden jets is presented. This model results in good agreement between predicted and experimentally observed values over a wide variety of surfactant concentrations and jet conditions and was shown to be useful for both the oil-water and water-air systems, within the axisymmetric jetting regime.

THE EFFECT OF SURFACTANTS ON THE BREAKUP OF AN AXISYMMETRIC LAMINAR LIQUID JET

By

Justin R. Walker

Dissertation submitted to the Faculty of the Graduate School of the
University of Maryland, College Park, in partial fulfillment
of the requirements for the degree of
Doctor of Philosophy
2012

Advisory Committee:

Professor Richard V. Calabrese, Chair
Professor James Duncan
Professor Panagiotis Dimitrakopoulos
Professor Srinivasa R. Raghavan
Professor Andre Marshall

Acknowledgements

I would like to thank my supervisor, Prof. Richard Calabrese, for his support. Without his valuable guidance and assistance, this project would have not been possible.

Secondly, I would like to thank my colleagues – Paul Reuger, Meng Yang, B.N. Murthy, and Derrick Ko for their insightful input, meaningful discussions, and constructive criticism throughout the length of my project.

I would like to thank the members of the High Shear Mixing Research Program (HSMRP) consortium for their financial support, as well as their helpful suggestions regarding experimental and analytical techniques, especially in the early stages of the project.

I would also like to thank Prof. Duncan and his students for the use of their High Speed Camera, optics, and computational equipment, as well as their time and expertise.

Finally, I would like to thank my wife Lindsay, as well as my parents, Donald and Shirley, my brother and sister Matt and Kristin, my parents-in-law Gail and Michael, and all of the other members of my extended family for their continued support.

Table of Contents

List of Tables

List of Figures

Chapter 1: Introduction

1.1: Motivation and Purpose

The breakup of a laminar axisymmetric jet is a well-studied fluid dynamics phenomenon, first studied by Savart (1833) and Rayleigh (1879) in the 1800's. Many papers have been published over the years describing the theory of jet breakup, such as the paper by Tomotika (1935) and the volume by Chandrasekhar (1961). More recently, many studies have been performed using various computational simulations to better understand the mechanics of jet breakup, notable among these are Homma et al. (2006), and García and González (2008).

Despite the extensive literature on the topic, the impact of surface active agents on jet breakup has received limited attention, whether due to the system's inherent complexity or a poor understanding of the mechanics of the action of surface active agents themselves. Indeed; the recent extensive review paper on the Physics of Liquid Jets (Eggers and Villermaux (2008)), only has a brief mention of surfactants, and even so only makes generalizations on the topic, in stark contrast to the detailed analytical analysis of most other aspects of jet physics.

Jet breakup is applicable to many fields, notably inkjet printing, fuel injector design, irrigation technology, liquid jet propulsion, manufacturing, and preparation of liquid dispersions, among others. The final entry on that list is the most relevant to this body of work. The High Shear Mixing Research Program (HSMRP) at the University

of Maryland has been studying the preparation of liquid dispersions of various systems for several years, and certain unanswered questions motivated this study.

1.2: Approach

The drop size distribution and jet breakup length resulting from the breakup of liquid jet systems were studied. Jets were formed by forcing a fluid through a narrow capillary using pneumatic pressure, to assure no external disturbances were introduced into the flow. These systems are divided into three primary groups. Firstly, jets of water or aqueous surfactants were issued into air, providing an experimental scenario where the viscosity of the continuous phase is negligible compared to the dispersed (jet) phase. Secondly, jets of silicone oils (Dow Corning 200 fluid) of various grades were issued into water, aqueous methanol solutions, and aqueous surfactant solutions, providing an experimental scenario where the viscosity of the continuous phase is non-negligible but the viscosity ratio is still large. Finally, jets of water or aqueous surfactant solutions were injected into silicone oils, providing a case where the viscosity ratio is small (less than unity), and the breakup is governed by the continuous phase properties.

The surfactants chosen in this study were Octyl Phenol Ethoxylate (more commonly known by the trade name Triton X-100) and a proprietary branched ethoxylate known as Tergitol TMN-6. These are low molecular weight, non-ionic surfactants whose properties are well established in the literature. The absorption behavior of these surfactants is will characterized by the well-known Ward and Tordai (1946) approach

for diffusion-controlled absorption. Aqueous methanol solutions allow for comparison of surfactant free systems with the same equilibrium interfacial tension as an aqueous surfactant solution, and consequently allow the decoupling of the interfacial phenomena from the kinetic surfactant-absorption phenomena in experiments operating far from equilibrium.

In order to quantify the surfactant properties, their static and dynamic interfacial tension was measured using the pendant drop technique. These measurements allowed for an estimation of the Critical Micelle Concentration (CMC) of the surfactant as well as various other physicochemical properties of the system, allowing for the construction of a model correlating the observed results of the experiment.

1.3: Organization of the Dissertation

This dissertation is divided into 7 chapters. Chapter 1 (the present chapter) is the introductory chapter. Chapters 2 and 3 provide background information on the topics of jet physics and surfactants, respectively. Chapter 4 contains details of the experimental methods, measurement techniques and semi-empirical models used in this study.

Experimental results are presented in Chapters 5-6. Results for aqueous jets into air are presented in Chapter 5, for both clean and surfactant-laden cases. The effects of jet velocity, capillary size, as well as surfactant type and concentration on jet breakup length (the distance from the capillary tip to the point at which the liquid column

breaks up into discrete droplets) and droplet size are presented and discussed, and the data is compared to existing correlations and models from the literature. Chapter 6 focuses on the liquid-liquid system. Results for jets of viscous oils into clean water, methanol-water solutions, and surfactant solutions are presented. Additionally, results for jets of aqueous solutions – both clean and surfactant laden – into viscous oils are presented. The effects of viscosity ratio, surfactant phase, jet velocity, capillary diameter, interfacial tension, surfactant type, and surfactant concentration are presented and discussed. The semi-empirical model presented in Chapter 4 is validated against the experimental data. Finally, comparisons are drawn between the laminar jet breakup system utilized in this study and the high shear mixing system which motivated it.

Chapter 7 presents the conclusions of this study, summarizes the findings, and proposes recommendations for future complementary studies to further the knowledge of surfactant laden jets.

Chapter 2: Background

2.1: Background and Existing Literature

Savart (1833) and Rayleigh (1879) first studied the breakup of liquid jets into droplets in the 1800's. Savart observed that fluid issuing from a circular orifice on the base of fluid reservoir formed a coherent liquid jet for a certain distance downstream from the reservoir, and performed many measurements on the relationship between the orifice diameter, the fill level of the reservoir, angle of the jet relative to vertical, and the type of fluid used on the jet length. Savart found that breakup occurs spontaneously, and does not depend on factors like the angle or direction of the jet, and noted that the jet did indeed break up into discrete droplets – as a "thin object" could be passed through the latter portion of the jet without being wetted.

Rayleigh's work provided the first insights into the mechanism of jet breakup. Utilizing the revolutionary new 'phenakistoscope' (a type of stroboscopic camera utilizing electric sparks of very short duration for illumination), invented by Joseph Plateau, Rayleigh was able to observe the formation of wavelike instabilities on the surface of the jet prior to breakup, as well as the formation of both larger primary droplets and smaller satellite droplets. Rayleigh went on to propose a model describing jet breakup utilizing linear dynamics. Rayleigh's linear jet breakup model will be discussed in greater detail in the following sections. Rayleigh also determined that out of all the possible disturbance wavelengths imposed on the jet, there will be only one dominant wavelength that will grow quickly in amplitude and cause the jet

to destabilize. He also realized that only wavelengths which exceeded the circumference of the jet would drive the jet toward breakup. This 'most amplified wavelength' is one of the critical components to his linear breakup analysis.

The next major work in the field of jet breakup is the paper by Tomotika (1935)**.** Expanding on the work by Rayleigh, Tomotika expanded the linear stability models to include the viscosity of the surrounding fluid – something previously neglected in Rayleigh's models. He went on to show that in the limiting case where the jet fluid viscosity is much larger than that of the continuous fluid, his model reduced to that of Rayleigh, and in the opposite case, when the viscosity of the surrounding fluid is very large compared to the jet fluid, that the value of the most amplified wavelength also becomes very large – which is to say the jet becomes extremely stable.

Linear analysis (so called because it is based on a linearization of the Navier-Stokes equations) is limited in its ability to accurately capture the physics of jet breakup. Most notably, satellite droplets are not predicted by linear breakup theory, as it predicts that the jet will break up based on a single dominant wavelength. Several subsequent papers have attempted to improve upon the results of Rayleigh and Tomotika by including higher order terms or performing other types of analysis. One such paper is the work by Geer & Strikwerda (1983). They proposed a method known as 'slender jet' theory, where the shape of the interface of a jet can be determined numerically by solving a nonlinear 2-dimensional set of equations in the cross-sectional plane of the jet. They compared the oscillations on the jet observed in

their calculations to those found experimentally by Rayleigh, and found them to agree qualitatively. Keller (1983) further analysed the oscillations using slender jet theory and found better agreement by taking into account variations in the velocity and radius of a falling jet.

Lafrance (1974) made an important contribution to the field by extending Tomotika's method to include terms up to the 3rd order. His results show that these nonlinear terms are responsible for the appearance of satellite droplets. He also showed that the overall jet length and primary droplet diameters were not significantly changed by the inclusion of higher order terms. Utilizing this method, the authors were able to achieve good quantitative agreement with experimental data. However, as with any higher order analysis, no analytical solution is possible, and so any solution must be performed numerically.

With the advancing capability of modern computers, the bulk of recent studies have focused on improved numerical solutions to the problem. One notable numerical study is the direct numerical simulation performed by Homma et al (2006). In this work the authors calculate the exact solution to the Navier-Stokes equations at very small length scales to accurately simulate jet breakup without any modeling equations. The authors identified several phases of jet behaviour and were able to accurately reproduce experimental data. However, this type of simulation remains prohibitively expensive to perform on more than a tiny subset of conditions due to the extremely long run times of DNS simulations. García and González (2008) provide

an excellent review of the various recent jet simulation papers, including their simulation methods and types of initial conditions. They found that the accuracy of many simulation schemes were strongly dependent on the choice of initial conditions. This limits the usefulness of these types of simulations because in the case of unforced jets – such as this study – determining the precise initial conditions of the experimental jet instability is often impossible.

In order to rectify this problem, many jet studies impose a forcing frequency – using some form of mechanical oscillation of the capillary used to form the jet or by introducing pressure pulses into the fluid – to provide a well characterized initial condition on the jet. Das (1992), Kalaaji et al (2003), and González and García (2006) provide examples of experimental studies of forced liquid jets. By imposing a dominant frequency on the jet, the system can be driven to produce monotonic droplets by breaking up at that imposed wavelength, rather than the wavelength determined by the physical properties of the system. This is useful for applications such as inkjet printing where consistent sized droplets are desired, but is less useful for understanding the mechanism by which the physical properties of the system interact to modify jet breakup (such as the case where surfactants are added to the system).

2.2: Jet Breakup Analysis Techniques

2.2.1 Linear Stability Analysis

A cylindrical jet of fluid is hydrodynamically unstable, having a larger surface area than a sphere of equal volume. As such, surface tension drives the jet to break up.

The dynamics of the system drive the jet to break up into a series of spheres, rather than a single one. According to Rayleigh, if the column becomes varicose with wavelength λ exceeding the circumference ($2\pi r$) of the cylinder, the cylinder will decay into droplets such that each fluid 'node' comprises one drop. Figure 2.1 shows the relevant geometry.

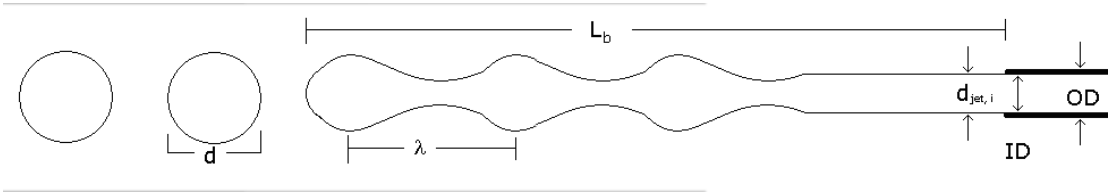

Figure 2.1 – Schematic diagram of jet with relevant geometry

L_b is the jet breakup length, d is the droplet diameter, $d_{jet,i}$ is the initial jet radius, and ID and OD are the inner and outer diameter of the capillary tube, respectively. If the breakup of an inviscid fluid cylinder is assumed to be driven only by capillarity (eg, the influence of the outer fluid is ignored), and we work in the jet's reference frame (eg, the jet velocity in the axial direction is zero), the Navier-Stokes equations may be linearized and rearranged to form Equation 2.1 (see Eggers and Villermaux (2008) for a detailed derivation)

$$\omega^2 = -\frac{\sigma}{\rho r_0^3}(kr_0)\left[1-(kr_0)^2\right]\frac{I_1(kr_0)}{I_0(kr_0)} \qquad (2.1)$$

Where ω is the growth rate of the instabilities, ρ is the fluid density, σ is the interfacial tension between the jet fluid and its surrounding fluid, r_0 is the initial jet

radius, k is the wave number of the instability, and I_0 and I_1 are modified Bessel functions of the first kind of order 0 and 1, respectively. The most unstable wave number is found by locating the value of k which maximizes ω. Figure 2.2 shows a plot of ω vs k. The most amplified wave number is k_{max}=0.698. This wave number is known as the Rayleigh breakup mode.

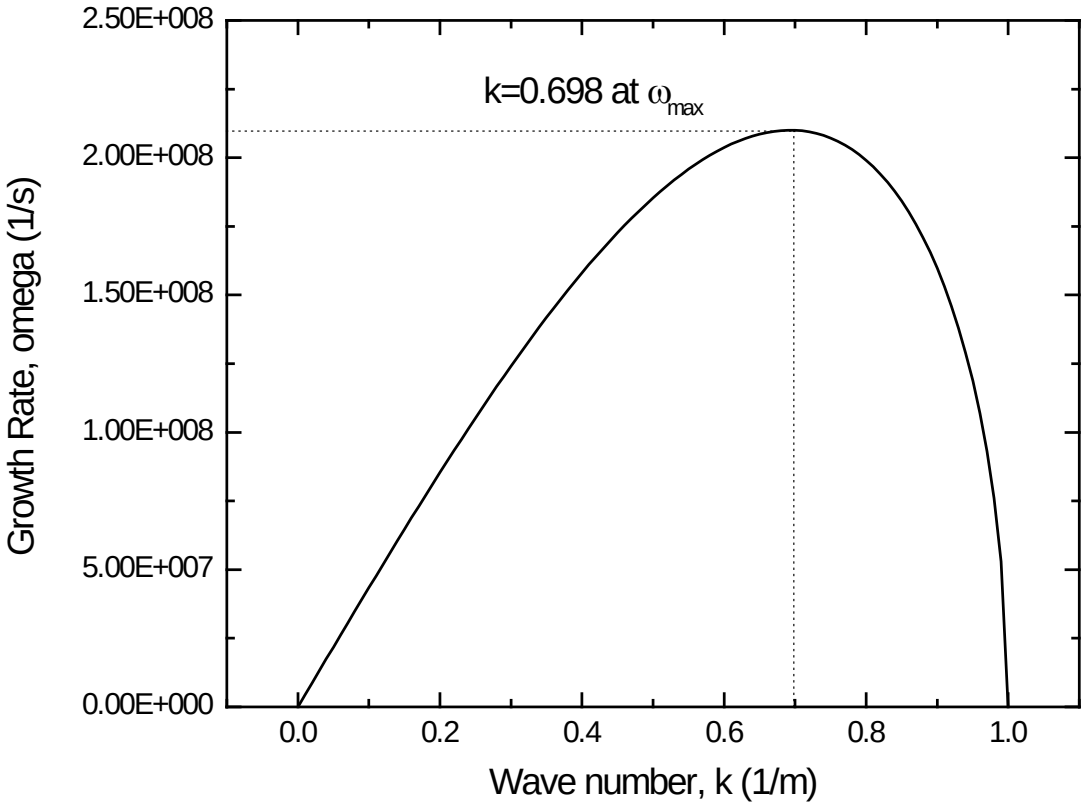

Figure 2.2 – Growth rate vs wave number for the Rayleigh mode

If we no longer assume the jet to be inviscid, a similar derivation results in Equation 2.2

$$\omega^2 = -\frac{\sigma\eta}{\rho r_0^3}\left[1-\eta^2\right]\frac{I_1(\eta)}{I_0(\eta)} - \frac{3\mu k^2}{\rho}\omega \qquad (2.2)$$

Where $\eta = k \cdot r_0$ is substituted for convenience and μ is the fluid viscosity. It is shown in Figure 2.3 that as viscosity increases, the most unstable wave number approaches zero, corresponding to longer breakup wavelengths.

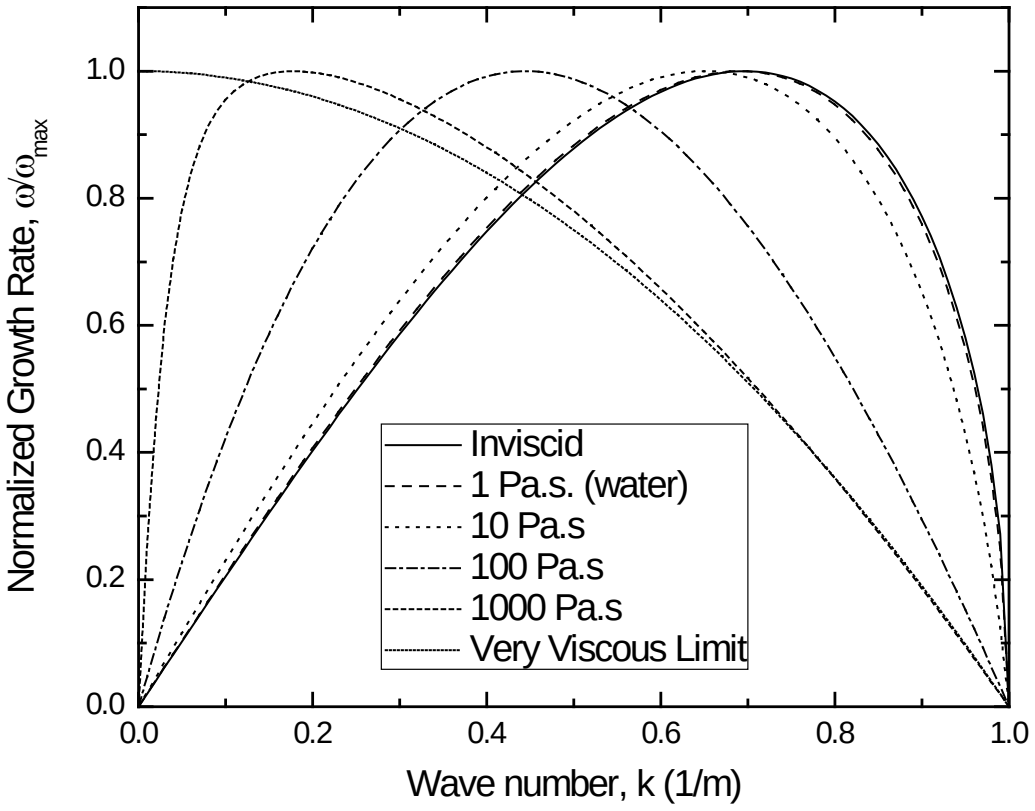

Figure 2.3 – Effect of viscosity on normalized growth rate

It is generally convenient to work in dimensionless units, so utilizing the 'dimensionless growth rate':

$$w = \omega \sqrt{\frac{\rho r_0^3}{\sigma}} \tag{2.3}$$

And the Ohnesorge Number

$$Oh = \frac{\mu}{\sqrt{\rho \sigma r_0}} \tag{2.4}$$

Equation 2.2 can be recast in dimensionless form:

$$w^2 = \eta\left(1-\eta^2\right)\frac{I_1(\eta)}{I_0(\eta)} - 3\eta^2 Oh\, w \tag{2.5}$$

Solving for w (ignoring the nonphysical negative root), we get

$$w = \frac{1}{2}\left(-3\eta^2 Oh + \sqrt{9\eta^4 Oh^2 + 4\eta\left(1-\eta^2\right)\frac{I_1(\eta)}{I_0(\eta)}} \right) \tag{2.6}$$

Figure 2.4 shows the effect of the Ohnesorge number on the η-w maxima. From the value of η_{max}, the dimensionless droplet size (d^*) can be calculated using Equation 2.7, which is derived from a simple geometric reduction (a spherical droplet is formed from a cylindrical section of length η).

$$d^* = \frac{d_{drop}}{d_{jet,i}} = \left(\frac{3\pi}{2\eta_{\max}} \right)^{1/3} \tag{2.7}$$

where d_{drop} is the equivalent spherical diameter of the droplet, and $d_{jet,i}$ is the initial diameter of the fluid jet (equal to the inner diameter of the capillary tube).

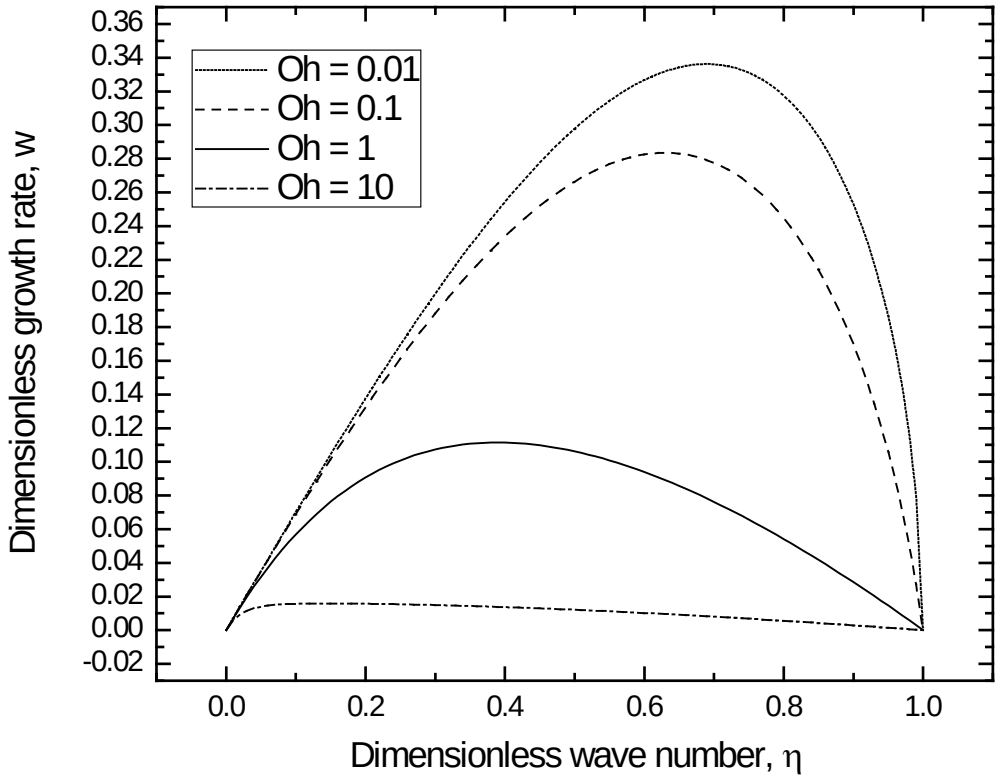

Figure 2.4 – Effect of Ohnesorge number on dimensionless growth rate

Figure 2.5 shows the predicted dimensionless drop size (normalized by capillary diameter) vs. the Ohnesorge number.

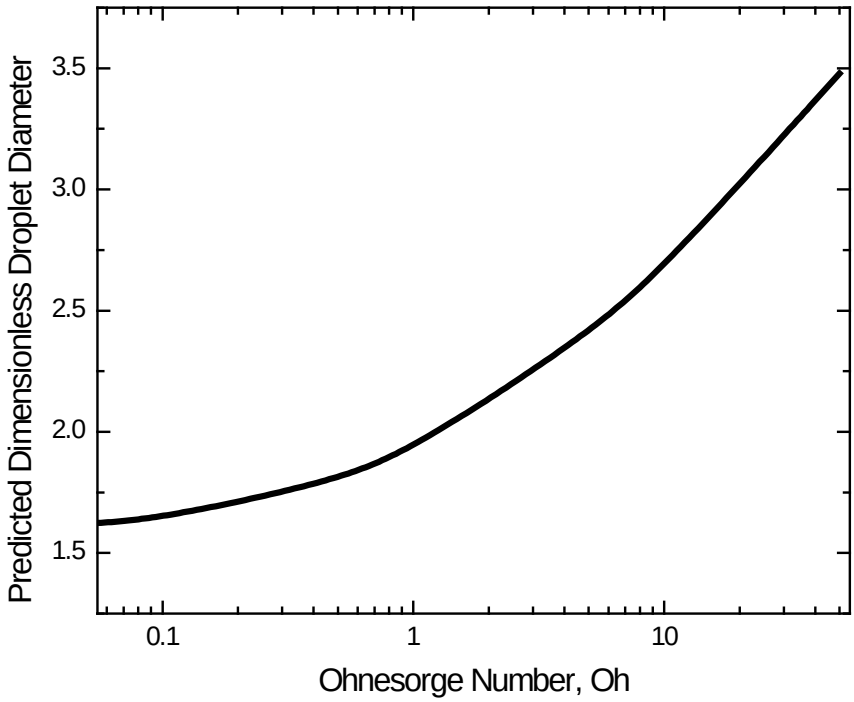

Figure 2.5 – Predicted variation in dimensionless droplet diameters with Ohnesorge number

It is also possible to predict the jet breakup length using the linear stability model. Using the instability growth rate found above, coupled with knowledge of the jet's geometry and velocity, an estimate of the time until the instability grows to exceed the jet diameter can be made. This quantity is known as the breakup time. From the breakup time, the breakup length can be calculated knowing the jet velocity. However, accommodations must be made for the fact that the jet increases in diameter as it becomes varicose, and as such slows down.

Das (1997), working off the earlier results of Rayleigh (1879), derived the following expression for jet breakup length L_b:

$$L_b = \frac{U_n}{\omega} \ln\left(\frac{r_0}{\delta_0}\right) \tag{2.8}$$

where U_n is the average (superficial) jet velocity, and δ_o is the amplitude of an infinitesimal disturbance on the surface of the jet. Since the value of δ_o cannot be determined experimentally, Das (1997) and Scheele and Meister (1968) both found that using $\ln(r_o/\delta_o) = 6$ successfully predicted breakup lengths for liquid-liquid systems. For this prediction, the value of ω from Equation 2.1 or 2.2 is used, as appropriate. The dimensionless breakup length (L_b^*) is found by dividing by the initial jet diameter:

$$L_b^* = \frac{We^{1/2}}{2w}\ln\left(\frac{r_0}{\delta_0}\right) \tag{2.9}$$

where We is the Weber Number, defined by Equation 2.10:

$$We = \frac{\rho U_n^2 d_{jet,i}}{\sigma} = \frac{16\rho Q^2}{\pi^2 \sigma d_{jet,i}^3} \tag{2.10}$$

and Q is the volumetric flow rate. The form of Equation 2.9 is in agreement with the semi-empirical correlation proposed by Goldin et al. (1969), which correlated breakup length with the Weber number and Reynolds number using equation 2.11:

$$L_b^* = C_1\left[We^{1/2} + 3\frac{We}{\mathrm{Re}}\right] = C_1\left[We^{1/2} + 3Ca\right] \tag{2.11}$$

where C_1 is an empirical fitting parameter, Re is the Reynolds number, defined by Equation 2.12, and Ca is the Capillary number, equal to We/Re. Both equations show a $We^{½}$ dependence, however Equation 2.9 is a more mechanistic approach, and so is generally preferable.

$$\mathrm{Re} = \frac{\rho U_n d_{jet,i}}{\mu} = \frac{4\rho Q}{\pi d_{jet,i} \mu} \tag{2.12}$$

2.2.2 Nonlinear Analysis

The model presented in section 2.2.1 assumes that the jet breaks up linearly into monosized droplets. In practice, this is not the case. In most situations, jets break up into large primary droplets separated by one or more satellite drops. Generally these satellite drops are much smaller than the primary drops and contribute less than 3% of the total volume of the system, so the linear theory above can be safely used to predict the primary droplet diameter. In order to predict the size of satellite drops, higher order terms need to be accounted for. This type of modeling is known as nonlinear analysis.

Neyfeh (1970) performed a second-order expansion of Rayleigh's equations and found that there was a critical wavenumber above which disturbances oscillate stably, in agreement with the linear stability results. However, he also determined that the frequency of these oscillations is amplitude-dependent, contrary to the findings utilizing only the 1st-order equations. Lafrance (1974) extended Tomotika's method to include terms up to the 3rd order. He proposed that since the system is initially at rest, the flow is entirely potential. Therefore, the dimensionless velocity potential ϕ must satisfy Laplace's equation:

$$\nabla^2 \phi = 0 \tag{2.13}$$

The boundary conditions are:

$$\left[\frac{\partial}{\partial t}+\left(\nabla\phi\cdot\nabla\right)\right]\eta=\frac{\partial\phi}{\partial r} \tag{2.14}$$

and

$$\phi_t+\frac{1}{2}\left(\phi_r^2+\phi_z^2\right)=\frac{\eta_{zz}}{\left(1+\eta_z^2\right)^{3/2}}-\left(1+\eta\right)^{-1} \tag{2.15}$$

He then assumes that the surface disturbance and velocity perturbation can be expanded in terms of η_0, which he designates the "smallness parameter".

$$\eta(z,t)=\sum_{n=1}^{\infty}\eta_0^n\eta_n(z,t) \tag{2.16}$$

$$\phi(r,z,t)=\sum_{n=1}^{\infty}\eta_0^n\phi_n(r,z,t) \tag{2.17}$$

A Taylor expansion of the boundary and initial conditions at r=1 provides successive orders of approximation. These approximations are solved in order, starting with the lowest. For the first order, the results are the same as Rayleigh's linear theory, presented above. The results for the 3rd order are presented as equations 2.18-2.20

$$\nabla^2\phi_3=0 \tag{2.18}$$

$$\begin{aligned}&\phi_{3,r}-\eta_{3,t}=-\eta_2\phi_{1,rr}-\eta_1\phi_{2,rr}-\frac{1}{2}\eta_1^2\phi_{1,rrr}\\&+\eta_{1,z}\left(\eta_1\phi_{1,rz}+\phi_{2,z}\right)+\eta_{2,z}\phi_{1,z}\end{aligned} \tag{2.19}$$

$$\begin{aligned}&\phi_{3,t}=\eta_{3+}\eta_{3,zz}-\frac{3}{2}\eta_{1,z}^2\eta_{1,zz}-2\eta_1\eta_2+\eta_1^3-\eta_2\phi_{1,tr}-\frac{1}{2}\eta_1^2\phi_{1,trr}\\&-\eta_1\phi_{2,tr}-\eta_1\phi_{1,r}\phi_{1,rr}-\phi_{1,r}\phi_{2,r}-\eta_1\phi_{1,z}\phi_{1,zr}-\phi_{1,z}\phi_{2,z}\end{aligned} \tag{2.20}$$

His results show that these nonlinear terms are responsible for the appearance of satellite droplets. As with any higher order analysis, no analytical solution is possible, meaning the results of these models must be achieved numerically.

A similar approach by Yuen (1968) showed that the maximum growth rate of an instability occurred at a wavenumber k=0.7, which closely agrees with the linear stability results shown by Rayleigh and Tomotika, proving that the introduction of higher order terms did not significantly affect the prediction of overall jet parameters such as the breakup length and primary droplet size. Chaudhary and Redekopp (1980) used a 3rd order solution to show that for wavenumbers $k < 0.65$, no satellite droplets formed. For wavenumbers $k \geq 0.65$, the jet broke up into primary droplets interspersed with small satellite droplets. They further showed that the presence of satellite droplets can be controlled by imposing a harmonic oscillation onto the jet externally, in addition to the fundamental oscillation frequency.

Geer & Strikwerda (1983) proposed a method known as 'slender jet' theory, where the shape of the interface of a jet can be determined numerically by solving a nonlinear 2-dimensional set of equations in cylindrical coordinates.

If we allow the velocity potential of the jet to be denoted by equation 2.20 (similar to above):

$$\phi = \phi(r, z, t; \varepsilon) \tag{2.20}$$

And the shape of the free surface to be denoted by equation 2.21:

$$r = \xi(\theta, z; \varepsilon) \tag{2.21}$$

The parameter ε is the slenderness ratio of the jet, which is the ratio of the typical radius of the jet to the typical length, defined precisely by Geer (1977). For small values of ε, Geer & Strikwerda (1983) showed that:

$$\phi = \frac{2}{3}(1+z)^{3/2} + \varepsilon^2 \phi(r,\theta,z) + O(\varepsilon^4) \tag{2.22}$$

$$\xi = S(\theta, z) + O(\varepsilon^2) \tag{2.23}$$

Where ϕ and S satisfy the conditions:

$$\frac{\partial^2\phi}{\partial r^2} + \frac{1}{r}\frac{\partial\phi}{\partial r} + \frac{1}{r^2}\frac{\partial^2\phi}{\partial\theta^2} = -½(1+z)^{-½} \qquad (z>0, 0 \le r < S(\theta,z)) \tag{2.24}$$

with

$$\frac{\partial\phi}{\partial r} - \frac{1}{S^2}\frac{\partial S}{\partial\theta}\frac{\partial\phi}{\partial\theta} = (1+z)^{½}\frac{\partial S}{\partial z} \tag{2.25}$$

$$\left(\frac{\partial\phi}{\partial r}\right)^2 + S^{-2}\left(\frac{\partial\phi}{\partial\theta}\right)^2 + 2(1+z)^{½}\frac{\partial\phi}{\partial z} = W^{-1}\frac{SS_{\theta\theta} - S^2 - 2S_\theta^2}{\left(S^2+S_\theta^2\right)^{3/2}} \tag{2.26}$$

W is defined by:

$$W = \frac{2g^2b^3\rho}{\gamma U^2} \tag{2.27}$$

Where g is the acceleration due to gravity, b^2 is the cross-sectional area of the jet at z=0, ρ is the density of the fluid, γ is the surface tension, and U is the velocity of the jet at z=0. To find ϕ and S, the following solution to equation 2.24 is used:

$$\phi = -\frac{1}{8}(1+z)^{-½} r^2 + \psi \tag{2.28}$$

where ψ satisfies Laplace's equation. After significant further manipulation, the authors arrive at the following equation:

$$(1+\beta^2)\frac{1}{p}\frac{\partial}{\partial p}(p\frac{\partial \psi}{\partial p}) - \frac{\partial \beta}{\partial \theta}\frac{1}{p}\frac{\partial \psi}{\partial p} + \frac{1}{p^2}\frac{\partial^2 \psi}{\partial \theta^2} - 2\beta\frac{1}{p}\frac{\partial^2 \psi}{\partial p \partial \theta} = 0$$
$$(0 \le \theta \le 2\pi,\ 0 \le p < 1,\ z \ge 0) \tag{2.29}$$

where

$$\beta = \frac{1}{S}\frac{\partial S}{\partial \theta} = \frac{1}{2}\frac{1}{R}\frac{\partial R}{\partial \theta} \tag{2.30}$$

$$p = \frac{r}{S(\theta, z)} \tag{2.31}$$

$$R(\theta, z) = \frac{1}{2}S(\theta, z)^2(1+z)^{½} \tag{2.32}$$

The system of equations are solved numerically using a forward-backward MacCormack scheme. Further details are given in Geer & Strikwerda (1983). The shape of the surface oscillations predicted by their calculations agrees qualitatively with experimental observations, however this model was unable to predict actual jet breakup.

Keller (1983) extended the slender-jet model to allow for jet breakup, and allows for jets of initial shapes other than circular (elliptical, triangular, and square jet shapes are analyzed). These results showed better agreement with experimental results.

All of the higher order term models presented neglect the continuous phase, and so are only applicable to liquid jets in an inviscid phase (eg, water jets into air). The mathematical modeling for a viscous continuous phase simply becomes too difficult for this type of analysis. As a result, most recent studies have utilized full numerical (eg, Computation Fluid Mechanics) methods.

2.2.3 Numerical Methods

In order to predict jet breakup behaviour for a viscous jet breaking up in a viscous continuous phase and fully determine all of the parameters of the flow (satellite droplets, jet breakup length, etc.), the full Navier-Stokes equations need to be solved for both the inner and outer fluids. Since the Navier-Stokes equations do not have an analytical solution for this case, we must resort to Computational Fluid Dynamics (CFD), where our domain is divided into many small regions and the solution to the equations are solved for each region at each time step. There are many different types of CFD simulation schemes available, primarily depending on the scale of the subdivided regions. The smaller these regions are, the more computationally expensive the simulation is, in terms of run time and computer RAM and CPU usage. However, the larger these regions are, the less accurate the solution can be, as everything inside the region is assumed by the simulation to be homogenous. If the regions are small enough that the assumption of homogeneity can be upheld, the Navier-Stokes equations can be solved directly. This type of simulation is known as a Direct Numerical Simulation (DNS), and is the most accurate but most expensive

type of simulation. In most cases, the regions are sufficiently large that we must utilize a "sub-grid model", or some kind of model to determine the gradients in the various calculated quantities (velocity, pressure, density, etc.) within the region. In the case that all of the regions are large enough to require sub-grid modeling, we cannot solve the Navier-Stokes equations themselves, but rather a time-averaged version of the equations, introducing additional terms known as the 'Reynolds Stress'. This nonlinear term requires additional modeling to solve, and there are several different models (such as the k-ε model) to solve. This type of simulation is known as a Reynolds Averaged Navier-Stokes (RANS) simulation, and is the least expensive, but generally least accurate type of simulation.

Between these two extremes lies a family of simulation types known as Large Eddy Simulations (LES) or Detached Eddy Simulations (DES), whereby the complete Navier-Stokes equations are solved in some regions (eg, where gradients are small and homogeneity can be assumed), and sub-grid scale models are utilized in other regions (where gradients are large). These have a moderate computational cost and achieve reasonable accuracy in many cases.

In addition to these models, since this system is a multiphase system, an additional set of models must be taken into account to calculate the shape of the interfaces and the values of interfacial tension. Again, several models exist, but the most commonly utilized model is the Volume of Fluid (VoF) method. Further information about the formulation of this method is found in Hirt & Nichols (1981). This method is an advective method, meaning that the VoF equations must be solved in addition to the

Navier-Stokes equations at each point along the interface at each time step. Therefore, this adds significant complexity and cost to the simulations.

The equations and methodology of these CFD simulations are beyond the scope of this (experimental) study. However, a discussion of existing simulations and their methodology is given by Eggers (1997), Lin (2003) and García and González (2008).

2.3: Jet Regime Transition Analysis

2.3.1 Jet Regimes

Depending on the velocity of the fluid exiting a capillary, several different phenomena are possible. Jet behaviour falls within 4 distinct regimes; dripping flow, axisymmetric jetting, asymmetric jetting, and atomization. Figure 2.6, reproduced with permission from Homma et al (2006), shows the effect of jet velocity on jet breakup length and the relationship of the various jet regimes. Sample images from the jet regimes observed in this study are presented in Figure 2.7.

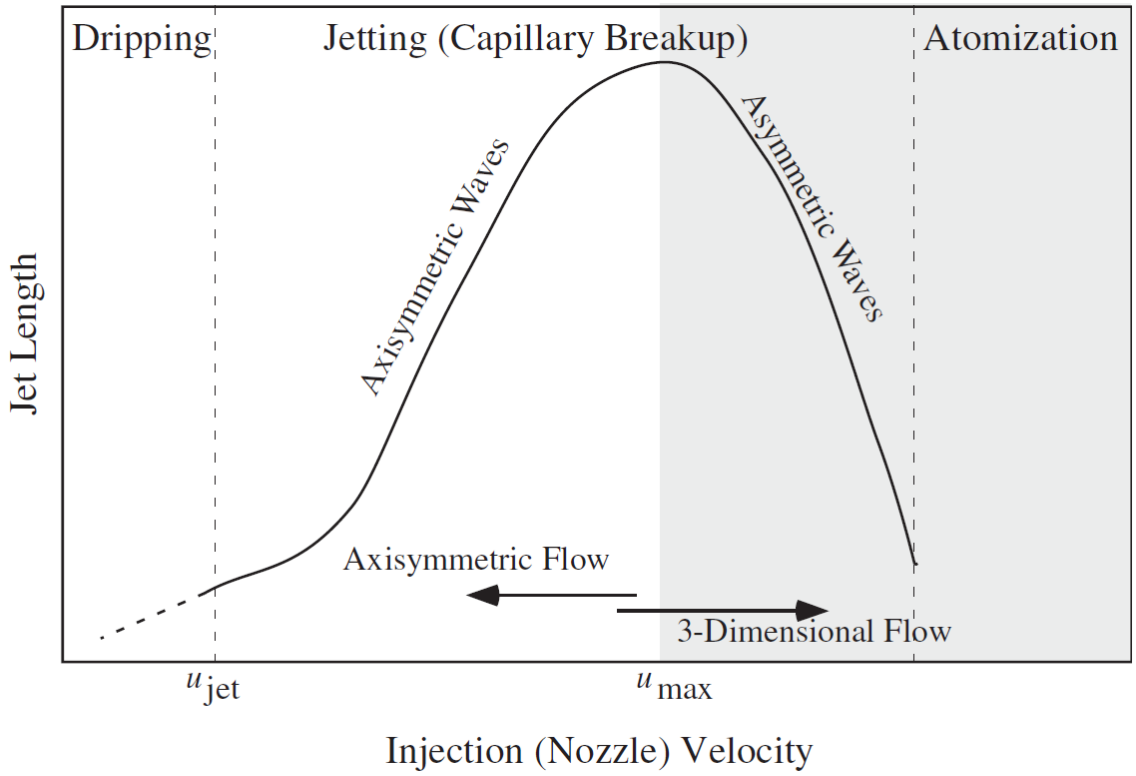

Figure 2.6 – Predicted effect of jet velocity on breakup length based on DNS simulation results (reproduced with permission from Homma et al. (2006))

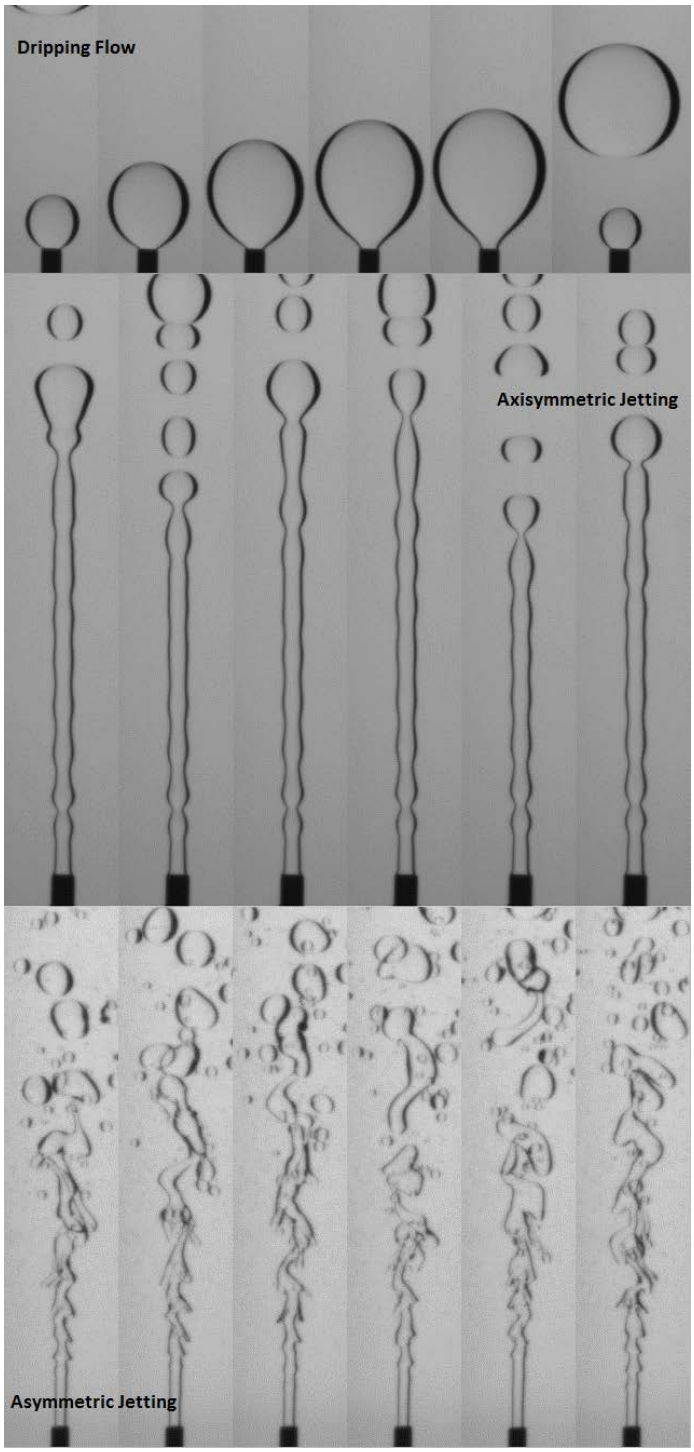

Figure 2.7 – Sample images of oil-water jets from three different flow regimes. Each row represents a series of frames from the same experiment. Time progresses from left to right. Jet velocity increases from top to bottom. Atomization is not observed under the experimental conditions in this study

As seen in figure 2.6 and 2.7, at low jet velocity no true jet is formed, but rather a droplet slowly forms at the tip of the capillary and grows in size until its buoyancy exceeds the force of adhesion holding it to the capillary, at which time an individual droplet detaches. At some critical velocity, discussed further in section 2.3.2, the jet transitions from dripping flow to jetting flow, and a stable column of liquid begins to form. At low velocity, axisymmetric instabilities form on the surface of the jet and eventually destabilize the jet to break up into a series of spherical droplets. The breakup length increases with jet velocity in this regime (known as the 'axisymmetric jetting' regime). At some other critical velocity, there is an onset of asymmetric instabilities caused by interactions between the jet and the continuous fluid that causes the jet to begin to destabilize in an asymmetric manner. Further increases in jet velocity serve to increase the magnitude of these asymmetric instabilities, causing the jet length to rapidly decrease with increasing velocity. This regime is known as the 'asymmetric jetting' regime. Finally, at some higher velocity (well above the range of conditions utilized in this study), a 4^{th} regime is identified, known as the 'atomization' regime. In this regime many small droplets are produced at the capillary tip without the presence of any jet due to strong entrained continuous fluid flow patterns.

2.3.2 Transitions from Dripping Flow to Jetting Flow

The nature of the transition between dripping and jetting flow is a much-studied topic in and of itself, with several recent papers on the topic.

Clanet and Lasheres (1999) propose a critical Weber number, defined by equation 2.33, at which the transition from dripping to jetting occurs. The Weber number is defined by equation 2.34, and the Bond number by equation 2.35.

$$We_c = 4\frac{Bo_o}{Bo}\left[1 + KBo_o Bo - \left(\left(1 + KBo_o Bo\right)^2 - 1\right)^{1/2}\right]^2 \qquad (2.33)$$

$$We = \frac{\rho U_0^2 D}{\sigma} \qquad (2.34)$$

$$Bo = \left(\frac{\rho g D^2}{2\sigma}\right)^{1/2} \qquad (2.35)$$

where Bo and Bo_o are the Bond numbers based on the inner and outer diameters of the capillary tube, respectively. K is an empirical constant (K = 0.37 for clean water injected into air), ρ is the jet fluid density, U_0 is the superficial jet velocity exiting the tube, D is the tube diameter, g is the acceleration due to gravity, and σ is the interfacial tension between the jet and continuous fluids. The authors determined that the critical value of the Weber number is subject to a hysteresis of approximately 10% (eg, there exists a narrow range of Weber numbers in which a jet could exhibit either jetting or dripping flow, depending on the previous conditions of the jet). As such, the critical Weber number predicted by equation 2.33 should be regarded as approximate. The reader will also note that equation 2.33 does not take into account the viscosity of the jet phase; therefore this expression gives the critical Weber number at the inviscid limit.

Ambravaneswaran et al (2004) utilized high speed photography as well as developing new mathematical models to explore the effects of jet flow rate and viscosity on the value of the critical Weber number. They present a phase diagram detailing regions of complex and simple dynamics, and describing the boundaries between simple dripping (as described above), an intermediate phase they label 'complex dripping' (referred to in this text as 'unstable jetting'), and jetting phases. They find that for values of the Ohnesorge number greater than ~0.5, the critical Weber number collapses to the inviscid limit. For Ohnesorge numbers of between 0.01 and 0.5 the value of the critical Weber number can exceed the inviscid limit critical Weber number by as much as 2 orders of magnitude. For reference, the Ohnesorge numbers used in this study are typically on the order of 0.05-0.1.

Subramani et al (2006) further characterizes the transition between these phases and identifies a total of 5 critical weber numbers between simple dripping flow and jetting flow, classifying the regions due to the presence or absence of satellite droplets, and by the periodicity of the droplets produced (eg, in simple dripping all droplets are of the same size, in period 2 dripping, two droplets of one size are produced followed by a droplet of another – typically smaller – droplet, and so on). These critical values are presented as a phase diagram covering a broad range of the Bond number and Ohnesorge number space. A numerical modeling technique to predict the presence or absence of satellite droplets under simple dripping (of period n) is also presented and validated against experimental data.

Cramer, Fischer, & Windhab (2004) experimentally studied the formation of drops for two immiscible co-flowing fluids, focusing on dripping flow, and in particular the production of monodisperse droplets. They also explored the parameter space of the properties of the external fluid on the transition point between dripping and jetting, finding that increasing the flow rate of either the inner or outer phase pushed the system toward jetting behaviour, and that increasing viscosity ratio also pushed the system toward the jetting regime. Decreasing interfacial tension also promoted jetting flow. They also found that the viscosity ratio had little effect on the ultimate droplet size produced, and that droplet size was strongly influenced by the flow rates of the inner and outer fluid. Thus, the system could be 'tuned' to produce monodisperse droplets of a target size even with varying viscosity solutions.

2.4: Tensiometry (Measurement of Interfacial Tension)

There are several methods available to measure the interfacial tension of one fluid in another, for example the Du Noüy Ring, the Wilhelmy Plate, the Bubble Pressure method, the Spinning Drop method, and the Pendant Drop method, among others. The Pendant Drop method is the method chosen for this study.

The pendant drop method determines interfacial tension based on the shape of the droplet. For a droplet such that the forces due to surface tension and buoyancy are of comparable magnitudes, a droplet will be deformed from a spherical shape due to buoyancy but still adhere to a capillary tube due to surface (interfacial) tension. The

interfacial tension can then be determined from measurements of the shape of the drop or bubble (Adamson (1976)).

Figure 2.8 shows an image of a pendant drop with the relevant coordinate system. Using this coordinate system, the balance between the buoyancy force and the surface tension force can be expressed by means of the Young-Laplace Equation (2.36)

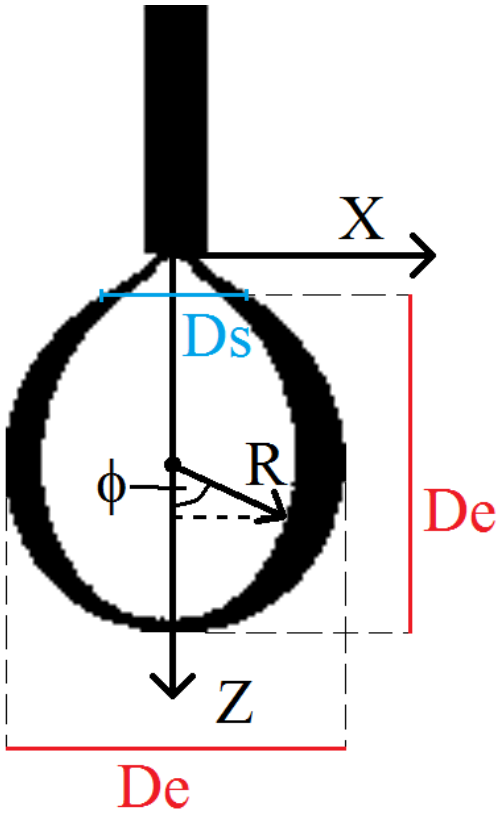

Figure 2.8 – Image of a pendant drop showing the coordinate system and the parameters (De, Ds) needed to calculate the Shape Parameter

$$\sigma\left(\frac{1}{R_1}+\frac{1}{R_2}\right)=\frac{2\sigma}{b}+\Delta\rho g z \qquad (2.36)$$

where R_1 is the radius of curvature on the x-z plane, R_2 is the radius of curvature on the plane normal to z, and b is the radius of curvature at the apex of the drop (since

the drop is symmetric, R_1=R_2 at the apex). If this expression is rearranged as a function of ϕ, it is known as the Bashforth-Adams equation (Hiemenz and Rajagopalan (1997)):

$$\frac{1}{R_1 b} + \frac{\sin(\phi)}{x/b} = 2 + Bo\frac{z}{b} \tag{2.37}$$

where Bo is the Bond number, defined by equation 2.35 above. As the exact value of b is difficult to measure experimentally due to spherical aberration, it is convenient to utilize a model based on the so-called 'Shape Parameter', S:

$$S = \frac{Ds}{De} \tag{2.38}$$

De and Ds are defined as the equatorial diameter of the drop and the diameter of the drop at a distance from the apex equal to De, respectively, and are illustrated in figure 2.8. We may then combine the parameter b with the Bond number to define a variable H:

$$H = Bo\left(\frac{De}{b}\right)^2 \tag{2.39}$$

The relationship between the Shape Parameter S and the variable H is determined experimentally, and presented in tabulated form in Adamson (1976). Padron (2005), provided the following equation as a best-fit to the data:

$$\frac{1}{H} = 0.315S^{-2.608} \tag{2.40}$$

Utilizing this relationship allows us to determine the interfacial tension of the drop from the shape parameter:

$$\sigma = \frac{\Delta\rho g\, De^2}{H} \tag{2.41}$$

Chapter 3: Surfactants

3.1: Background on Surfactants

All of the relationships discussed thus far are valid for 'clean' systems, that is, those with unpopulated fluid/fluid surfaces. However, our system of interest is a surfactant laden system, where the fluid surfaces are partially or completely coated with amphiphillic chemicals which significantly affect interfacial phenomena.

Surfactants are commonly modeled as having an ionic, hydrophilic 'head', and an organic hydrophobic 'tail'. Thus, when exposed to an aqueous interface, the molecules have a tendency to orient themselves such that the hydrophobic group protrudes from the aqueous phase into the neighbouring fluid phase. Figure 3.1 shows a sketch of this phenomenon.

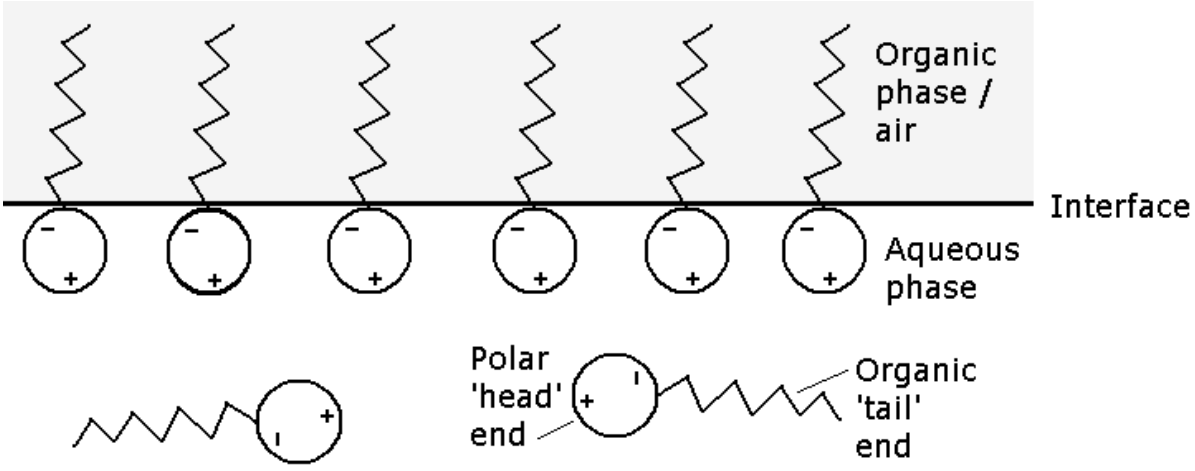

Figure 3.1 – Surfactant geometry

When an interface is not present, surfactants will tend to self-organize if their concentration is sufficiently high. Above the Critical Micelle Concentration (CMC),

surfactants will spontaneously form micelles, spherical structures where the molecules organize to minimize the contact of the hydrophobic end of the molecule with the surrounding aqueous phase. A similar phenomena, reverse micelles, occur in oil-soluble surfactants where the hydrophilic (and thus lipophobic) head groups are within the micelle. Figure 3.2 shows sketches of normal and reverse micelles. Micelles are in equilibrium with free surfactant molecules in solution, so if the bulk concentration of surfactant changes – for example by the creation or destruction of new surfaces, or by the addition of chemical, micelles can break or form to maintain the bulk free surfactant concentration at the critical micelle concentration. In this manner, micelles act as a surfactant buffer and maintain the bulk interfacial tension constant at any surfactant concentration above the CMC. Figure 3.3 shows a sketch of the relationship between surfactant concentration and interfacial tension, illustrating the location of the CMC.

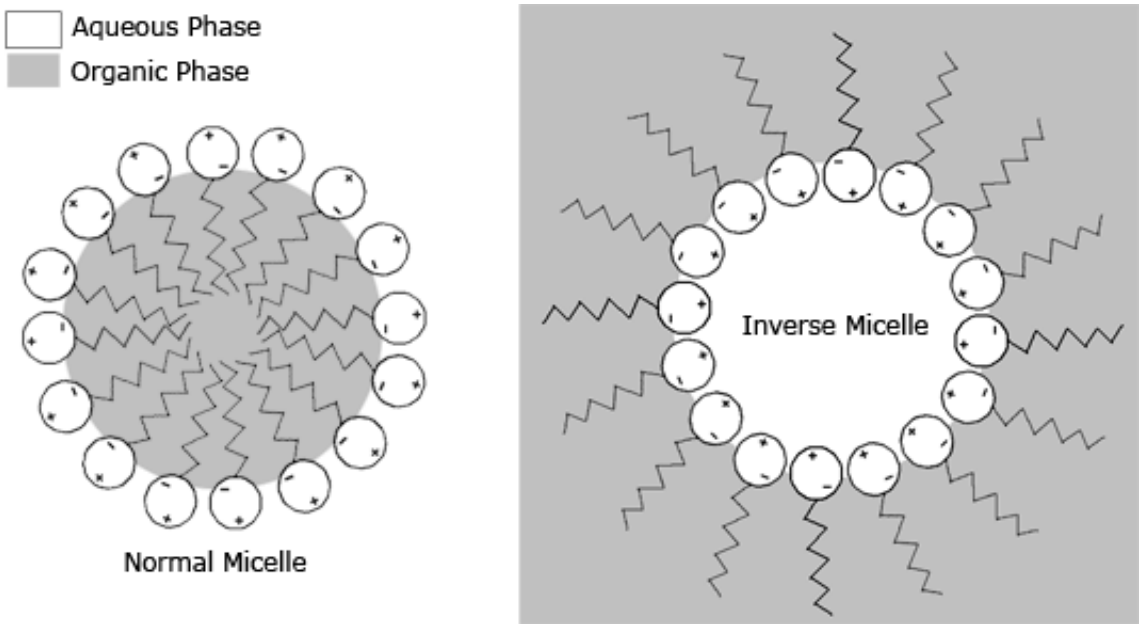

Figure 3.2 – Illustration of normal and inverse micelles

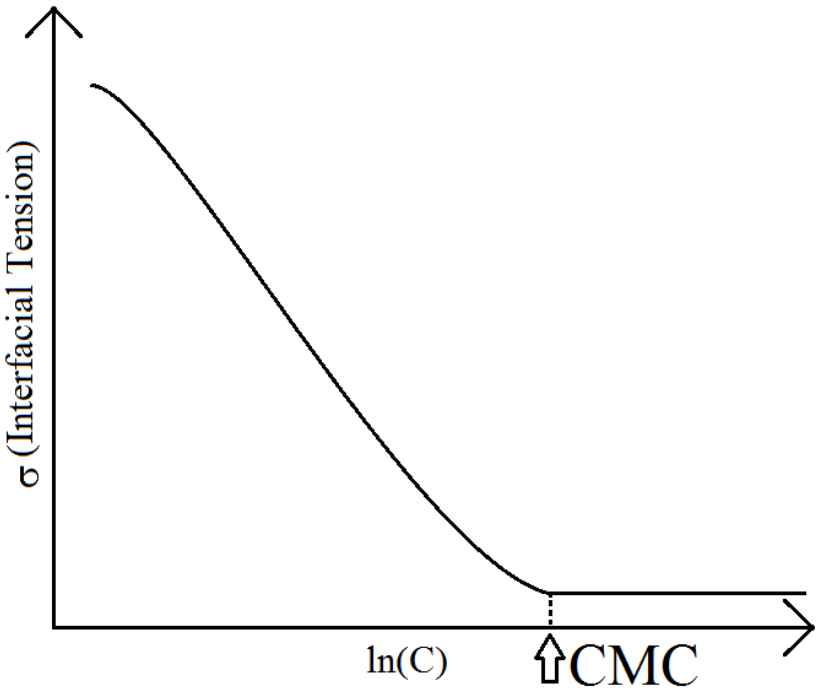

Figure 3.3 – Relationship between interfacial tension (σ) and surfactant concentration (C), identifying the location of the Critical Micelle Concentration (CMC)

If concentrations are increased significantly above the CMC, other structures such as double micelles, cylindrical micelles and bi-layer sheets can form. Surfactant concentrations in this study were maintained at relatively low levels, so it is unlikely that any of these secondary structures were formed.

The primary action of surfactants is to act as a 'bridge' between phases, reducing the interfacial tension. Surfactant molecules also add rigidity to interfaces, as any change in surface area or orientation causes gradients in the surface concentration of surfactant, resulting in Marangoni stresses which oppose these changes. Depending on the diffusivity of the surfactant in question, these Marangoni stresses can have significant effects on jet breakup, as they act to damp out surface oscillations and stabilize the jet against breakup.

Surfactants also have significant effects on drop coalescence (Stone and Leal (1990), Yang et al. (2001)). While this study is not specifically investigating droplet coalescence, there are frequently droplet collisions very close to the breakup region of the jet that sometimes result in coalescence – especially the collision of energetic satellite drops with the larger, slower moving primary drops. Thus, when the droplet size is measured downstream from the breakup event, the droplets observed may be the product of coalescence events. Generally; the coalescence of a satellite drop with a primary drop does not significantly change the diameter of the primary drop due to the disparity in volume between them, so coalescence phenomena will only be discussed qualitatively.

3.2: Physical and Chemical Properties of Surfactants

A surfactant (often referred to as a Surface Active Agent, or SAA) is a substance whose molecules are amphiphillic, meaning that part of them have an affinity for water (hydrophilic), and another part has an affinity for organic phases (lipophilic). As a result of this duality, these molecules tend to migrate to and populate water-oil and water-gas interfaces. While surfactants come in many forms, they generally fit within 3 broad classes: Ionic, Amphoteric, and Non-ionic. Ionic surfactants are ones whose hydrophilic head group contains a salt which, upon introduction into an aqueous phase, ionizes to form either an anion (negative charge), or cation (positive charge). Anionic surfactants are the most common – most soaps, such as that made by the saponification of fats in lye, fall into this category. Ionic surfactants, due to

their electrically charged head group, create complex electrical interactions along the oil-water interface, resulting in an electrical double layer which concentrates oppositely-charged ions in the aqueous phase near the interface to balance the charge of the head group. This, in turn, causes a region of unbalanced charge in the near-interface region which can have significant effects on interfacial rheology, and is strongly affected by changes in dissolved ion concentrations in the aqueous phase.

Amphoteric surfactants have a head group which can have either a positive or negative charge, depending on the pH of the solution, or can have both charges simultaneously (Zwitterionic surfactants). These types of compounds are almost exclusively biological in nature and are very rarely used.

Non-ionic surfactants are synthetic molecules whose head group has no ionic charge, but instead are water soluble due to the presence of highly polar functional groups. They have several advantages over the other types of surfactants as they are relatively insensitive to pH and dissolved ion concentrations. Both of the surfactants used in this study are non-ionic surfactants, more specifically alcohol ethoxylates (alcohol functional groups attached to chains of ethylene oxide of various lengths and structures). Tergitol TMN-6 is a highly branched ethoxylated alcohol of proprietary chemical structure, and Triton X-100 (Octyl Phenol Ethoxylate) is a straight chain ethoxylated alcohol. Table 3.1 gives some of the relevant properties of these surfactants.

Table 3.1 – Selected physical properties of the two non-ionic surfactants utilized in this study: a) provided by manufacturer/vendor, b) determined experimentally c) From Padron (2005)

	Triton X-100	**Tergitol TMN-6**
Molecular Weight[a]	624 g/mol	543 g/mol
HLB (Hydrophilic-Lipophilic balance)[a]	13.5	13.0
Critical Micelle Concentration (CMC)[b]	2.19×10^{-4} mol/l	1.03×10^{-3} mol/l
Saturation Surface Excess Concentration (Γ_∞)[c]	2.87×10^{-6} mol/m²	2.44×10^{-6} mol/m²

3.3: Effect of Surfactants on Jet Breakup

3.3.1 Single Drop Studies

One of the first studies to investigate the effect of surfactants on droplet breakup is that of Stone and Leal (1990), where they extended their earlier work (Stone, Bentley, and Leal (1986)) on drop breakup to include insoluble surfactants. They found the inclusion of surfactants made drops harder to deform, which they attributed to the surfactant being swept towards the drop poles, resulting in Marangoni stresses. Milliken et al. (Milliken, Stone, and Leal (1993); Milliken and Leal (1994)) then expanded their studies to include viscous drops and soluble surfactants. Marangoni stresses were found to decrease with both increasing drop viscosity and surfactant solubility. Soluble surfactants were found to have a less significant effect on droplet breakup than insoluble surfactants; however the Marangoni stresses were never negligible.

Eggleton and Stebe (1998) investigated the surfactant adsorption on the deformation of drops in extensional flow. When the adsorption is kinetically controlled, the deformation of the drop decreases with increasing surfactant concentration (due to Marangoni stresses). At higher concentration, adsorption is fast enough to alleviate the Marangoni stress and the droplet remains in equilibrium with the solution.

A study of the deformation of water drops in oil in simple shear flow with non-ionic surfactants performed by Janssen, Boon, and Agterof (1994) found that the critical capillary number for breakup goes through a maximum as surfactant concentration increases, and that this maximum coincided with the concentration at which the surface dilatational modulus (defined by equation 3.9) also reached its maximum value. They further proposed the use of an 'effective' interfacial tension to correlate their data, defined by equation 3.11

$$E^{sd} = \frac{E_0}{\sqrt{1 + 2\zeta + 2\zeta^2}} \tag{3.9}$$

where E_0 and ξ are defined as

$$E_0 = \frac{d\pi}{d \ln \Gamma} \qquad \text{and} \qquad \zeta = \frac{dC}{d\Gamma}\sqrt{\frac{D_{AB}}{2\omega}} \tag{3.10a,b}$$

where π is the surface pressure, Γ is the surfactant surface concentration, C is the surfactant bulk concentration, D_{AB} is the binary diffusion coefficient, and ω is the deformation frequency.

$$\sigma_{eff}(C) = \sigma(C) + \beta E^{sd} \tag{3.11}$$

where β is an empirically derived parameter that is a function of the viscosity ratio. This relationship holds well for large droplets (~1mm) where the exchange of surfactant occurs within the diffusion layer around the drop – thus bulk convection of the surfactant can be neglected.

3.3.2 Capillary Jets and Fluid Threads

The first investigation of surfactant-covered fluid jets was the study by Anshus (1973). He theoretically studied the effect of an insoluble surfactant on the breakup rate of fluid cylinders. He found that, generally, the presence of surfactant slows the breakup of the jet. The effect is most pronounced for fluids of higher viscosity. He modeled the surfactant as a surface film, and considered the cases when this film was compressible and incompressible. He found that the incompressible case causes a much more significant decrease in breakup rate. Since the surfactant is insoluble and cannot leave the interface, his model does not take into account any of the adsorption/desorption kinetics, and local surface tension gradients are due solely to changes in geometry.

Skelland and Walker (1989) performed an experimental study of the effect of anionic, cationic, and non-ionic surfactants on the breakup of liquid jets in another immiscible liquid phase. They utilized a variety of empirical correlations to relate the jet breakup length and droplet size to the equilibrium interfacial tension of the system, as well as various hydrodynamic parameters. The data was found to follow these correlations within what the authors refer to as a “rather broad limit of accuracy”.

Craster, Matar, and Papageorgiou (2002) studied the breakup of viscous threads covered with insoluble surfactants. They utilized a one-dimensional numerical simulation, and introduced the following mass balance equation to calculate the surfactant flux from the bulk to the interface:

$$J = \Gamma_t - \frac{S_t S_z \Gamma_z}{1+S_z^2} + \frac{1}{S(1+S_z^2)^{1/2}}\left(\frac{S\Gamma(w+uS_z)}{\left(1+S_z^2\right)^{1/2}}\right)_z - D_s \frac{1}{S\left(1+S_z^2\right)^{1/2}}\left(\frac{S\Gamma_z}{\left(1+S_z^2\right)^{1/2}}\right)_z + \frac{\Gamma\left(u-wS_x\right)}{\left(1+S_z^2\right)^2}\left(\frac{1+S_z^2}{S} - S_{zz}\right) \tag{3.12}$$

Their model assumes a uniform initial concentration of surfactant, and that the jet is perfectly axisymmetric:

$$\Gamma(z,0) = \Gamma_0 \qquad \Gamma = f(z,t) \tag{3.13a,b}$$

The location of the surface is determined by the function S, which is initially a cylinder of radius r:

$$S(z,0) = r_0 \qquad r = S(z,t) \tag{3.14a,b}$$

D_S is the surface diffusion coefficient, and w and u are the velocity components in the r and z directions, such that:

$$S_t + wS_z = u \tag{3.15}$$

Equations 3.15 and 3.12 are coupled by the surface equation of state corresponding to the Langmuir isotherm:

$$\sigma = \sigma_0 + gT\Gamma_\infty \ln\left(1 + \frac{\Gamma}{\Gamma_\infty}\right) \tag{3.16}$$

where σ_0 is the interfacial tension of a clean interface, g is the gas constant, T is the absolute temperature, and Γ_∞ is the maximum surface concentration of surfactant the surface can accommodate. They showed that the size of satellite droplets decreased with increasing initial surfactant concentration, which they attributed to "interface rigidification". They also proposed the following useful relationship for the effective interfacial tension:

$$\sigma_{eff} = 1 + \beta \ln\left(1 - \Gamma_{eff}\right) \tag{3.17}$$

where β and Γ_{eff} are defined as:

$$\beta = \frac{gT\Gamma_\infty}{\sigma_0} \qquad \Gamma_{eff} = \frac{\int_{-z_{\min}}^{z_{\min}} S\Gamma dz}{\left(3\int_{-z_{\min}}^{z_{\min}} S^2 dz\right)^{2/3}} \tag{3.18a,b}$$

Timmermans and Lister (2002) present a very similar one-dimensional numerical analysis of a surfactant-covered liquid thread. They find that if the surfactant effects a critical value of the dimensionless surface tension gradient, β, the system transitions from extensionally dominated inertial flow to shear-dominated viscous flow. They find that the presence of surfactant has no effect on the minimum wavelength for instability, and suggested that the Frumpkin surface equation of state (equation 3.19) would be more appropriate for the surfactant-laden jet than the more commonly used Langmuir isotherm.

$$\sigma = \sigma_0 + RT\Gamma_\infty \ln\left(\frac{\Gamma_\infty - \Gamma}{\Gamma_\infty - \Gamma_0}\right) \tag{3.19}$$

Jin, Gupta, and Stebe (2006) studied the evolution of individual buoyant viscous drops injected into a viscous fluid in the presence of surfactants. They found these droplets form by the rapid formation and pinching of the neck of the droplet. Upon the introduction of a soluble surfactant, they found that significant accumulation of surfactant in the neck region due to the rapid reduction in surface area caused the surfactant molecules to 'pile up' in these regions, meaning that the breakup is dominated by the kinetics of the surfactant adsorption/desorption process. If the surfactant is able to desorb back into the bulk rapidly enough, no Marangoni stresses are observed and the droplet breaks up similarly to a surfactant-free droplet. If the surfactant desorption step is rate-limiting, then droplets can form secondary necks or fail to neck at all due to Marangoni stresses opposing the necking mechanism. A series of numerical simulations across the parameter space were performed to construct a phase diagram of necking behaviour, reproduced as Figure 3.4

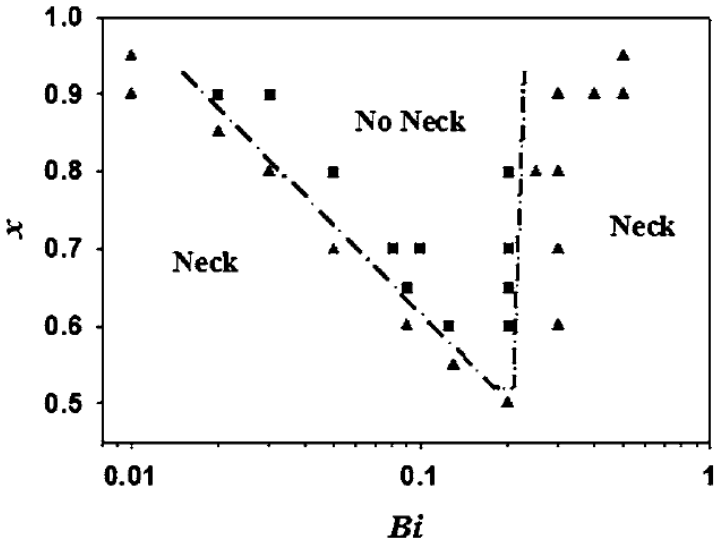

Figure 3.4 – Phase diagram of necking and non-necking drops as a function of equilibrium surface coverage x, and the Biot number, Bi, reproduced from Jin, Gupta & Stebe (2006)

The Biot number describes the rate of surfactant desorption to surface dilatation. Therefore, at low Bi, the surfactant desorbs very slowly, and so no Marangoni stresses are formed as the surface behaves as if it were a clean interface of lower interfacial tension. At high Bi, the surfactant desorbs quickly enough to cause negligible Marangoni stresses, and only at moderate Bi are sufficient Marangoni stresses created to oppose necking. Interestingly, the higher limit of the Bi is found to be independent of equilibrium surface coverage, while the lower limit is a linear function of x.

McGough & Basaran (2006) numerically studied the breakup of a surfactant-covered liquid jet utilizing the slender-jet model. They observed the formation of thin fluid threads between droplets, which can lead to the formation of satellite droplets. Upon further investigation, they also observed smaller fluid threads between the satellite

droplet and the primary droplet, and found that the geometry and breakup mechanism of these threads were self-similar and approaches the Eggers (1997) solution for clean interfaces. Figure 3.5, reproduced from their paper, shows the series of progressively smaller fluid threads and how each produces a successively smaller satellite droplet.

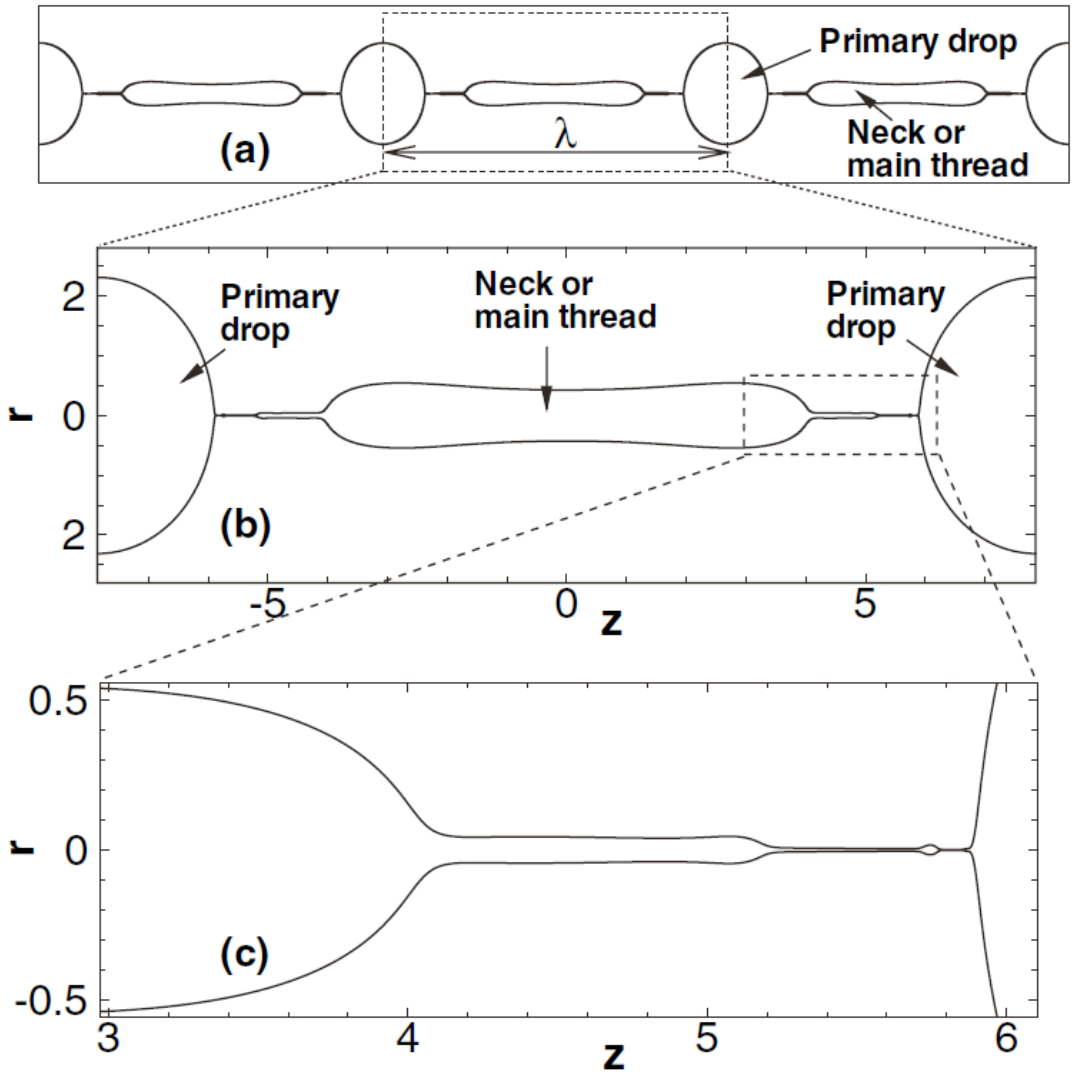

Figure 3.5 – Shape of a surfactant-covered jet just before breakup, showing the existence of several different length scales of fluid threads, each producing a series of successively smaller satellite droplets. Reproduced from McGough and Basaran (2006)

Xue et al (2008) studied the effect of surfactant-laden liquid jet breakup in shear-thinning fluids. A Carreau fluid covered with an insoluble surfactant and studied using a two-dimensional finite element method with adaptive meshing. Their simulations predict a strong synergistic interaction between the non-Newtonian fluid and surfactant effects. They make recommendations to suppress the creation of satellite droplets during applications such as inkjet printing, spray drying, and crop spraying, which they believe will decrease waste and environmental pollution.

3.4: Effect of Surfactants on Tensiometry

Surfactant kinetic effects can be measured using time-dependent tensiometry experiments. By measuring the interfacial tension as a function of time, the long time limit of the Ward-Tordai equation (Equation 3.20) can be used to estimate the diffusion coefficient of the surfactant in that system (Eastoe et al. (1997)).

$$\sigma(t)_{t\to\infty} = \sigma_{eq} + \frac{RT\Gamma_\infty^2}{2C}\sqrt{\frac{\pi}{D_s t}} \tag{3.20}$$

Where σ_{eq} is the equilibrium surface/interfacial tension, T is the temperature, R is the gas constant, Γ_∞ is the equilibrium surface excess concentration, C is the bulk surfactant concentration, D_s is the Fickian diffusion coefficient, and t is the time, starting from when the interfacial area was created.

Figure 3.6, reproduced from Padron (2005), shows a fit of Equation 3.20 to surface tension measurements for an aqueous solution of Triton X-100 surfactant in air over a

time period of several minutes, showing that as surfactants diffuse to the interface, the surface tension asymptotically approaches the equilibrium value.

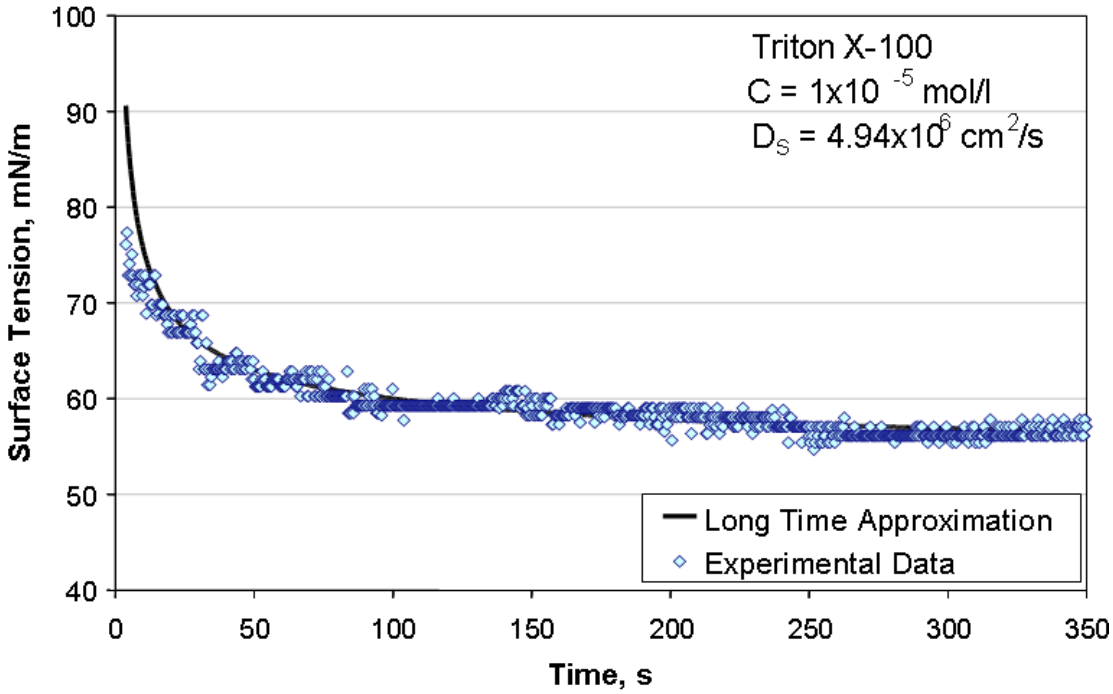

Figure 3.6 – Change in surface tension over time due to surfactant diffusion, reproduced from Padron (2005)

Another important measurable quantity related to surfactant chemistry is the Critical Micelle Concentration. By measuring the equilibrium surface tension of a surfactant solution with another phase, the CMC can be determined by finding the concentration at which addition of surfactant no longer decreases σ (since these additional surfactant molecules simply form micelles). Fitting the plot of concentration vs time to the Langmuir - von Szyszkowski equation (equation 3.21), allows one to calculate Γ_∞ needed in Equation 3.20 above. It also allows the value of the Langmuir constant (a_L) to be identified. Knowledge of a_L and Γ_∞ allows use of the Langmuir adsorption isotherm to characterize the interfaces rheological properties.

$$\sigma_{eq} = \sigma_0 - \Gamma_\infty RT \cdot \ln\left(1 + \frac{C}{a_L}\right) \tag{3.21}$$

Figure 3.7, reproduced from Padron (2005), shows the fitting of Equation 3.21 to the concentration-σ curves for 3 different non-ionic surfactants. The CMC is taken to be the intersection point of the linear decay line and the constant interfacial/surface tension line. This method was utilized in this study to determine the properties of the two surfactants used, shown above in Table 3.1.

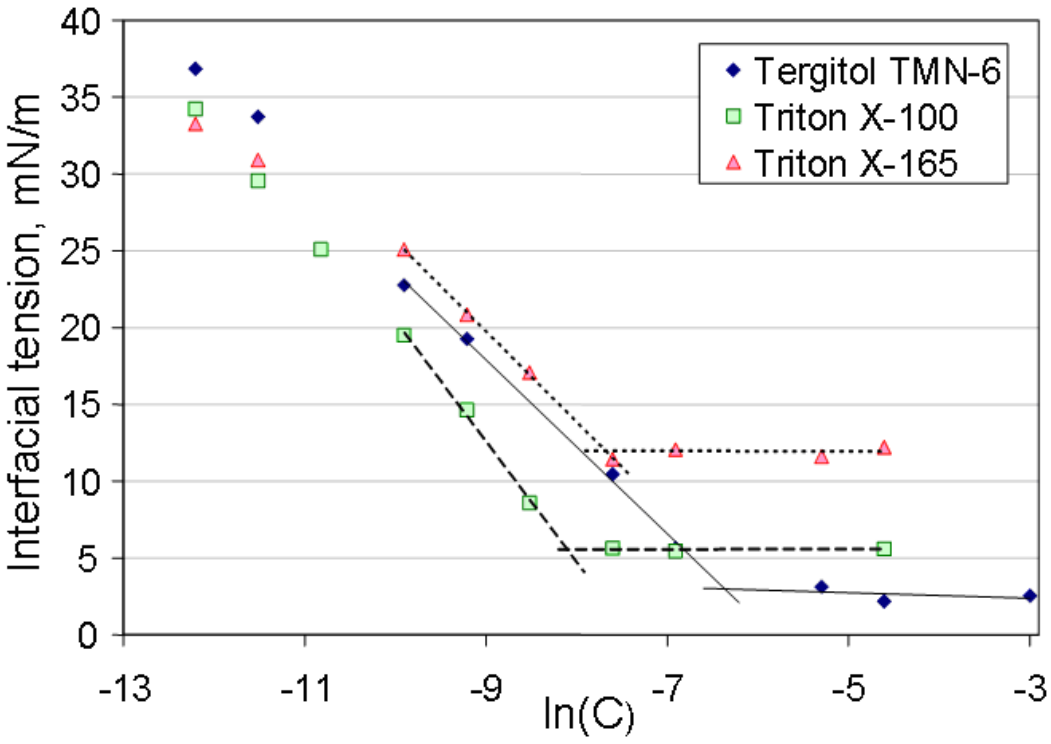

Figure 3.7 – Determination of CMC, a_L, and Γ_∞ using Equation 3.21, reproduced from Padron (2005)

Chapter 4: Methods and Models

4.1: Tensiometry

4.1.1 General Experimental Method

Dynamic and static surface/interfacial tension measurements were performed using the pendant drop technique. For this purpose a cuvette constructed from 2”x3” glass microscope slides was filled with the desired ambient fluid (or left empty for surface tension), and a syringe filled with the droplet phase fluid was fitted to a needle with either a straight or hooked end, to accommodate either positive or negative buoyancy. The entire apparatus was placed atop a pneumatic vibration isolation table. In the case of static measurements, droplets were formed manually, and then the system was left to come to equilibrium for several minutes. After the system had equilibrated, several images were acquired on the hanging drop using a high resolution CCD camera. The drop was then ejected and a fresh drop formed. This process was repeated several times to ensure good results. Figure 4.1 shows a schematic diagram of this procedure.

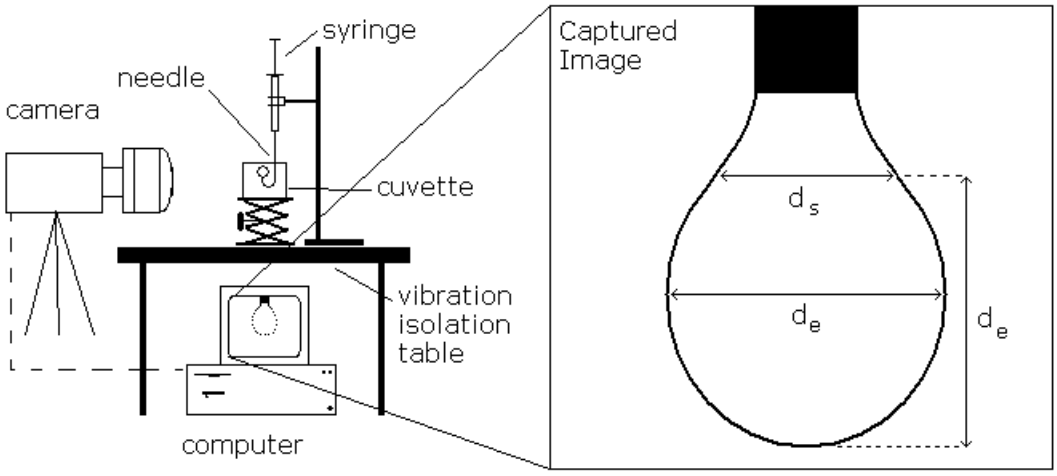

Figure 4.1 – Schematic diagram of Pendant Drop apparatus

For dynamic surface tension measurements, droplets were formed as quickly as possible, and the CCD camera was set to automatically acquire images at regular intervals as soon as the drop had stopped noticeably oscillating (due to the vibrations introduced by touching the syringe). In this manner, the change in surface tension with time could be measured; starting approximately 20-30 seconds after the droplet was formed.

4.1.2 Image Processing

Images were acquired from the CCD camera and stored on the computer's hard drive as .tiff images. These images were analyzed using the software package ImageJ. While the detailed computer algorithm is given in the appendices, the general steps performed are as follows (see Figure 4.2 for sample images):

1. Images are opened as a stack and cropped to remove extraneous areas. Images are also rotated if necessary to ensure proper orientation of the droplet
2. A bandpass filter is used to eliminate gradients in the images due to uneven lighting
3. Images are converted into binary images (black/white – no gray scale values) using thresholding
4. Binary images are then converted into data files containing the X,Y coordinates of each black pixel
5. Data files are processed using a MATLAB algorithm which calculates the quantities De and Ds from Equation 2.38, as well as determining the scale of the image using the width of the capillary bore at the top of the image
6. Interfacial tension values are then automatically calculated using 2.41
7. This process is repeated for several hundred images to determine the average value

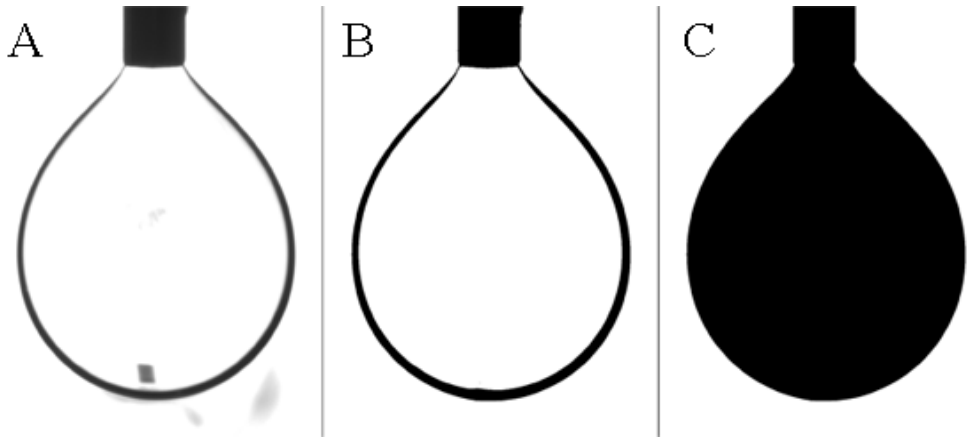

Figure 4.2 – Example images during image processing – A) original image as captured by the camera, B) image after filtering and thresholding, C) final binary image sent to MATLAB

4.2: Breakup of Viscous Jets

4.2.1 General Experimental Method

Clean and surfactant-laden water jets were injected into otherwise still air. Three capillaries were used to form the jets in this study, having inner diameters of 0.41 mm, 0.60 mm, and 0.84 mm, respectively. The capillaries were all 51mm long; enough to assure fully developed laminar flow profiles at the capillary tip. A one liter fluid reservoir, maintained at constant pressure through the use of a regulated nitrogen gas cylinder, was used to initiate the flow (see Figure 4.3). The flow rate of the jet phase was controlled using a needle valve and monitored using a rotameter. Flow rates were varied from 5-30 ml/min, corresponding to Reynolds numbers from 20-2000, depending on the capillary and fluid in use. The entire apparatus rests on top of a pneumatic vibration isolation table to prevent ambient vibrations from influencing the jet breakup experiments.

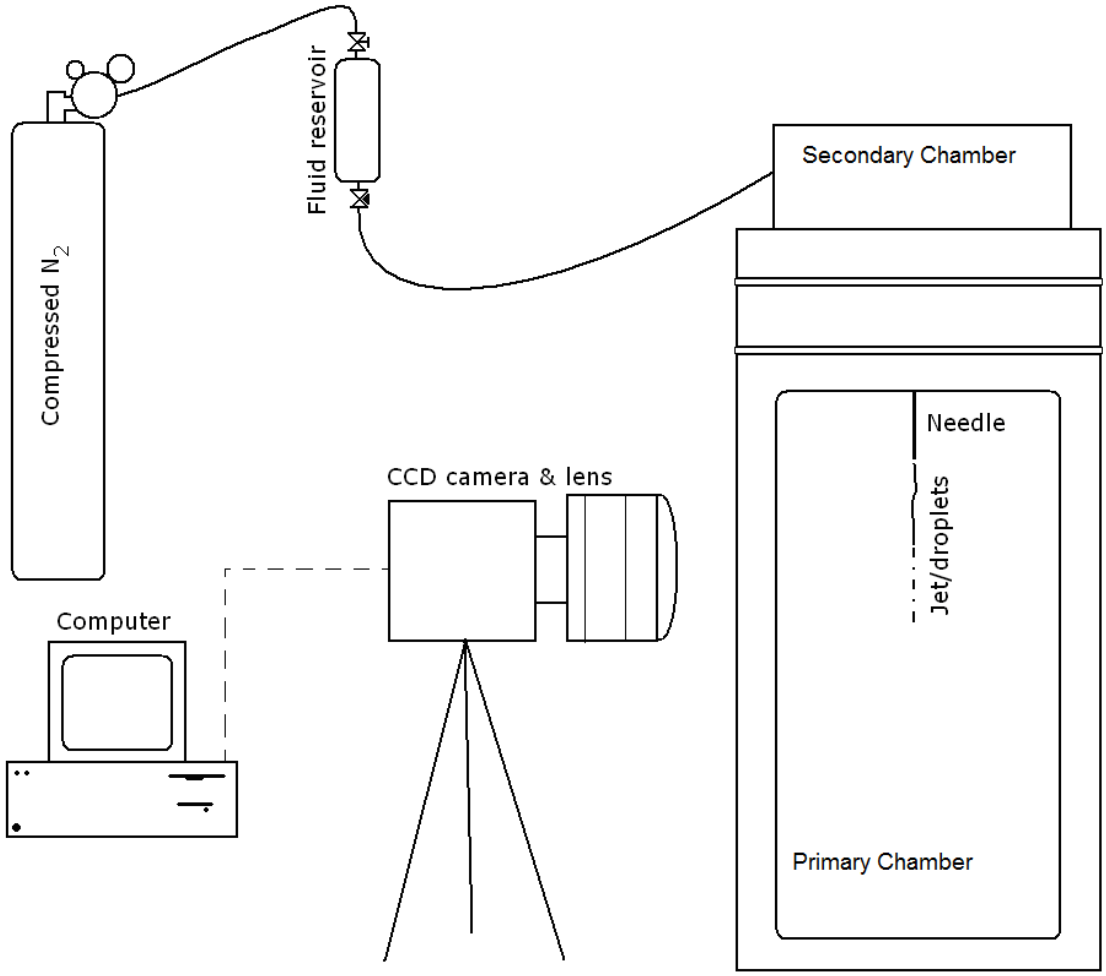

Figure 4.3 – Schematic diagram of experimental apparatus

Two distinct CCD cameras were used to image droplets. A low frame rate (30 fps), high resolution camera (Pulnix TM-1405GE) was used to measure breakup length and to quantify droplet population statistics. A high frame rate (up to 10,000 fps), moderate resolution camera (VRI Phantom V9) was employed to observe detailed breakup phenomena. A variety of Nikkor SLR lenses and extension bellows systems were used in conjunction with both of these cameras. An automated image processing algorithm (using a combination of ImageJ and MATLAB) was used to acquire droplet geometry and population statistics. See Figure 4.3 for a detailed

schematic diagram of the experimental apparatus. A set of mirrors set at complementary 45° angles were optionally set inside the jet chamber to allow the jet to be imaged in two orthogonal planes simultaneously. This allows for discrimination between prolate and oblate droplets to be made and the droplet volume to be estimated from a single frame. An automated algorithm is employed in MATLAB to perform this calculation and report the equivalent spherical diameter (ESD) of the droplets. A similar automated algorithm is utilized to calculate the breakup length (L_b). Satellite drop sizes were calculated by using a second set of images at higher magnification and are treated in a similar manner to the primary droplet.

For oil-in-water experiments, the test cell was fitted with liquid-tight windows and filled completely with deionized water (or aqueous surfactant solutions). The entire experimental apparatus was inverted, such that the needle was at the bottom of the cell. The fluid reservoir was still filled with deionized water in order to maintain the calibration of the rotameter, and the secondary chamber at the bottom of the test cell was filled with the desired grade of silicone oil. In this manner, water flowed from the fluid reservoir, through the metering valve and flowmeter into the secondary chamber, where it displaced oil and slowly filled the secondary chamber. The displaced oil was forced through the needle, creating an oil jet in the upper water-filled primary chamber. An overflow keeps the cell chamber at constant pressure. The entire apparatus rests on top of a pneumatic vibration isolation table to prevent ambient vibrations from influencing the jet breakup experiments.

Silicone oils (Dow Corning 200 Fluid) of viscosity grades between 5 and 200 cSt were used as a model oil in this study. The viscosity of these oils was verified using a cone and plate viscometer (TA Instruments AR2000EX). The interfacial tension of the oil-water system was found to be independent of viscosity grade (see Padron (2005)).

For water-in-oil experiments, the primary chamber was filled with 10cSt Dow corning 200 fluid, and the secondary chamber and fluid reservoir was filled with deionized water or aqueous surfactant solution. The apparatus was placed in downward-jetting orientation so the water jet flowed from the top of the cell to the bottom.

Triton X-100 and Tergitol TMN-6 surfactants were optionally added to the aqueous phase in all of these experiments. Both of these surfactants are insoluble in silicone oils, therefore, regardless of orientation, the surfactant must diffuse through the aqueous phase to the interface in all cases. This means that in the case of water-in-air or water-in-oil jets, the surfactant is present in the jet phase, while in the case of oil-in-water jets the surfactant is present in the continuous phase.

4.2.2 Image Processing

Similar to the processing of pendant drop experiments, images were acquired from the CCD camera and stored on the computer's hard drive as .tiff images. These images were analyzed using the software package ImageJ. The detailed computer

algorithms are given in an appendix; however, the general procedure is as follows (See Figure 4.5):

Breakup Length

1. Images are opened as a stack and cropped to remove extraneous areas. Images are also rotated if necessary to ensure proper orientation of the jet
2. A bandpass filter is used to eliminate gradients in the images due to uneven lighting
3. Images are converted into binary images (black/white – no gray scale values) using thresholding
4. The total length (in pixels) of the largest dark object (the capillary plus the contiguous liquid jet) is reported by the ImageJ software
5. The length of the capillary is subtracted to find the total breakup length
6. The known width of the capillary bore is used to convert the measurements from pixel units to dimensional units (mm)
7. This process is repeated for several hundred images to determine the mean and variance of the breakup length

Droplet Size

1. Images are opened as a stack and cropped to remove extraneous areas. Images are also rotated if necessary to ensure proper orientation of the jet

2. A bandpass filter is used to eliminate gradients in the images due to uneven lighting
3. Images are converted into binary images (black/white – no gray scale values) using thresholding
4. Watersheding is used to separate overlapping droplets
5. The ImageJ software automatically reports the area and dimensions of each droplet (perimeter, major and minor axis diameters, etc.) in pixel units
6. Pixel units are converted to dimensional units using a calibration image acquired using the same magnification
7. This process is repeated for several hundred images and the results combined to calculate the droplet size distribution

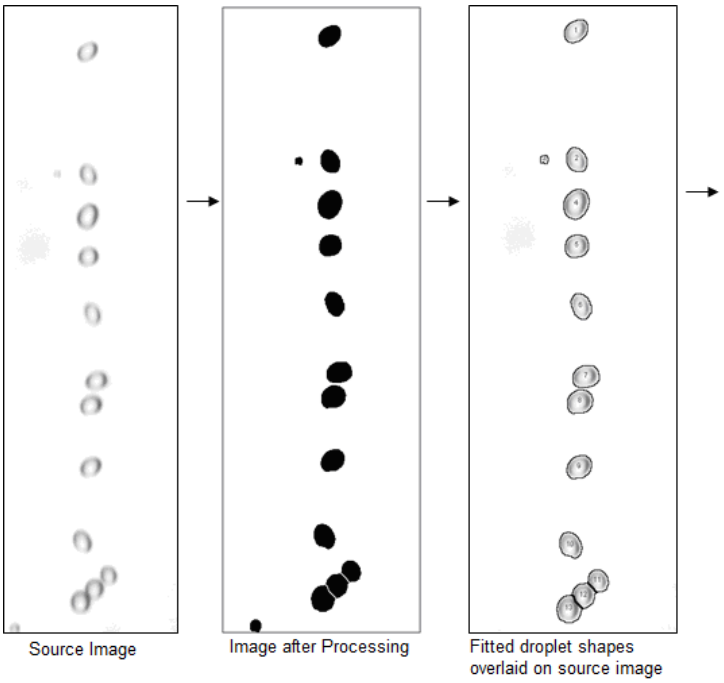

	Area (mm²)	Major (mm)	Minor (mm)
1	0.7049	1.0997	0.816
2	0.6667	1.0459	0.8116
3	0.0948	0.3539	0.3411
4	1.014	1.2763	1.0116
5	0.7368	1.0174	0.9221
6	0.6801	1.1042	0.7842
7	0.8192	1.1431	0.9125
8	0.8326	1.1119	0.9534
9	0.7749	1.1131	0.8865
10	0.7533	1.1168	0.8588
11	0.5822	0.9546	0.7766
12	0.6976	1.0096	0.8798
13	0.8553	1.1265	0.9667

Figure 4.4 – Illustration of image processing pipeline for finding droplet size distribution. Note that droplets touching the image edges are discarded

4.2.3 Determination of Droplet Volume

For droplets in an inviscid continuous medium (eg, water-in-air jets), there is insufficient viscous drag to damp out surface oscillations in the time period between jet breakup and droplet imaging, as is the case when the continuous phase is viscous. Therefore, the droplet may not be axisymmetric when imaged. From a single imaging plane, it is not possible to determine the 3-dimensional shape of the droplet, and therefore its volume cannot be found.

In order to resolve this problem, these droplets are imaged from two orthogonal planes using the mirror arrangement described in Section 4.2.1. The computer algorithm then processes both images simultaneously, and utilizing their relative dimensions and positions in the images, matches the droplets in one image to the corresponding droplet in the other image. Based on the droplet projections in the two imaging planes, it is possible to estimate the droplet volume, since the droplets are roughly spheroidal. This is done by comparing the major and minor axis of the droplet projections, using these values to determine the axis of symmetry of the droplet, and then calculating the droplet volume. Droplets whose dimensions are not spheroidal or droplets which cannot be matched with a mate from the other image (usually because the droplet is obscured by another droplet) are rejected. From the droplet volume, the equivalent spherical diameter is calculated using equation 4.1:

$$d_{es} = 2\left(\frac{3V}{4\pi}\right)^{1/3} \tag{4.1}$$

where V is the droplet volume. The individual equivalent spherical diameter values are then used to calculate the mean diameter (usually the Sauter mean diameter – equation 5.1), and any other relevant statistics pertaining to the droplet size distribution.

4.3: A Semi-Empirical Model for predicting Jet Breakup length in the presence of surfactants

In this section, a semi-empirical model relating the length of a surfactant laden jet to the length of a clean jet with the same hydrodynamic conditions is proposed. Starting by non-dimensionalizing the linear stability model equations proposed by Das (1997), we arrive at Equations 4.2 and 4.3:

$$w = \eta(1-\eta^2)\frac{I_1(\eta)}{I_0(\eta)} - 3\eta^2 Oh\, w \tag{4.2}$$

$$L_b^* = \frac{We^{1/2}}{2w}\ln\left(\frac{r_0}{\delta_0}\right) \tag{4.3}$$

If we assume that δ_0, the initial perturbation on the jet surface responsible for its destabilization, happens rapidly after the jet fluid interfaces come into contact, we can approximate that this value should be independent of the surfactant concentration of

the system, since the initial perturbation will occur prior to any surfactant interacting with the jet interface.

Therefore, we may relate the breakup length of a surfactant laden jet to that of a clean jet by solving for δ_0.

$$\delta_0 = r_0 e^{\frac{-2 L_b^* w}{We^{1/2}}} \tag{4.4}$$

$$r_0 e^{\frac{-2 L_{b,clean}^* w_{clean}}{We_{clean}^{1/2}}} = r_0 e^{\frac{-2 L_{b,surf}^* w_{surf}}{We_{surf}^{1/2}}} \tag{4.5}$$

Solving for L_b^* and eliminating common terms, we arrive at the following expression

$$L_{b,surf}^* = L_{b,clean}^* \frac{w_{clean}}{w_{surf}} \sqrt{\frac{We_{surf}}{We_{clean}}} \tag{4.6}$$

Equation 4.6 is the general case for our model. For a jet of particular nozzle geometry and velocity, the elongation caused by surfactant adsorption is proportional to the growth rate of the instabilities and the square root of the Weber number.

Equation 4.6 is mechanistic in the sense that no empirical parameters are needed to define it, although it is derived from a first-order approximation of the equations of fluid motion. However, in order to utilize this model, we require a method for estimating the interfacial tension as a function of interfacial age in order to determine w_{surf} and We_{surf}. This results in an empirical component to the model as the rate of change of the interfacial tension with time must be determined empirically.

Ward and Tordai (1946) derived the following expression for the Surface concentration of surfactant with respect to time:

$$\Gamma(t) = \sqrt{\frac{D_{AB}}{\pi}} \cdot \left[2C_0\sqrt{t} - \int_0^t \frac{C(0,\tau)}{\sqrt{t-\tau}} d\tau \right] \tag{4.7}$$

Where C(0,t) is the sub-surface concentration. The difficulty with this approach is that it contains the instantaneous sub-surface concentration, and as such must be solved via numerical integration. By using a suitable absorption isotherm as a boundary condition, we can derive both a short-time and a long-time asymptotic solution, both of which can be solved analytically. The short-time approximation is given by equation 4.8, and the long-time approximation was given above as equation 3.20.

$$\sigma(t)_{t\to 0} = \sigma_0 - 2nRTC_0\sqrt{\frac{D_{AB}t}{\pi}} \tag{4.8}$$

The short-time approximation utilizes the initial ('clean') interfacial tension as its boundary condition and predicts the decrease as surfactant is added, while the long-time approximation uses the equilibrium interfacial tension as its boundary condition and predicts the interfacial tension for a less saturated system. Both solutions diverge from measured values when extrapolated far from their initial conditions. Since we are most interested in situations where the interfacial tension deviates significantly from the initial 'clean' value, the long-time approximation is more appropriate. As seen in figure 3.6, the long-time approximation gives excellent agreement with measured values once the interfacial tension decreases by ~10% from its initial value. Also from figure 3.6, we can see that for very short times, the 1/t term in the equation causes the predicted interfacial tension to tend toward infinity. However, from our

experimental observations we know that at short diffusion times, the interface is essentially in the 'clean' state, and therefore for short times the 'clean' interface value for σ is used whenever a value larger than σ_0 is calculated. Although we could perform a piecewise solution where the short-time approximation was used for these conditions, we have observed experimentally that for these short times there is no significant effect of surfactant diffusion on the jet breakup. Therefore this step is unnecessary and the long-time approximation solution is sufficient for the model.

This approach requires the knowledge of the surfactant's diffusivity in that particular medium, as well as the surface excess concentration and Langmuir Constant. These quantities can be determined from static and dynamic tensiometry experiments (as discussed in Chapter 3) and have been determined by Padron (2005) for the aqueous Triton X-100/10 cSt silicone oil system, shown in Table 4.1.

Table 4.1 – Saturation Surface Excess Concentration (Γ_∞), Langmuir Constant (a_L) and Molecular diffusivity (D_{AB}) for Triton X-100 at the Silicone Oil-Water interface

Surfactant	Γ_∞	a_L	D_{AB}
Triton X-100	3.09×10^{-6} mol/m²	1.50×10^{-6} mol/l	5.02×10^{-10} m²/s

When calculating the solution, an initial estimate of the breakup time of 110% of the breakup time for a clean system is used. The value of Oh_{surf} allows for the calculation of w_{surf}. Utilizing the model, we are able to calculate an estimate for the jet breakup length. Since the breakup length and breakup time are proportional, the solution is iterative – with each subsequent iteration, the estimated breakup time is refined using the calculated breakup length, and new values of w and We calculated, leading to a

refined value of breakup length. This is repeated until convergence is achieved. The algorithm converges rapidly, generally converging to within 0.01% after 4-5 iterations.

Chapter 5: Water-Air Jets

5.1: Experimental Results

5.1.1 Clean (Surfactant Free) water-in-air jets

In order to validate our experimental methods, a series of tests using a 'clean' system – e.g. no surfactants present – was performed. In these tests, jets of water were ejected into otherwise quiescent air. Jet velocity and capillary diameter were varied to investigate a wide range of Reynolds numbers. As the water jets into air were primarily used as proof-of-concept and preliminary testing for the later liquid-liquid systems, more rigorous results will be found in the liquid-liquid systems, seen in Chapter 6.

Figure 5.1 shows a plot of dimensionless drop size vs. Reynolds number. Reynolds number was varied by varying the jet flow rate from 10-30 ml/min, and also by varying the capillary diameter between 0.41mm and 0.84 mm. This resulted in a range of Reynolds numbers of between 200 and 2000, based on the capillary diameter.

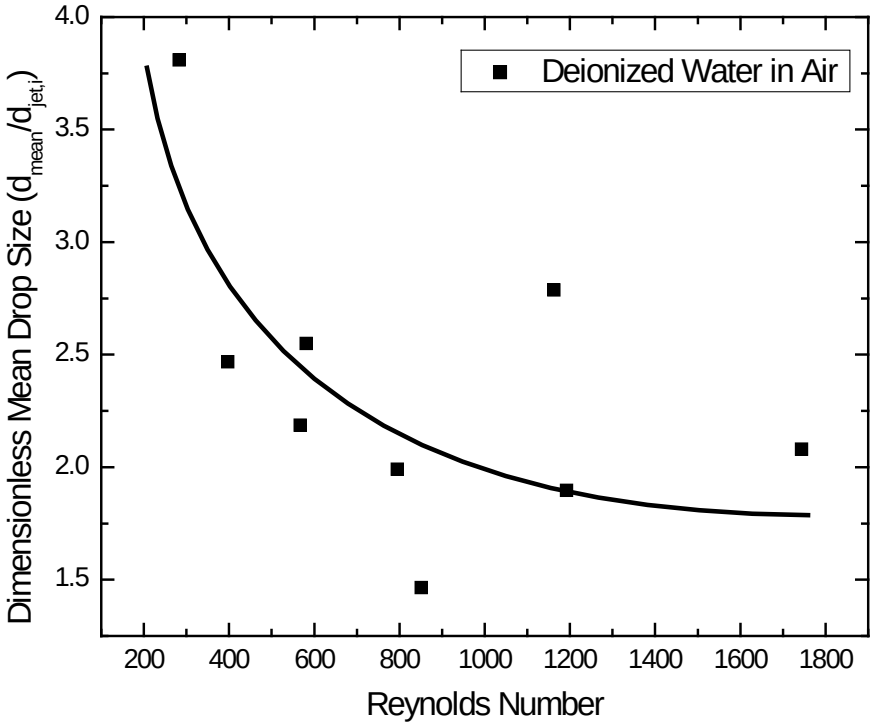

Figure 5.1 – Effect of Reynolds number on Dimensionless Mean Drop Size (the simple number mean), normalized by the initial jet diameter. The solid line indicates the data`s trend. Both primary and satellite droplets (if any) are included in the mean.

Another way to describe the data is with the Sauter Mean Diameter, d_{32}.

$$d_{32} = \frac{\sum d_i^3}{\sum d_i^2} \tag{5.1}$$

This quantity removes the influence of small drops, biasing the mean toward the primary droplets. d_{32} is also rendered dimensionless by normalizing by the initial jet diameter. Figure 5.2 shows the same data as in Figure 5.1, but instead shows the Sauter mean diameter instead of number mean (or simple mean) diameter.

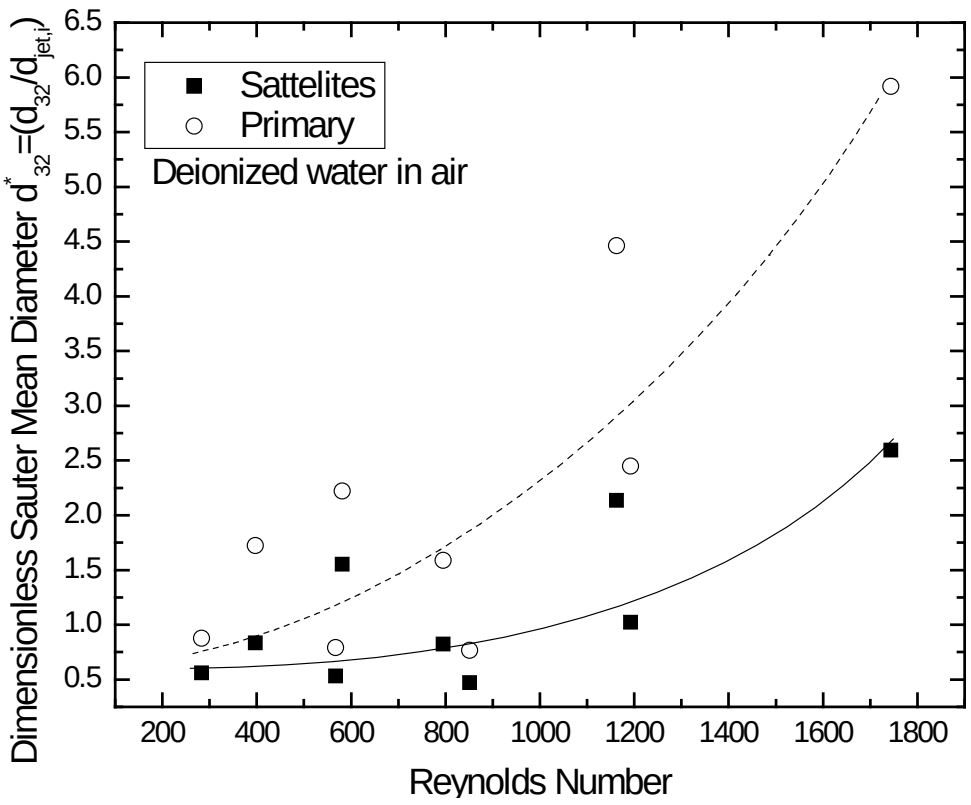

Figure 5.2 – Plot of d_{32}^{*} vs. Re. The solid and dashed lines indicate the trends of the satellite and primary droplets, respectively. A minimum of 1000 measurements were averaged for each condition

The other relevant quantity measured is the breakup length. For the purposes of this study, the breakup length was taken to be the longest contiguous fluid thread. Since images are captured instantaneously, the breakup length measured varies within the longest dominant wavelength, leading to a distribution of measurements. Error bars shown in the plot indicate the standard deviation of the measurements. Figure 5.3 shows the variation in dimensionless breakup length (normalized with initial jet diameter) with Reynolds number.

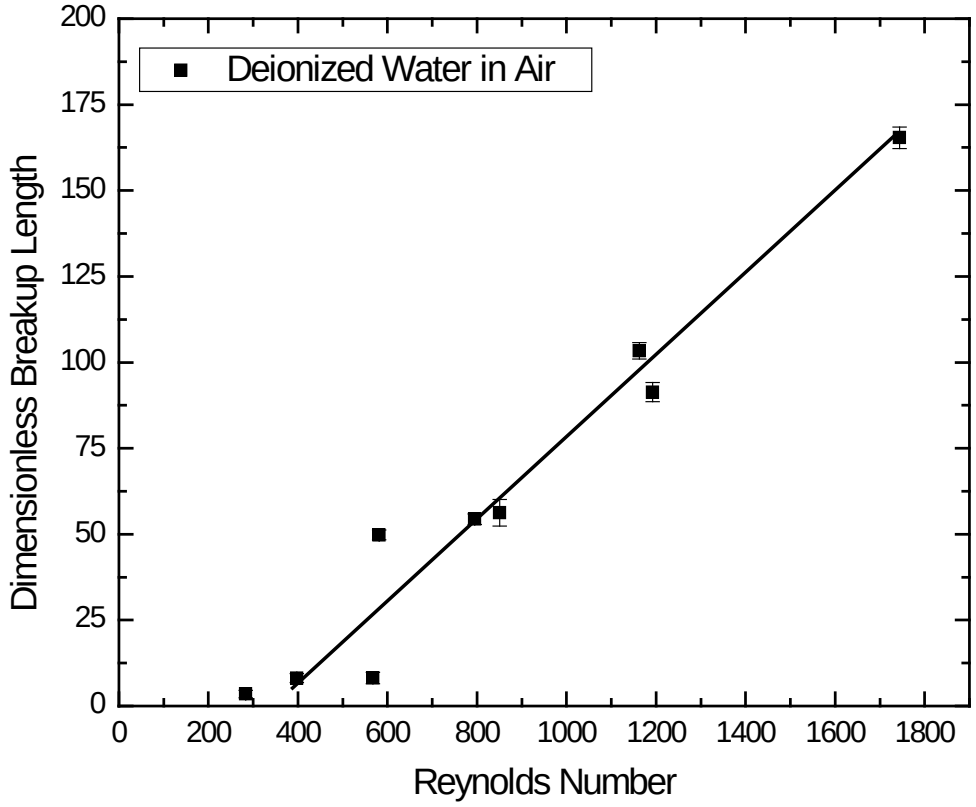

Figure 5.3 – Plot of L_b^* vs. Re for breakup of a jet of deionized water in air

5.1.2 Jets of aqueous surfactant solutions into air

The second set of experiments included varying the concentration and type of surfactant added to the system. The same flow conditions as above were employed. Surfactant concentration was varied from zero surfactant (pure deionized water) to 10 times the Critical Micelle Concentration (CMC). The CMCs of the two surfactants differ by approximately one order of magnitude (See Table 3.1), however their effectiveness scales with their concentration relative to the CMC, and as such their concentrations will be normalized by the CMC, so that more meaningful comparisons may be made.

Figure 5.4 shows the effect of Reynolds number of the dimensionless Sauter mean diameter for a variety of surfactant concentrations. Sauter mean diameter was calculated from the equivalent spherical diameter measurements, as discussed in Chapter 4.

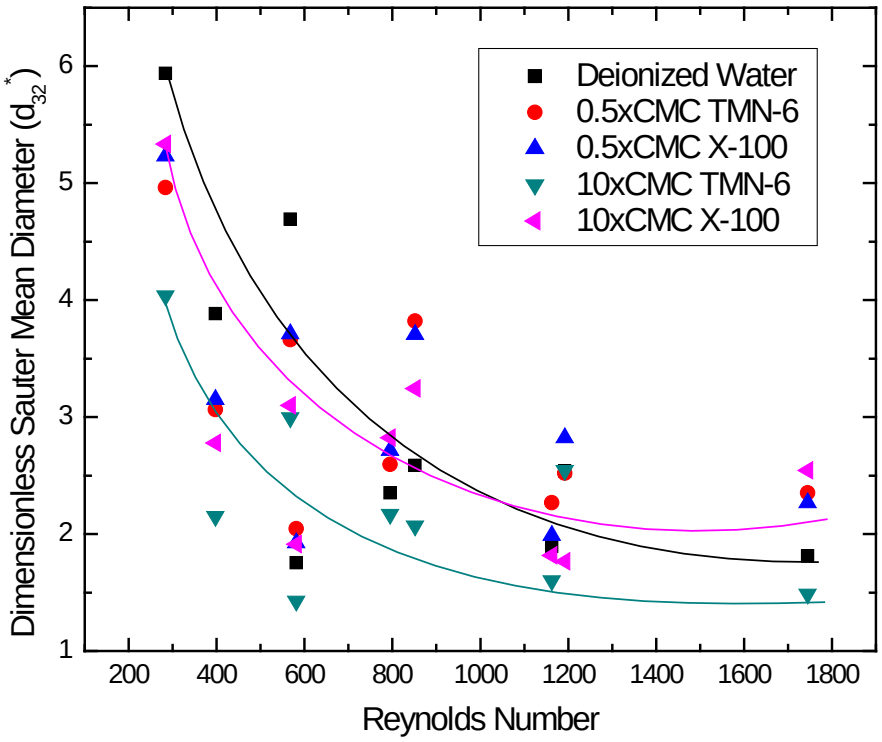

Figure 5.4 – Effect of Reynolds number on d_{32}^* for water jets into air at various surfactant concentrations. Trend lines for selected data sets are included (trend line colours correspond to data point colours)

Figure 5.5 shows the effect of surfactants on the dimensionless breakup length of the jets, for a selection of surfactant concentrations.

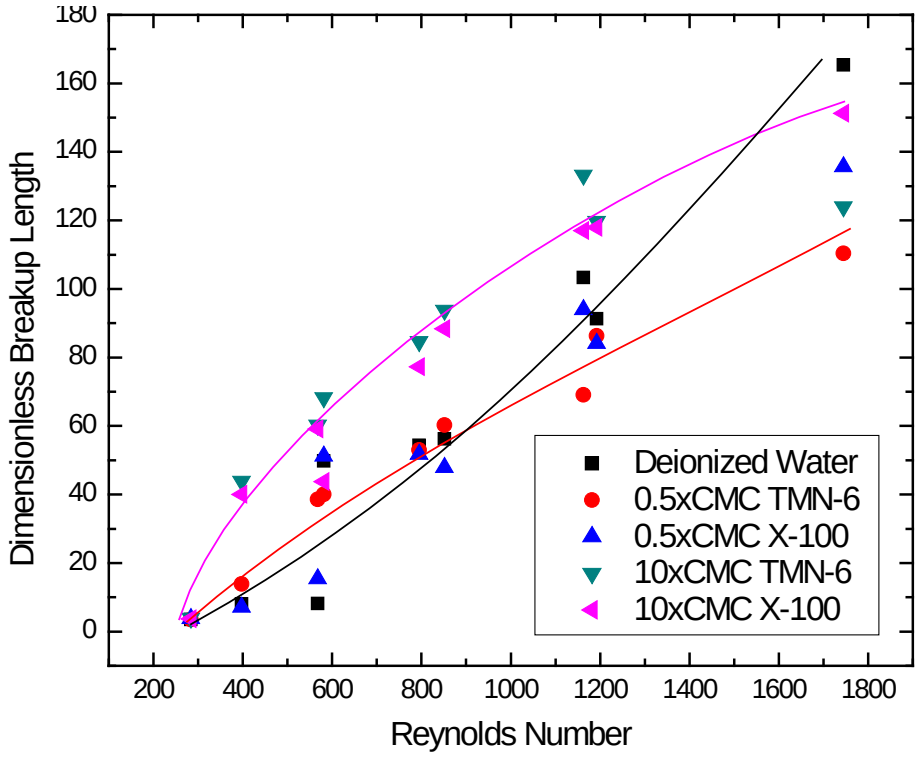

Figure 5.5 – Plot of L_b^* vs. Reynolds Number for water jets into air at various surfactant concentrations. Trend Lines follow data point colours.

In order to more easily observe the effect of surfactant concentration on the measured quantities, drop size and breakup length are plotted versus surfactant concentration. Sample results are shown in Figure 5.6 and Figure 5.7.

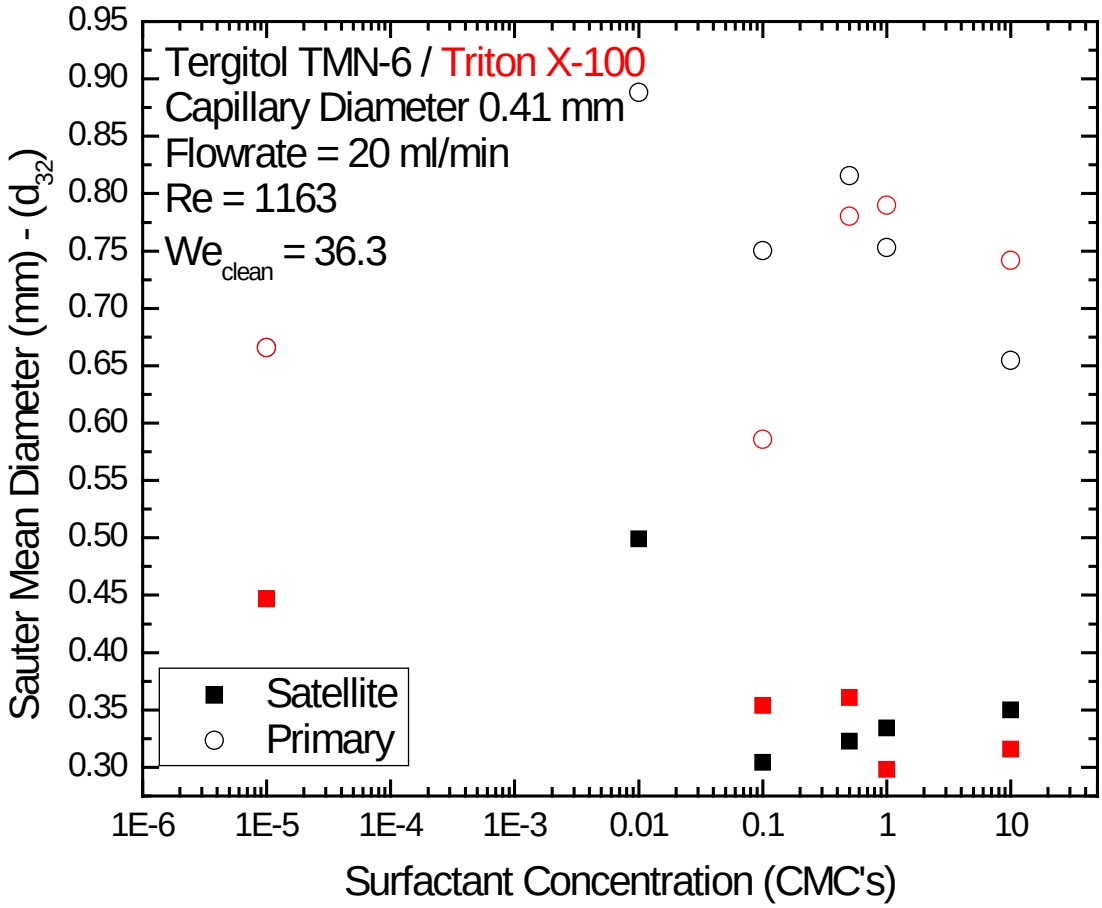

Figure 5.6 – Plot of d_{32}^{*} vs. Surfactant Concentration. Open symbols indicate primary drops, closed symbols indicate satellite drops. Red points correspond to Triton X-100 solutions, while black points correspond to Tergitol TMN-6 solutions.

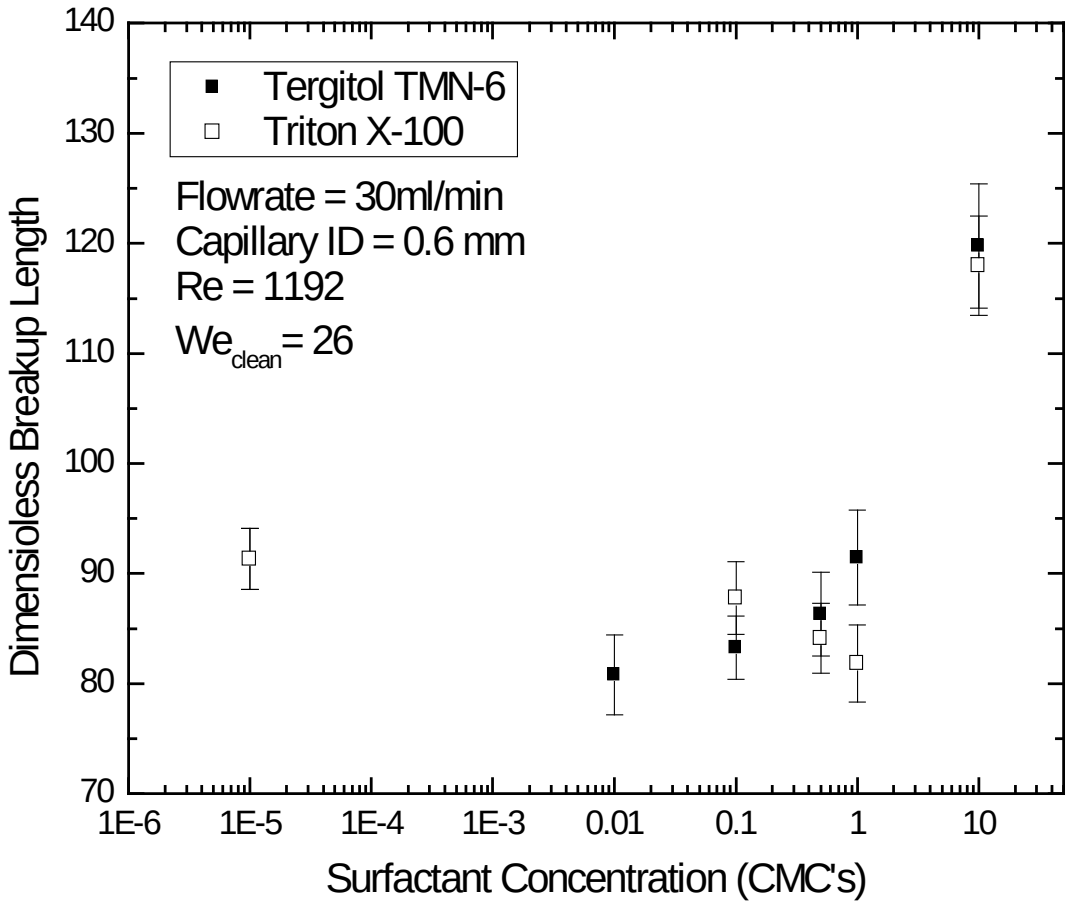

Figure 5.7 – Plot of L_b^* vs. Surfactant Concentration. Open symbols correspond to Triton X-100 solutions, while closed symbols correspond to Tergitol TMN-6 solutions.

Complete results are presented below. Figures are grouped either by experiments using the same capillary, or by experiments having the same flow rate. Figure 5.8 shows the dimensionless breakup length as a function of surfactant concentration with experiments grouped by capillary diameter. In order to directly compare the two different surfactants, surfactant concentration is expressed in units of CMCs (a dimensionless parameter). Figure 5.9 shows this same data again, this time grouped by flow rate.

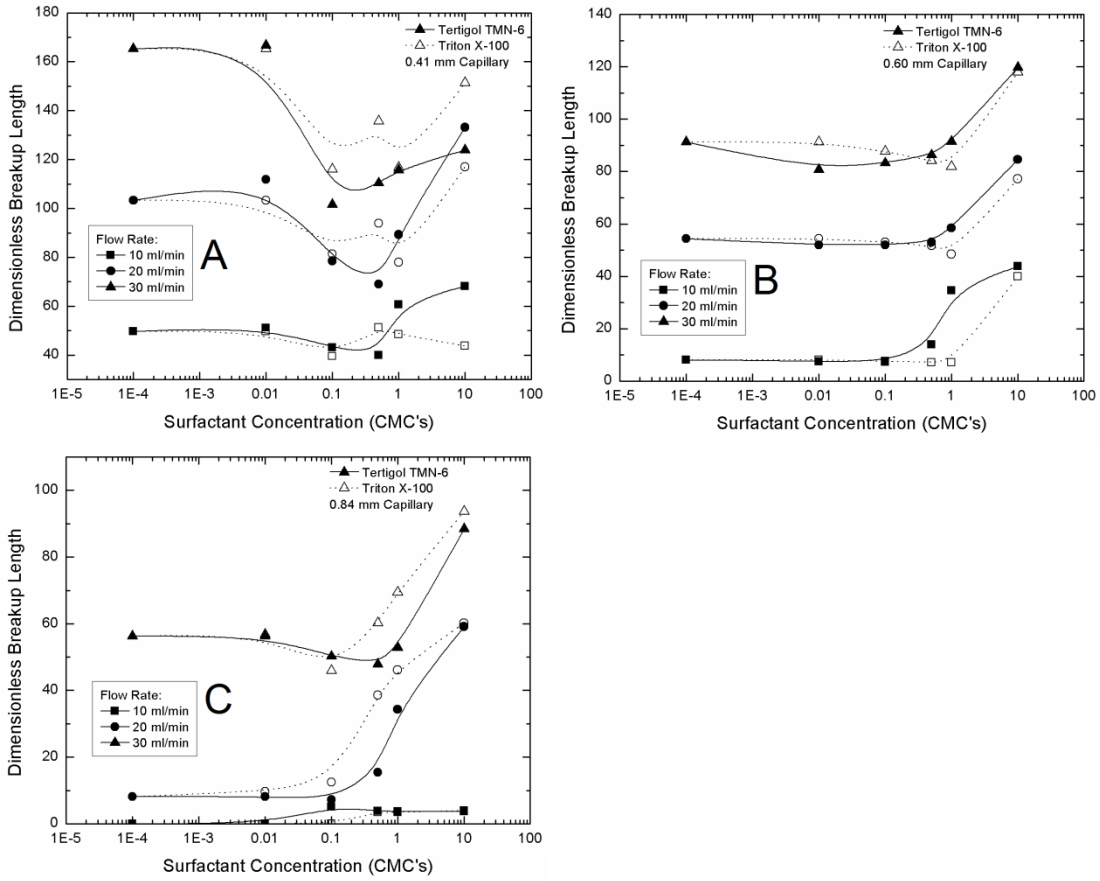

Figure 5.8 – Effect of surfactant concentration on L_b^*: aqueous surfactant solution jets into air, grouped by capillary size. Solid trend lines follow filled symbols (Tergitol TMN-6), while dashed trend lines follow open symbols (Triton X-100). Error bars are excluded for clarity (standard deviation for jetting flow is approximately 10% of the mean, and for dripping flow is less than 4% of the mean)

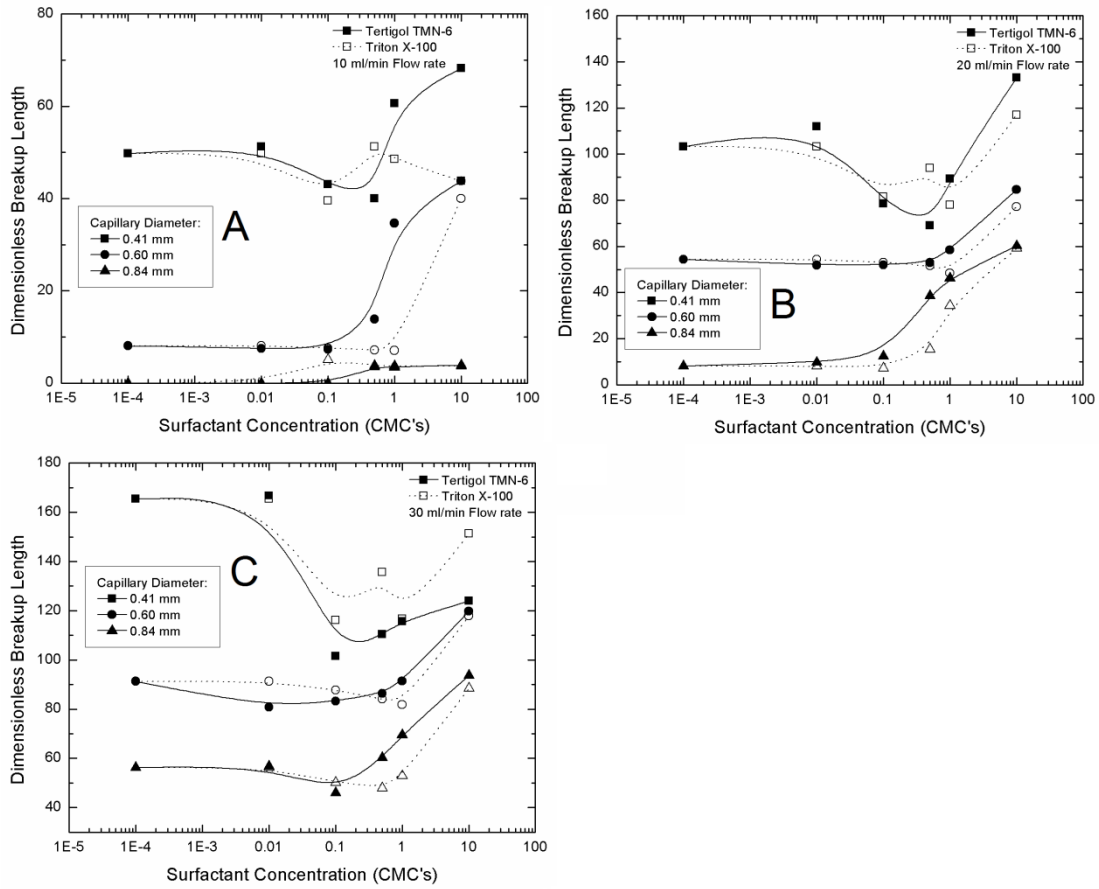

Figure 5.9 – Effect of surfactant concentration on L_b^*: aqueous surfactant solution jets into air, grouped by flow rate. Solid trend lines follow filled symbols (Tergitol TMN-6), while dashed trend lines follow open symbols (Triton X-100). Error bars are excluded for clarity (standard deviation for jetting flow is approximately 10% of the mean, and for dripping flow is less than 4% of the mean)

Figure 5.10 shows the dimensionless droplet diameter as a function of surfactant concentration with experiments grouped by capillary. Figure 5.11 shows this same data again, this time grouped by flow rate. Error bars show one standard deviation above and below the Sauter mean, indicating the width of the droplet size distribution. Error bars are only shown on the Tergitol TMN-6 data to reduce clutter, but are of comparable width for the Triton X-100 data. The Sauter mean diameter is

calculated from the equivalent spherical diameter data resulting from imaging the droplets simultaneously from 2 orthogonal planes.

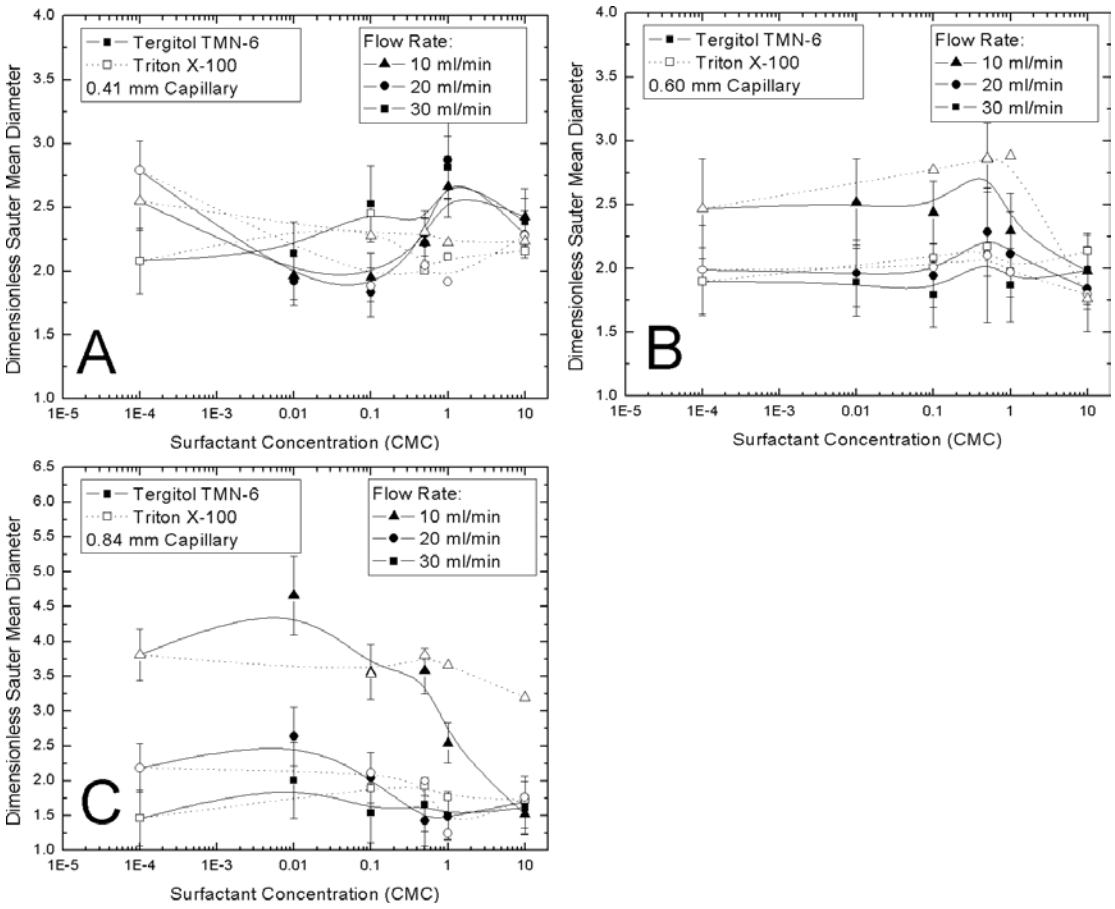

Figure 5.10 – Effect of surfactant concentration on d_{32}^{*}, grouped by capillary size. Solid trend lines follow filled symbols (Triton X-100), while dashed trend lines follow open symbols (Tergitol TMN-6). Error bars indicate the width of the droplet size distribution (±1 standard deviation)

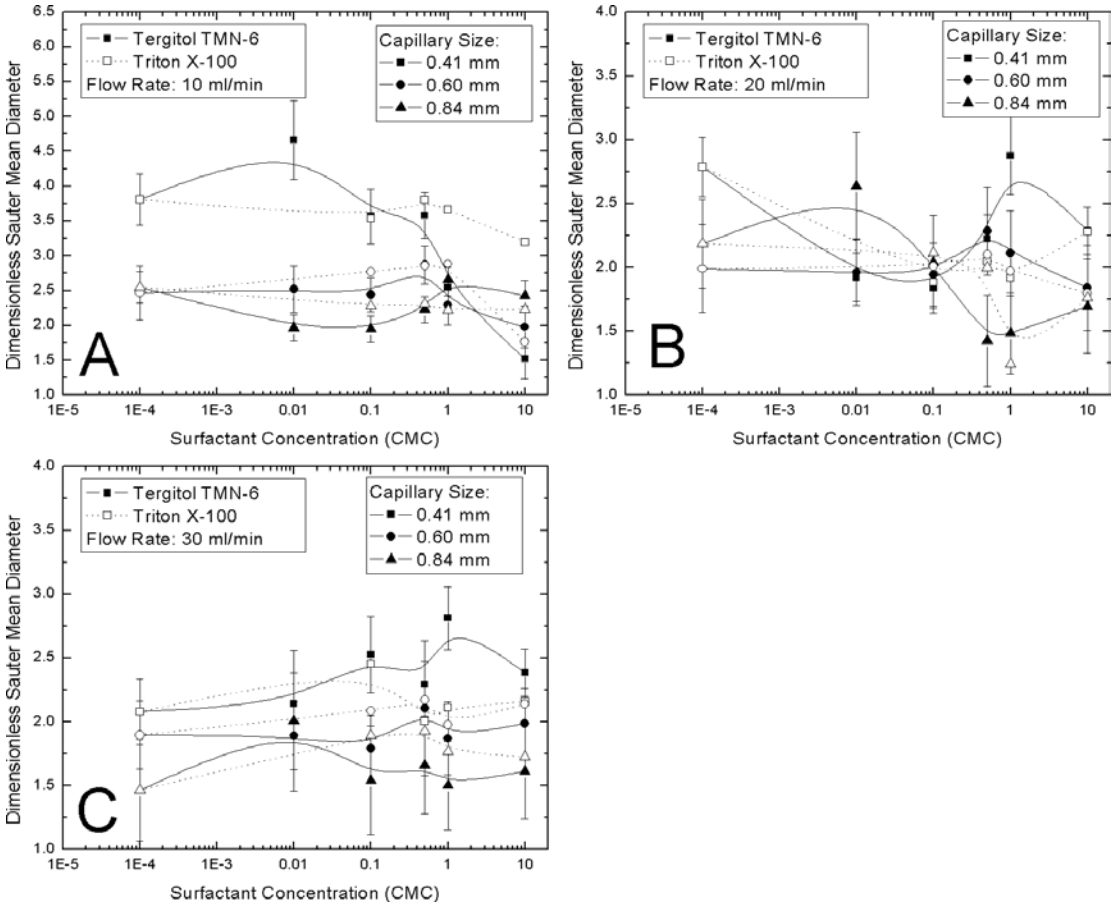

Figure 5.11 – Effect of surfactant concentration on d_{32}^{*}, grouped by flow rate. Solid trend lines follow filled symbols (Triton X-100), while dashed trend lines follow open symbols (Tergitol TMN-6). Error bars indicate the width of the droplet size distribution (±1 standard deviation)

5.1.3 Qualitative observations of droplet breakup using High Speed Imagery

Utilizing the high speed camera, detailed images and videos of the breakup events were obtained. Figure 5.12 shows a sequence of images showing the creation of a primary and satellite drop from a jet of deionized water in air. In this case, the satellite drop catches up with the primary drop and is reabsorbed into the primary droplet. Figure 5.13 shows a similar series of images for an aqueous 1 CMC Tergitol

TMN-6 solution in air, showing a similar production of primary and satellite droplets. In this case, the small satellite drop approaches the primary droplet, but instead of coalescing, ricochets off the surface of the drop and is ejected from the field of view.

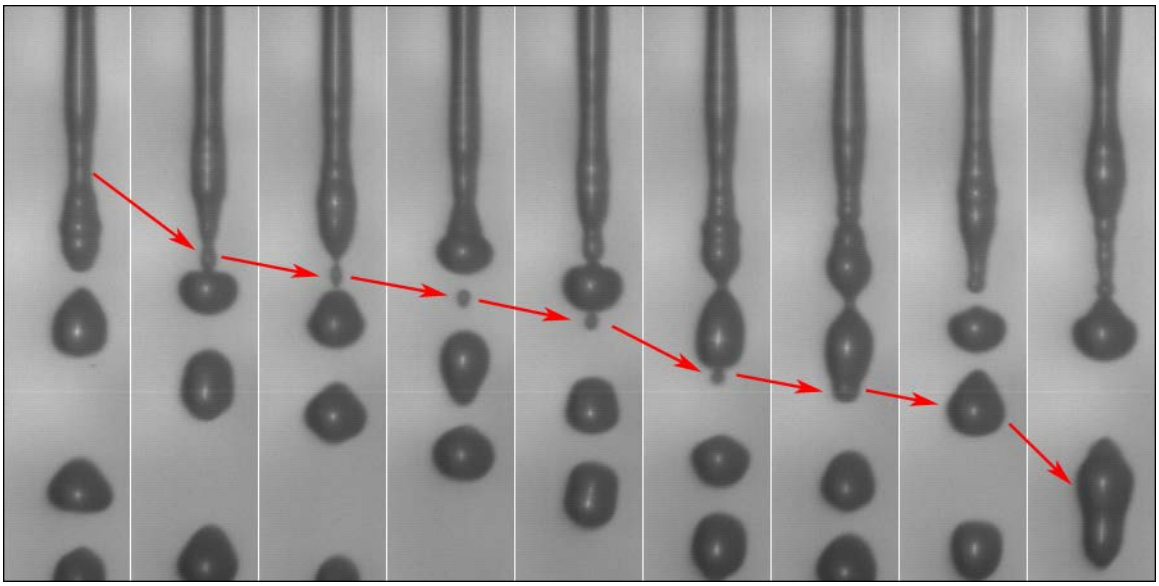

Figure 5.12 – High speed photography of a clean water-air jet. Initial jet diameter is 0.6 mm, flow rate is 10 ml/min

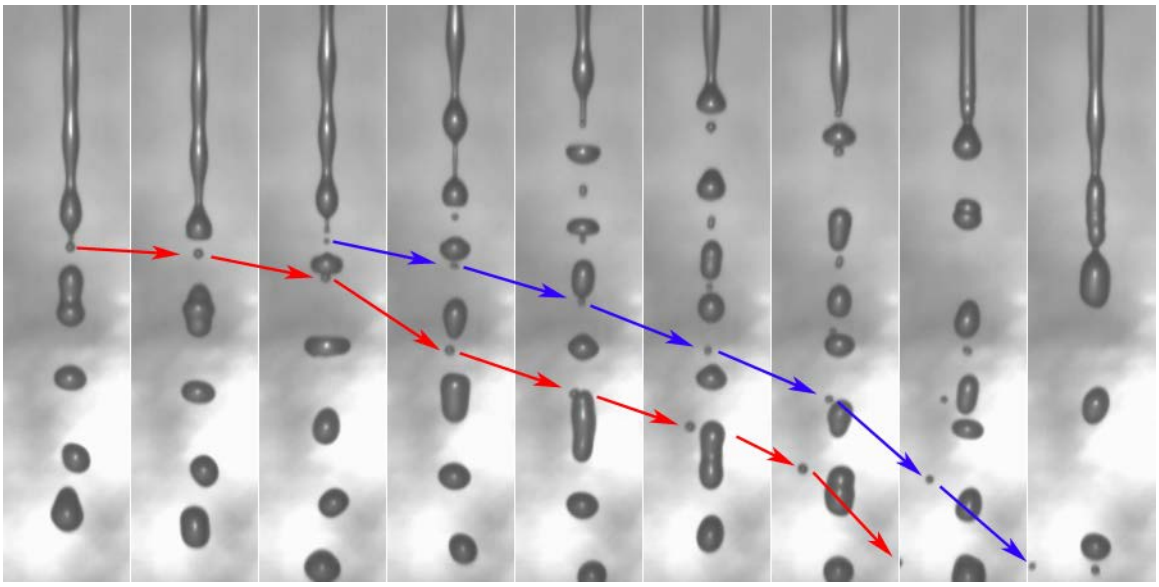

Figure 5.13 – High speed photography of a jet of 1 CMC Tergitol TMN-6 solution into air. Initial jet diameter is 0.6 mm, flow rate is 10 ml/min (Flow conditions are the same as Figure 5.12)

5.2: Comparison with theoretical predictions:

Equations 2.6 and 2.7 (linear stability model, see Chapter 2) were used to calculate the predicted primary droplet size for clean water-in-air jets. Figure 5.14 shows these predicted values compared to the actual measured quantities.

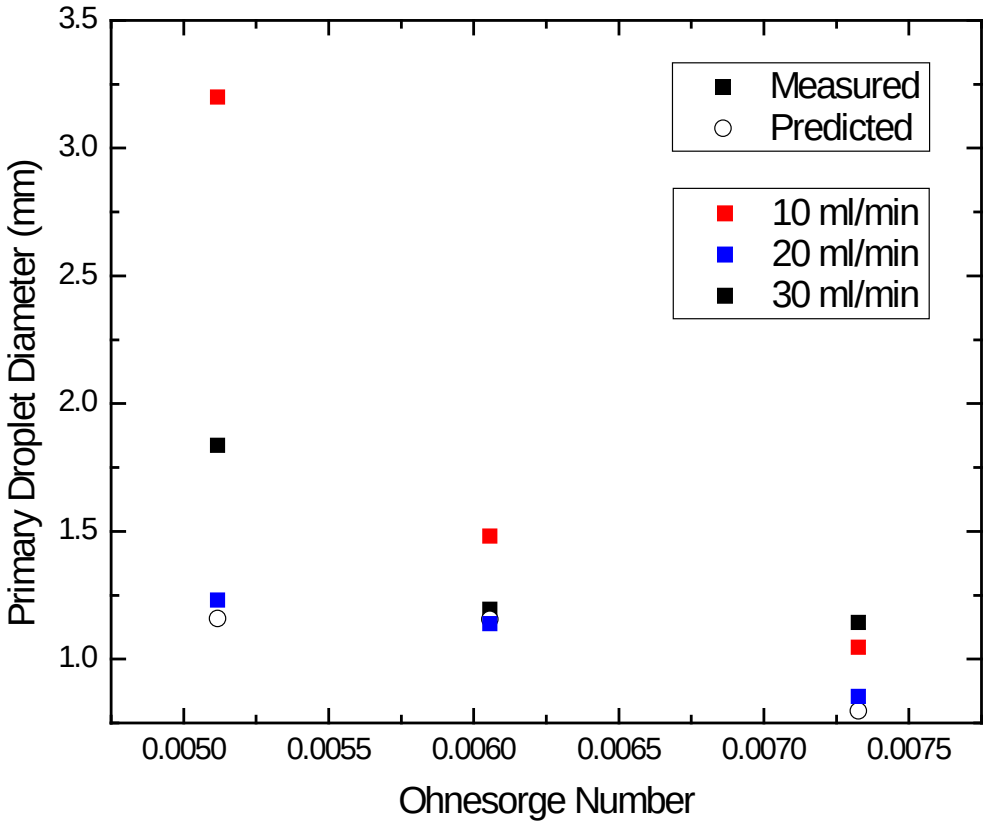

Figure 5.14 – Prediction of primary droplet size using linear theory for clean water jets in air, based on equations 2.6 and 2.7

Goldin et al. (1969) proposed that breakup lengths should follow Equation 2.11. The data presented above, as well as Goldin's published data is shown in Figure 5.15.

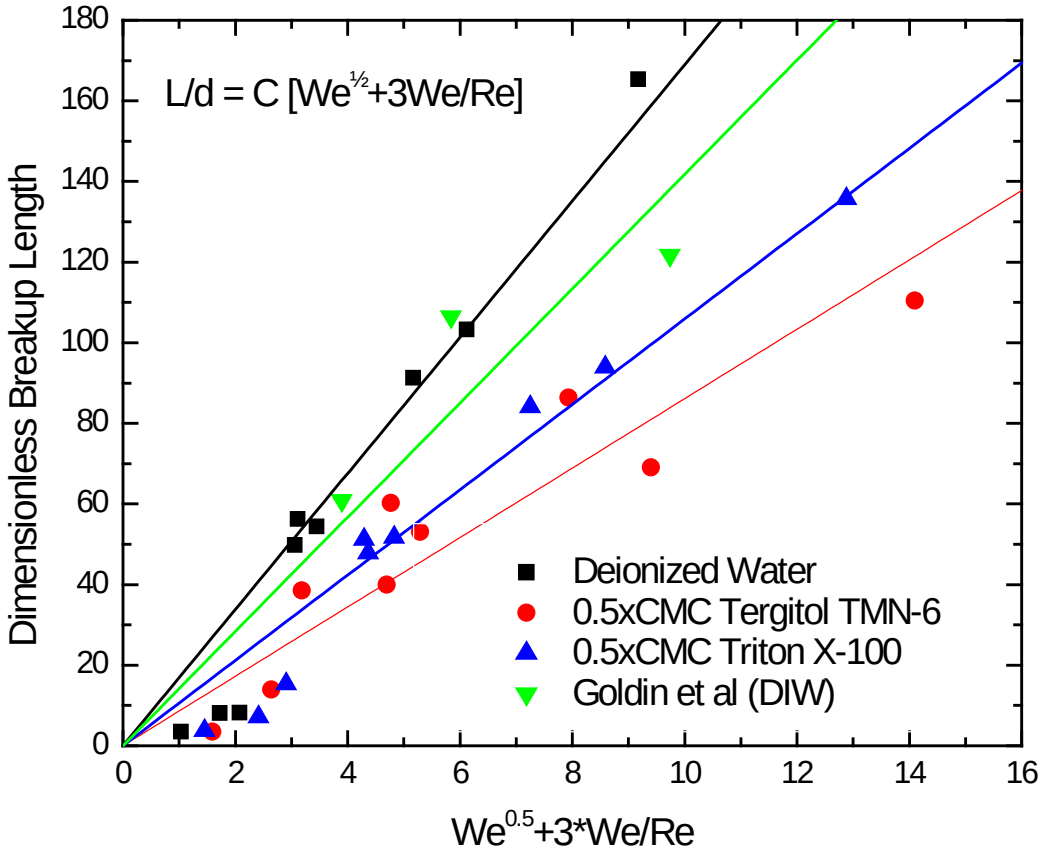

Figure 5.15 – Plot of L_b^* vs $We^{0.5}$+3 We/Re for water jets in air. "DIW" indicates deionized water

Based on Equation 2.9, the breakup length of clean water-in-air jets was predicted. Figure 5.16 shows the comparison with measured values. For the value of $\ln(r_o/\delta_o)$, the value of 6 proposed for liquid-liquid jets by Scheele and Meister (1968) was found to be unacceptable for water-air jets. A value of 11.6 was determined to fit our data well based on a least squares fit.

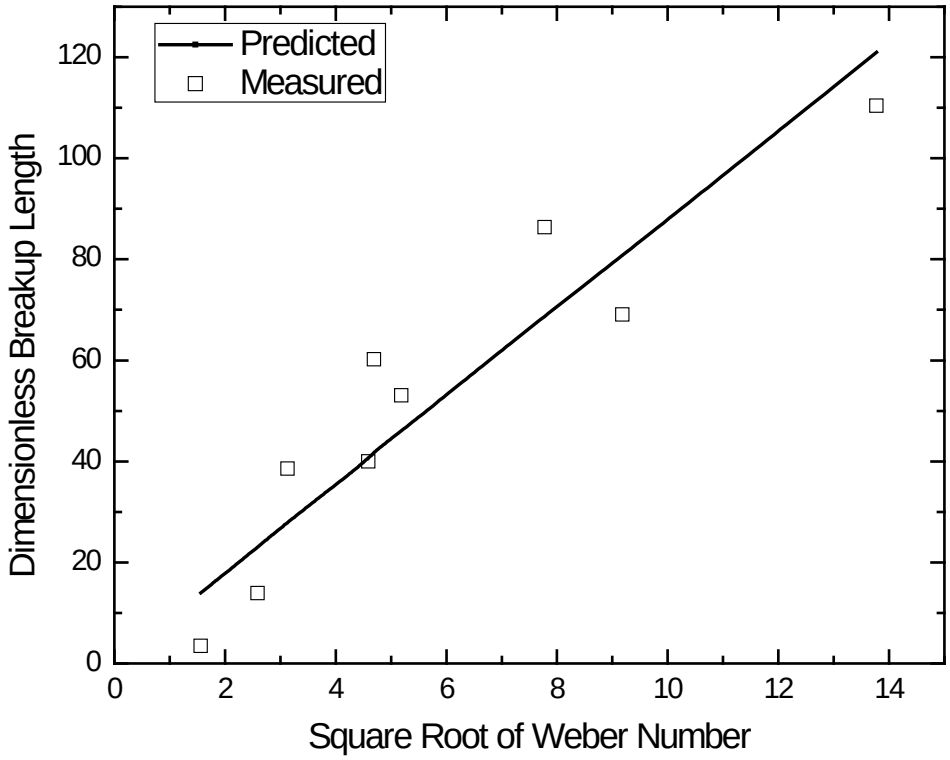

Figure 5.16 – Plot of dimensionless breakup length vs. $We^{0.5}$ for deionized water-in-air jets

5.3: Discussion of Results

The linear breakup theory developed by Rayleigh (1879) and Tomotika (1935) is a powerful tool to understand jet breakup. However, due to the assumptions inherent in the analysis, the method is limited to systems where the surrounding fluid viscosity is negligible, and is unable to predict satellite drop size. Another shortfall is that the model assumes a non-inertial reference frame, therefore failing to take into account the effect of the jet's velocity. This study has shown that jet velocity has a significant influence on jet breakup lengths and droplet sizes. Figure 5.2 shows that increasing Reynolds number causes a modest increase in droplet Sauter mean diameter once the Reynolds number exceeds a critical value of about 1000. Nonetheless, Figure 5.14

shows that the predicted droplet diameter using the linear model fits relatively well for air-water jets within the jetting regime (the outlier at 10 ml/min and the lowest Ohnesorge number was in Dripping flow). The effect of flow rate on jets is also evident in Figure 5.3, which shows that dimensionless breakup length increases linearly with Reynolds number once the Reynolds number exceeds a critical value (corresponding with the transition from dripping to jetting flow). Based on the DNS simulation results for a variety of liquid-liquid and gas-liquid systems presented by Homma et al. (2006), the value of breakup length should reach a maximum, and then decrease with Reynolds number once the jet transitions from an axisymmetric profile to an asymmetric profile, and then reach an equilibrium value once the jet transitions into turbulent flow (see Figure 2.6). For air-water jets, the conditions in this study were such that the majority of jets observed were in the axisymmetric flow regime.

Surfactants were also shown to significantly influence water-in-air jets. Breakup lengths increased slightly at low concentrations as compared to clean jets, but the effect was much more pronounced at high surfactant concentrations. At a surfactant concentration of 10 times the critical micelle concentration, breakup lengths increased by approximately 40% above the values observed for 'clean' systems, as seen in Figure 5.7. It was seen from Figure 3.6 that it takes 30-60 seconds for these surfactants to have a significant effect on the surface tension at a concentration of about 5% of the CMC, so we can safely assume that this is representative of the time it takes the surfactants to diffuse to the surface. Since the time scale of the jet formation is much less than one second, it is unsurprising that low concentrations do not affect jet breakup significantly, since surfactants have insufficient time to diffuse

to the surface of the jet. Since diffusive flux is proportional to the concentration gradient, by increasing the surfactant concentration, we increase the diffusion rate of the surfactant, allowing more surfactant to reach the surface of the jet in the time scale of the jet formation. This leads to a synergistic effect where the more the surfactant stabilizes the jet, the longer the jet lasts, allowing for more surfactant to diffuse, which accounts for the significantly longer jets observed at high surfactant concentrations. Therefore, at low concentrations (below 50% of the CMC), we can model these jets as 'clean' interfaces utilizing the linear stability model discussed above.

The mechanism by which the surfactants stabilize the jet is not entirely clear. Marangoni stresses should act to stabilize the jet by opposing the creation of any new interfacial area (a necessary step for instabilities to grow). Additionally, since surfactants act to reduce the interfacial tension, there is less of a surface force acting to destabilize the jet. These two factors together are likely responsible for the increased jet lengths observed at high surfactant concentrations. Surfactant films have also been proposed to increase the 'surface viscosity', by making the surface appear to be more rigid (viscous) than the bulk fluid properties. Based on Equation 2.2, it is seen that by increasing the viscosity of the solution, the growth rate of the instabilities is reduced, therefore stabilizing the jet from breakup. This 'interfacial viscosity' is a manifestation of the Marangoni stress, as the restoring surface force caused by the gradient in interfacial tension acts like an elastic stress along the interface, similar to how viscous stresses act.

For the case of droplet diameters, increasing surfactant concentration acts to decrease the interfacial tension, which increases the value of the Ohnesorge number. Based on Figure 2.5, it is seen that as Ohnesorge number increases, the predicted droplet diameter increases as well. The Marangoni stresses should also act to increase droplet diameters, as by acting to suppress the creation of interfacial area they should act to damp out the higher frequency oscillations and cause the lower frequency (and thus longer wavelength) disturbances to dominate, resulting in larger fluid nodes and ultimately larger droplets. However, Figure 5.10 shows that in most cases, primary droplet diameter does not change significantly with increasing surfactant concentration. In fact, Figure 5.10C in shows a ~50% decrease in droplet diameter for droplets created by a low flow rate jet (corresponding to a transition from dripping flow to jetting flow), and a 10% decrease for jets at higher flow rates. In Figure 5.10B, a modest increase in droplet size is observed through the intermediate concentration range, followed by a marked decrease for concentrations above the CMC.

These phenomena are not explainable using linear breakup theory. From investigation of the jet breakup phenomena from the high speed photography, it becomes evident that the 'one node, one drop' assumption is not correct. As the jet widens towards the breakup position, the axial velocity slows. This allows subsequent wave fronts to 'catch up' with the droplet. Consequently, each droplet produced is actually the summation of anywhere from 1 to 6 nodes of fluid, with most droplets containing 3 or 4 nodes of fluid. In the case of clean water jets, few, if any, additional nodes of fluid are added to the droplet before breakup, resulting in droplet

sizes similar to those predicted by the linear theory. For surfactant laden jets, the additional lifetime of the droplets, especially during the latter stages of droplet evolution, causes additional complexities. While the size of individual fluid nodes may increase, as predicted by linear jet theory, the number of nodes of fluid contributing to each droplet often decreases due to the increasing surface rigidity caused by the adsorption of surfactant on the surface of the droplet. Consequently, due to the interaction between the node size and number of nodes varying independently, the ultimate droplet size may increase or decrease. At very high surfactant concentration, the Marangoni stress acts to make the droplet less able to enlarge, therefore there is a general trend towards smaller droplets at very high surfactant concentration across all conditions. Beyond that singular observation, no general trends are observed, and a mechanism for decoupling the size of the fluid nodes from the number of nodes in a droplet is needed to achieve a greater understanding of the underlying physics. One possible solution to this is to fix the size of fluid nodes by using a forced jet – this is discussed in greater detail in the Future Work section in Chapter 7.

Satellite droplets at higher surfactant concentration were observed to deflect off primary drops in a collision, instead of being re-absorbed, as is the case at low surfactant concentration. This phenomenon is clearly observed in the high speed video (see Figures 5.12 and 5.13 above). This is most likely a result of primary droplets developing surface elasticity due to the formation of a surfactant monolayer at high surfactant concentrations. Therefore, the survival of satellite droplets is much higher at higher surfactant concentrations. Due to the loss of satellite droplets from

the imaging plane (either due to re-absorption into the primary droplets, or the satellite drops colliding with primary droplets and being ejected from the image) and their high rate of speed causing them to blur on the high resolution CCD camera; it was difficult to draw any conclusions regarding the effect of surfactant concentration on their droplet size distribution. However, based on the limited data extracted from the high-speed imaging, no significant changes were observed in satellite droplet size with surfactant concentration. Increasing surfactant concentration was generally observed to reduce the occurrence of satellite droplets; however it also increased their survival past the initial breakup event as they were more likely to ricochet off the primary droplets instead of being absorbed. Therefore, the net population of satellite droplets was not observed to be significantly affected by surfactant concentration. Overall, the net population of satellite droplets remained very low across all conditions, and their presence (or absence) had no significant effect on the Sauter mean diameter of the primary droplets. From Figures 5.12 and 5.13 it is observed that the satellite droplets are, in general, an order of magnitude smaller than the primary droplets. Therefore, if a 0.2mm satellite droplet (with a volume of 0.0042 mm^3) is re-absorbed by a 2 mm primary droplet (with a volume of 4.189 mm^3), its diameter only increases to 2.001 mm. Therefore, the relative population of satellite droplets is safely ignored in the analysis of the overall droplet size distribution, especially when the Sauter mean diameter (which is weighted to favour the largest droplets) is utilized.

The semi-empirical correlation shown in Figure 5.15 shows that dimensionless breakup length is well linearized when plotted against a function of $We^{½}$. This agrees

well with the mechanistic theory developed by Das (1997). It is also shown in Figure 5.15 that varying the surfactant concentration changes the value of the empirical fitting parameter, observable by the changing slope of the least squares line. The value of the parameter was not found to correlate with surfactant concentration, so it remains unclear if this correlation will prove useful for further analysis. Given the breadth of numerical modeling techniques for this system in the literature, further empirical modeling of the air-water system was not pursued. The mechanistic model developed for the liquid-liquid from Chapter 4 was also applied to the air-water system in section 5.4.

5.4: Model Validation

In Chapter 4 a semi-empirical model to determine the breakup length of a surfactant laden jet was proposed (Equation 4.6). Figure 6.30 shows the results from a surfactant laden water jet into air. Utilizing appropriate values for Γ_∞ and a_L for the air-water interface, results for Triton X-100 surfactant were calculated using our model. Departure from the no-surfactant case is predicted at a slightly lower surfactant concentration than is observed in the experimental data, but otherwise excellent agreement between the model and data is observed. The transition point between the no-surfactant case and elongated case is found to depend strongly on the value of Γ_∞, therefore, small inaccuracies in the measurement of Γ_∞ are likely responsible for the minor disagreement between the measured and modeled values. Precise measurement of Γ_∞ and D_{AB} for the air-water system is difficult, as it requires maintaining a liquid droplet on the tip of a capillary in air for a period of at least 20-30 minutes, over which time the droplet has a tendency to shrink due to evaporation,

even in a high humidity system. Since the measurement of interfacial tension is extremely sensitive to changes in the droplet shape (See Chapter 4), this decreases the accuracy of the calculation of Γ_∞ and D_{AB}. Further application and discussion of this model is presented in Chapter 6.

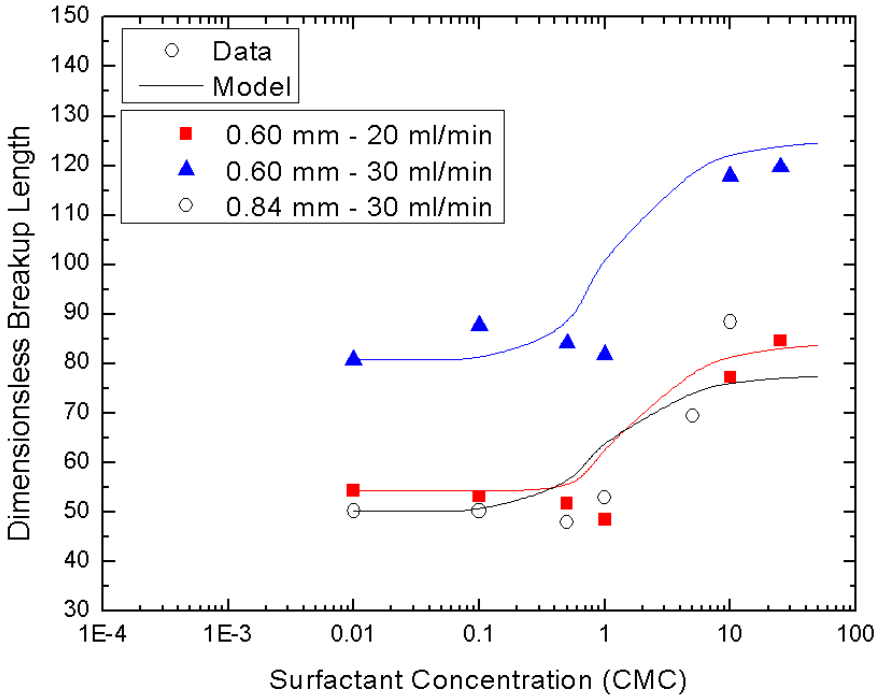

Figure 5.17 – Comparison of measured dimensionless breakup lengths with those calculated using equation 6.6, with instantaneous interfacial tension values predicted using equation 3.20 for a jet of aqueous surfactant solutions into air

Chapter 6: Oil-Water Jets

6.1: Experimental Results

6.1.1 Oil-in-Water Jets

Experiments were performed using 10 cSt silicone oil as the jet phase, into a quiescent phase of deionized water. Due to the increased viscosity of the jet phase, flow rates were lower than the water-in-air jets in order to stay within the appropriate Reynolds and Weber number ranges for the jetting flow regime. Increased continuous phase viscosity also resulted in oil droplets very quickly resolving into spheres, eliminating the need for the complementary mirrors and added computational complexity to calculate equivalent spherical diameter.

Figure 6.1 shows the effect of Reynolds number on the dimensionless Sauter mean diameter of oil drops in deionized water, and Figure 6.2 shows the effect of Re on the dimensionless breakup length of oil drops in deionized water. Trend lines are added as a guide to the eye and do not represent theoretical predictions. Open symbols indicate that the experimental conditions were below the critical velocity for jet formation; therefore individual droplets were periodically produced at the capillary tip (referred to as 'dripping flow'). The relationship of the different flow regimes was discussed in Section 2.3.1 above.

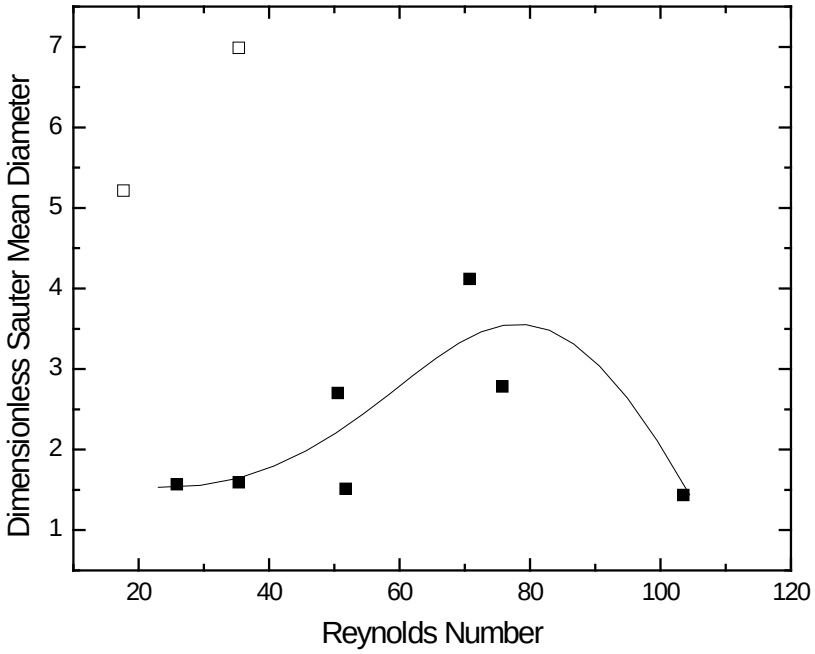

Figure 6.1 – d_{32}^{*} vs. Reynolds Number for oil-water jets (open symbols indicate a dripping flow regime)

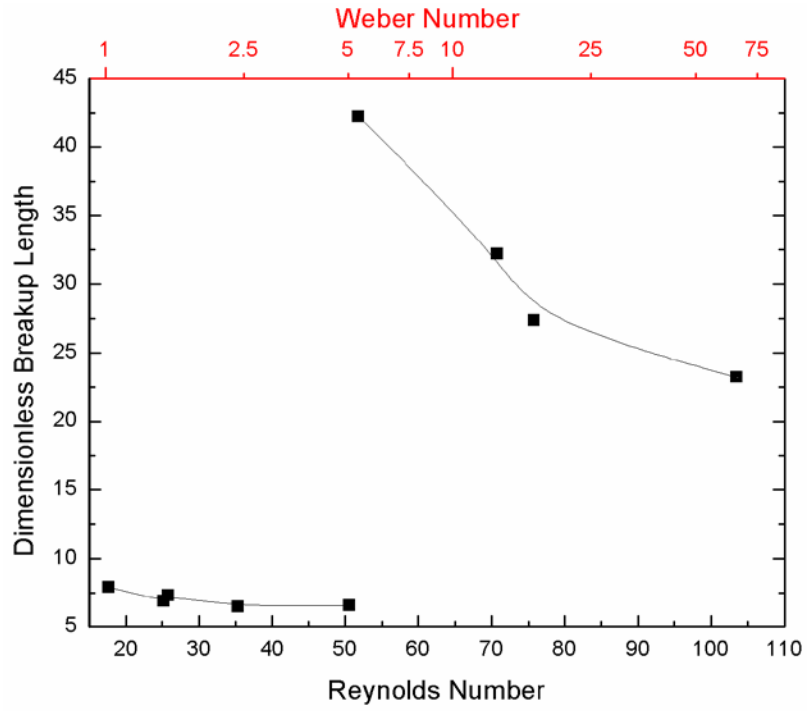

Figure 6.2 – L_b^{*} vs. Reynolds Number for oil-water jets. Corresponding Weber numbers are included on the upper horizontal axis

6.1.2 Surfactant-laden Oil-into-Water Jets

The effect of surfactants on the breakup of a 10 cSt silicone oil jet in aqueous solutions of Tergitol TMN-6 and Triton X-100 were studied. Since the Reynolds number incompletely correlates the experiments performed with different capillary diameters, subsequent results will be separated, and the capillary diameter or relative flow rate, rather than the Reynolds number, will be used to correlate the results. Figure 6.3 shows the effect of surfactant concentration on dimensionless Sauter mean diameter, with the data organized by relative flow rate. Figure 6.4 shows the same data, organized by capillary diameter. Note that for the flow rate groupings, the lowest, middle, and highest flow rates used for a given capillary are grouped together, meaning that the nominal flow rate in each figure is not the same for all 3 sets of data. Open symbols indicate a dripping flow regime, while closed symbols indicate a jetting flow regime (either axisymmetric or asymmetric jetting - refer to section 2.1.3 for definitions).

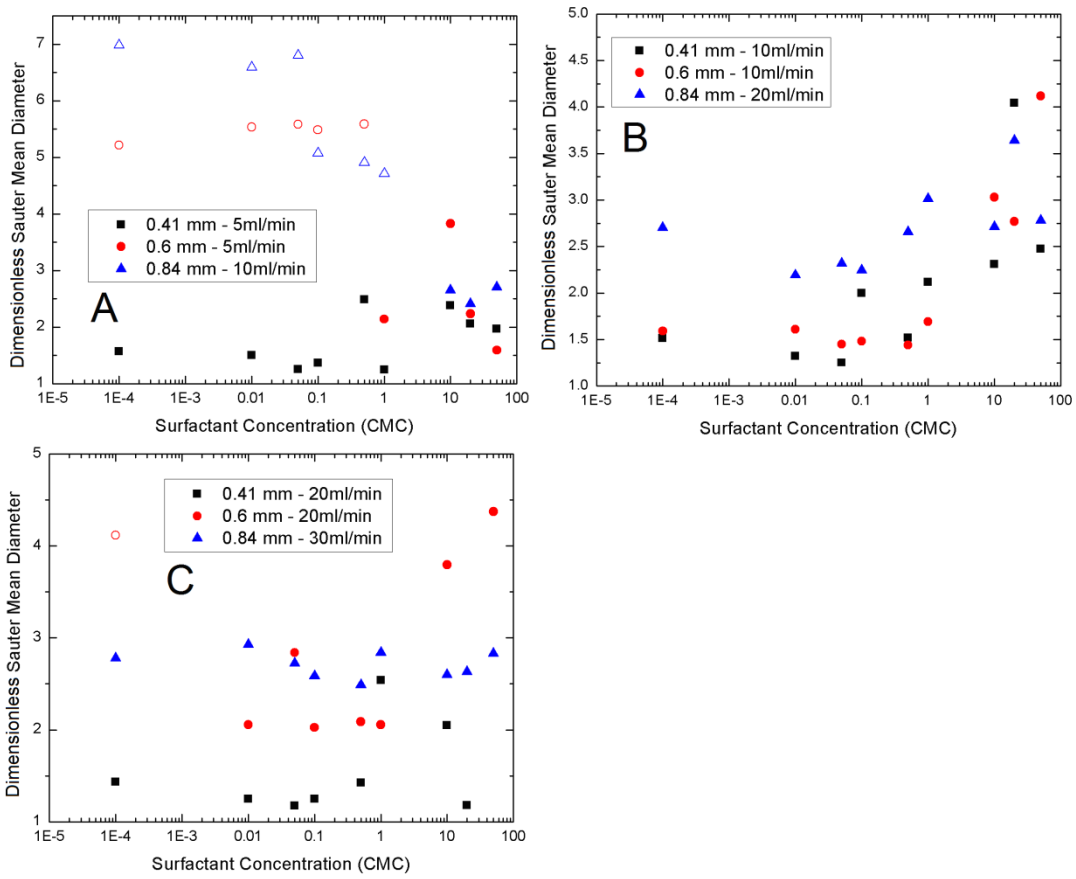

Figure 6.3 – Effect of surfactant concentration on d_{32}^{*} for 10 cSt silicone oil jets into aqueous Triton X-100 solutions. Open symbols indicate that no stable jet was formed (dripping flow regime). Data is grouped by relative flow rate

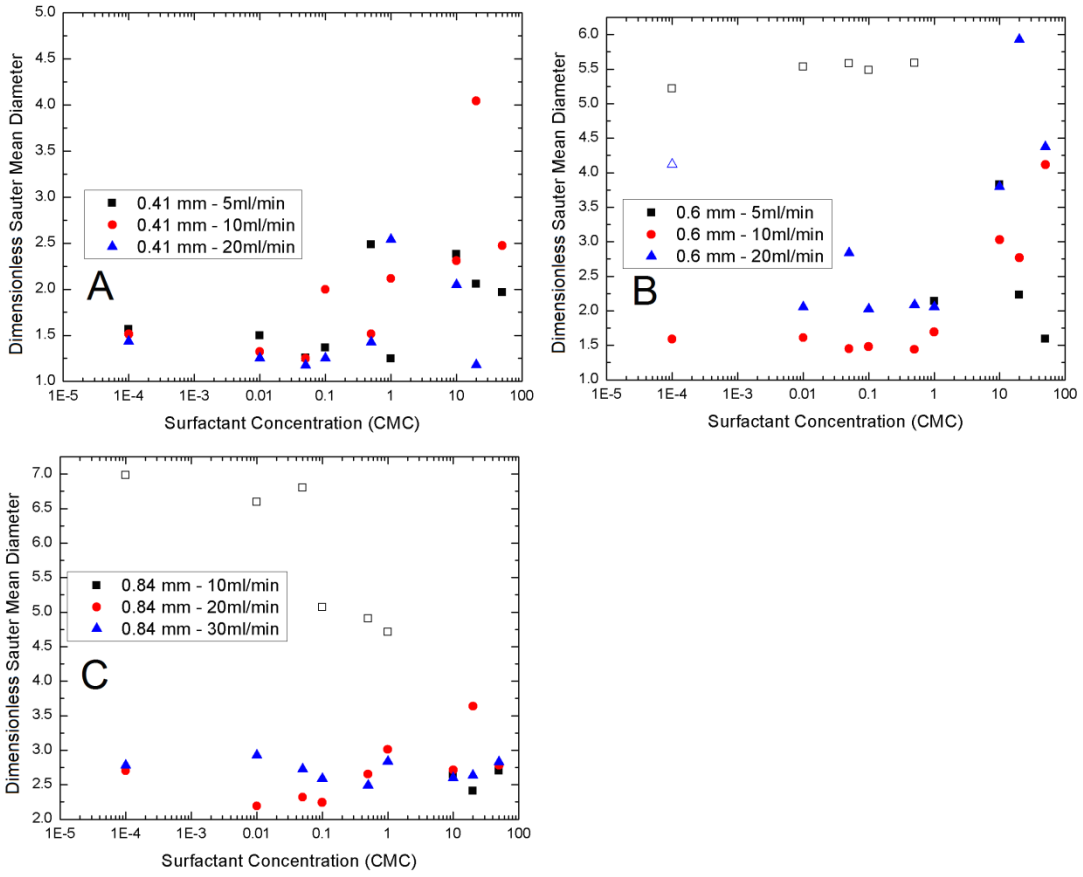

Figure 6.4 – Effect of surfactant concentration on d_{32}^{*} for 10 cSt silicone oil jets into aqueous Triton X-100 solutions. Open symbols indicate that no stable jet was formed (dripping flow regime). Data is grouped by capillary diameter

Breakup length was also measured for oil-water jets. Figure 6.5 shows dimensionless breakup length plotted as a function of surfactant concentration, organized by relative flow rate. Figure 6.6 shows the same data organized by capillary diameter.

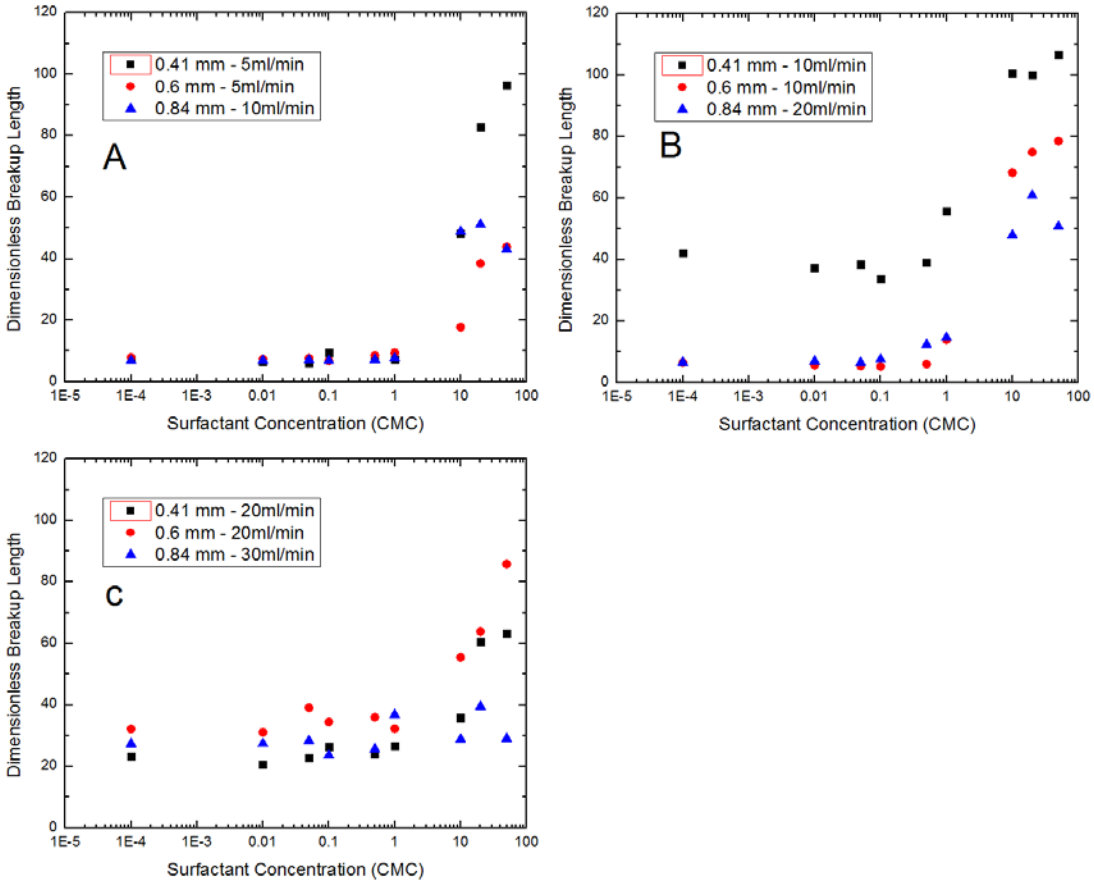

Figure 6.5 – Effect of surfactant concentration on L_b^* for 10 cSt silicone oil jets into aqueous Triton X-100 solutions. Data is grouped by relative flow rate

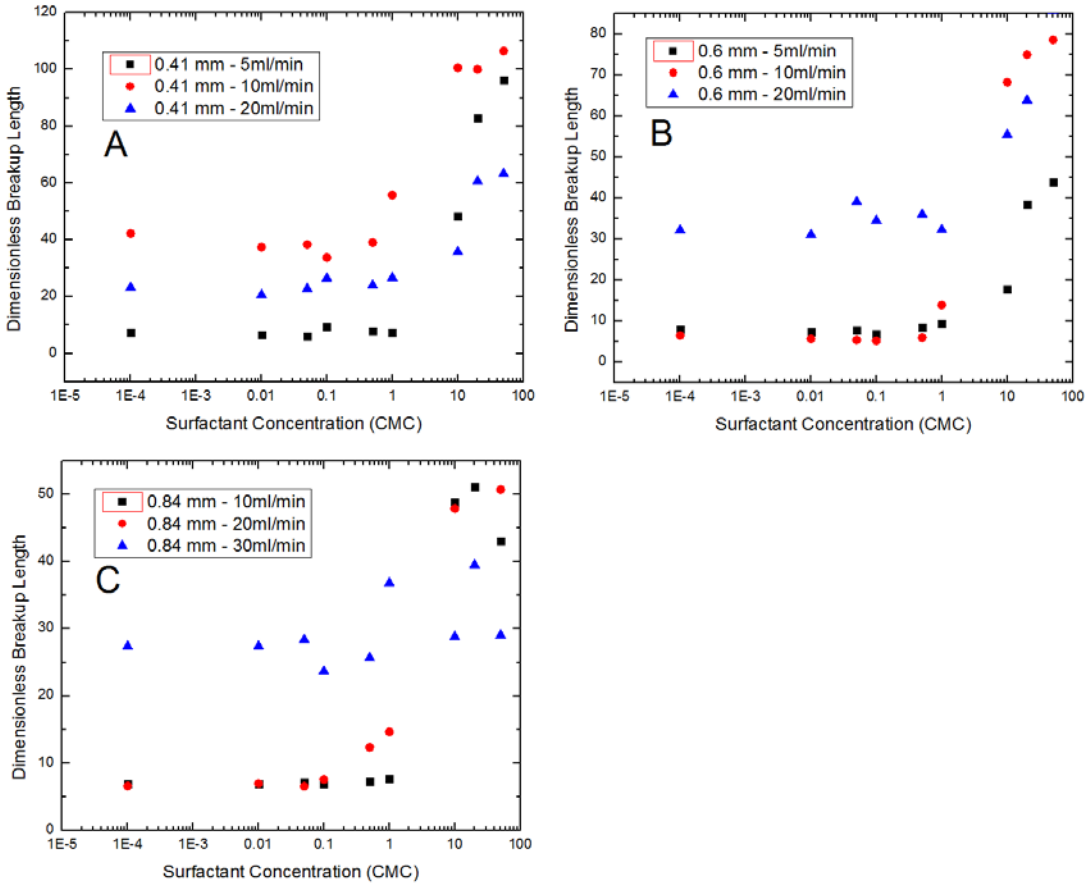

Figure 6.6 – Effect of surfactant concentration on L_b^* for 10 cSt silicone oil jets into aqueous Triton X-100 solutions. Data is grouped by capillary diameter

Experiments were also performed using Tergitol TMN-6 surfactant. Results for this set of experiments, as compared to the Triton X-100 Experiments, are presented in Figures 6.7 (droplet sizes) and 6.8 (jet breakup length).

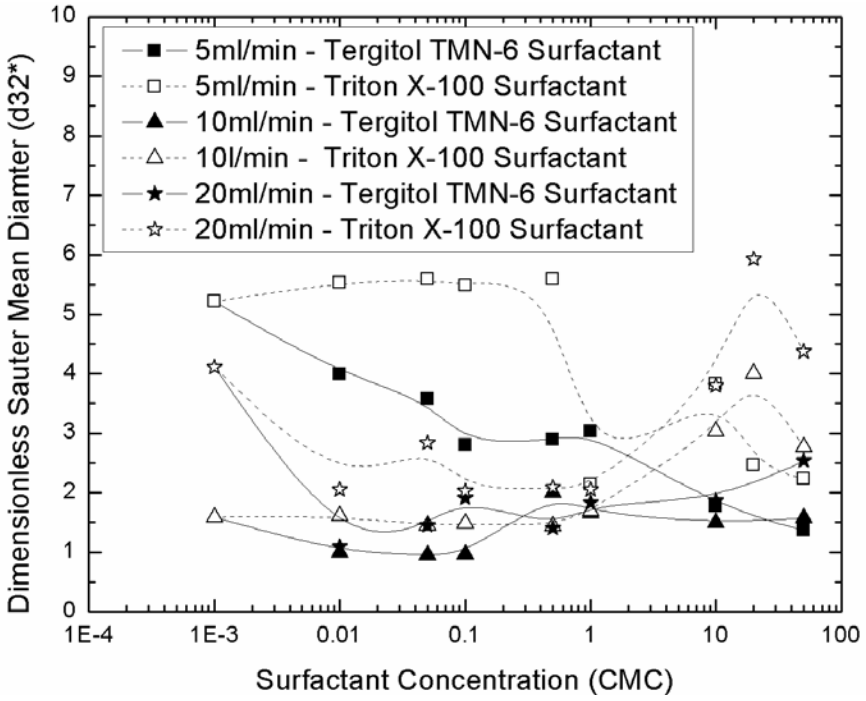

Figure 6.7 – Comparison of dimensionless Sauter mean diameters of droplets produced by a jet of 10 cSt silicone oil into aqueous solutions of Tergitol TMN-6 (solid symbols) and Triton X-100 (open symbols) surfactants

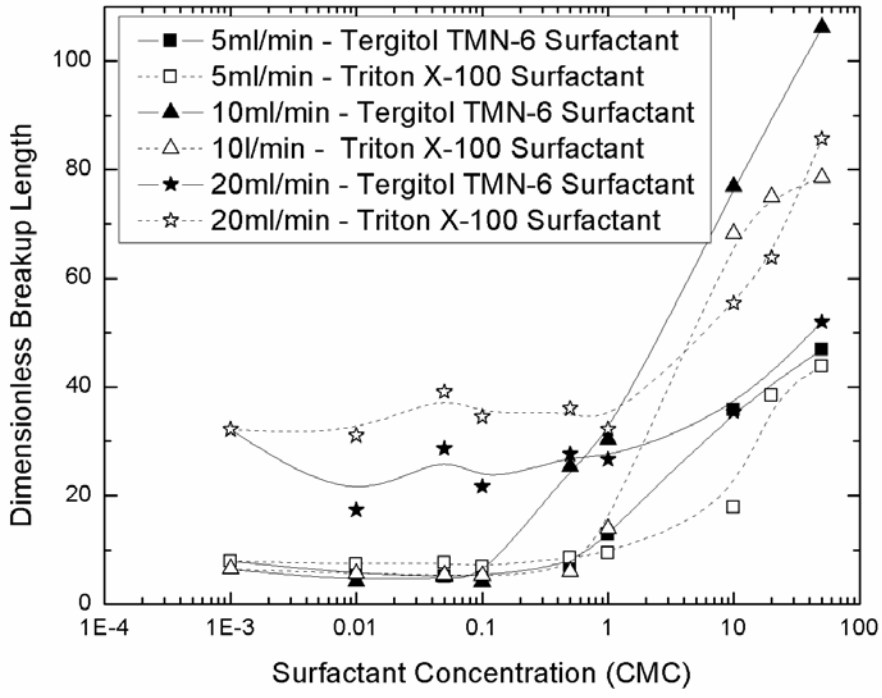

Figure 6.8 – Comparison of dimensionless jet breakup length for a jet of 10 cSt silicone oil into aqueous solutions of Tergitol TMN-6 (solid symbols) and Triton X-100 (open symbols) surfactants

6.1.3 Modified viscosity ratio Oil-into-Water Jets

In order to study the effect of viscosity ratio on the breakup of oil jets into water, a series of experiments were performed using silicone oils ranging in viscosity between 10 cSt and 50 cSt. These different viscosity grade silicone oils have the same density and interfacial tension with water as the 10 cSt grade oil (Padron, 2005). Figure 6.9 shows the effect of jet phase viscosity on the dimensionless Sauter Mean Diameter for these systems. Similarly, Figure 6.10 shows the effect of viscosity on the Jet Breakup Length.

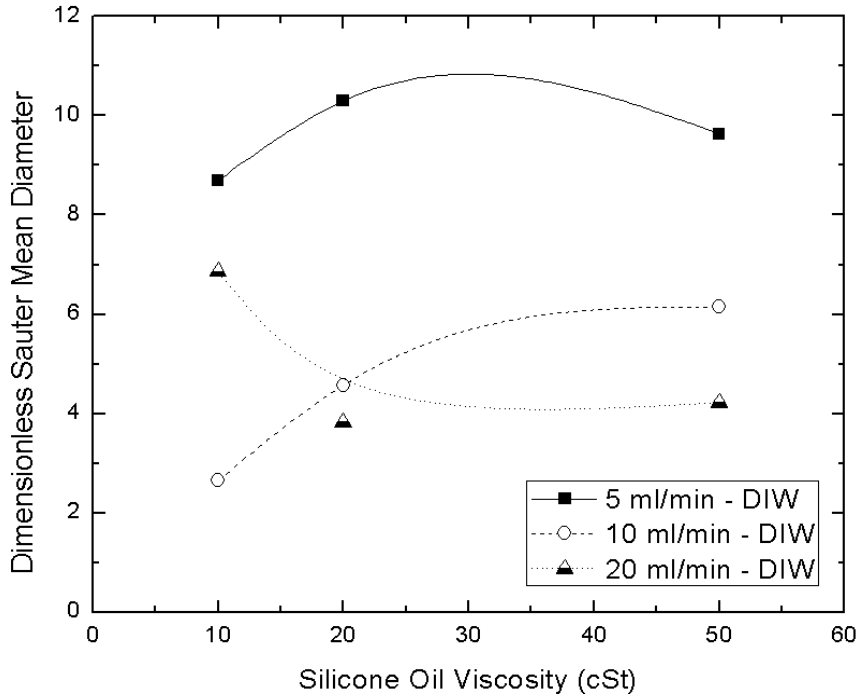

Figure 6.9 – Effect of jet phase viscosity on the dimensionless Sauter mean diameter of droplets produced by the breakup of a silicone oil jet into deionized water from a 0.6 mm capillary

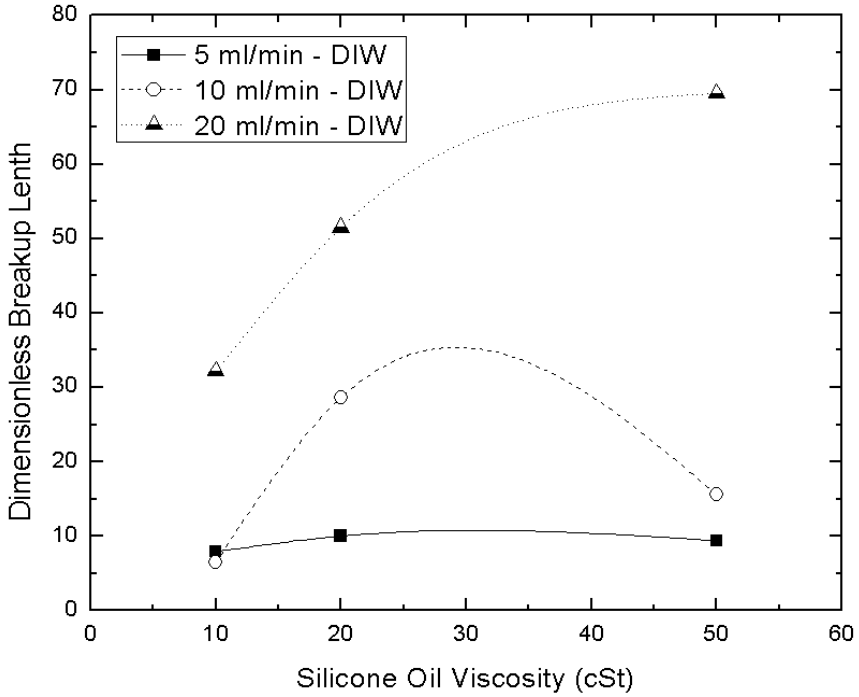

Figure 6.10 – Effect of jet phase viscosity on the dimensionless breakup length of a silicone oil jet into deionized water issued from a 0.6mm capillary

Experiments were also performed by adding Triton X-100 surfactant to the continuous phase with variable viscosity jet phase. The increased breakup time due to increased jet phase viscosity allowed more surfactant transport. The effect of jet phase viscosity on the droplet size for surfactant loaded jets is shown in Figure 6.11, and the effect on jet breakup length is shown in Figure 6.12.

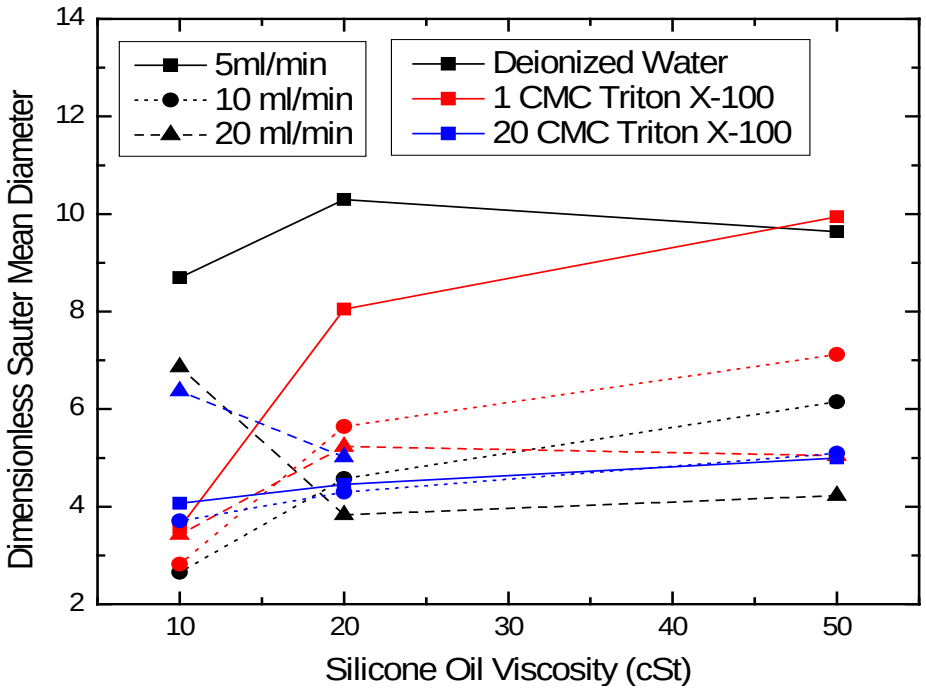

Figure 6.11 – Effect of jet phase viscosity on the dimensionless Sauter mean diameter of droplets produced by a silicone oil jet into aqueous surfactant solutions. The capillary diameter was 0.6 mm

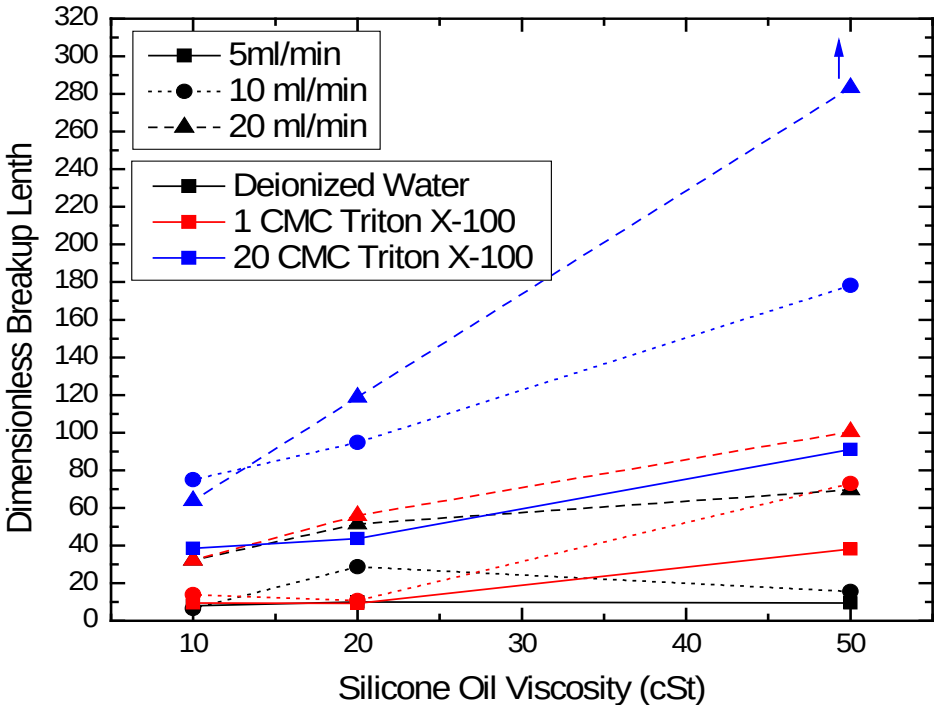

Figure 6.12 – Effect of jet phase viscosity on the dimensionless breakup length of a silicone oil jet into aqueous surfactant solutions. The capillary diameter was 0.6 mm

6.1.4 Modified Interfacial Tension Oil-in-Water Jets

It has been proposed in the literature (Eggers & Villermeaux (2008)) that the reduction of interfacial tension is the primary mechanism by which surfactants affect the breakup of viscous threads, droplets, and jets. To test this hypothesis, a series of experiments utilizing a methanol-water solution as the continuous phase were performed. A methanol-water solution's interfacial tension with silicone oil is a function of methanol concentration, varying from approximately 42 mN/m to 25 mN/m over the 0-30% methanol concentration range where the density change of the solution can be considered negligible (beyond 30% methanol, the density of the solution starts to approach the density of the silicone oil, confounding the problem by introducing neutral buoyancy effects). The density and interfacial tension of a methanol-water solution as a function of methanol concentration is presented in Figure 6.13.

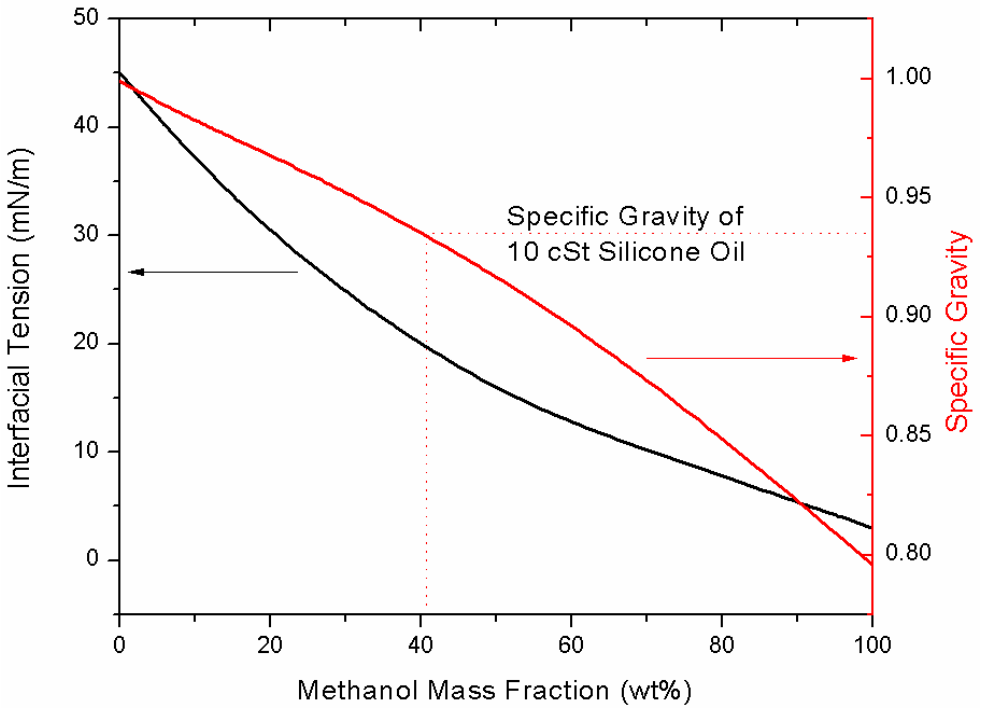

Figure 6.13 – Density and interfacial tension of a methanol-water solution as a function of methanol concentration

The effect of methanol concentration on the breakup length of an oil jet into surfactant-free MeOH-H_2O solution is presented in Figure 6.14. The effect of MeOH concentration on the size of droplets produced by an oil jet into MeOH-H_2O solutions is presented in Figure 6.15. Figures 6.16 and 6.17 compare the breakup length and droplet size (respectively) for the results of these methanol-water experiments with data from surfactant-laden jets, based on their equilibrium interfacial tension.

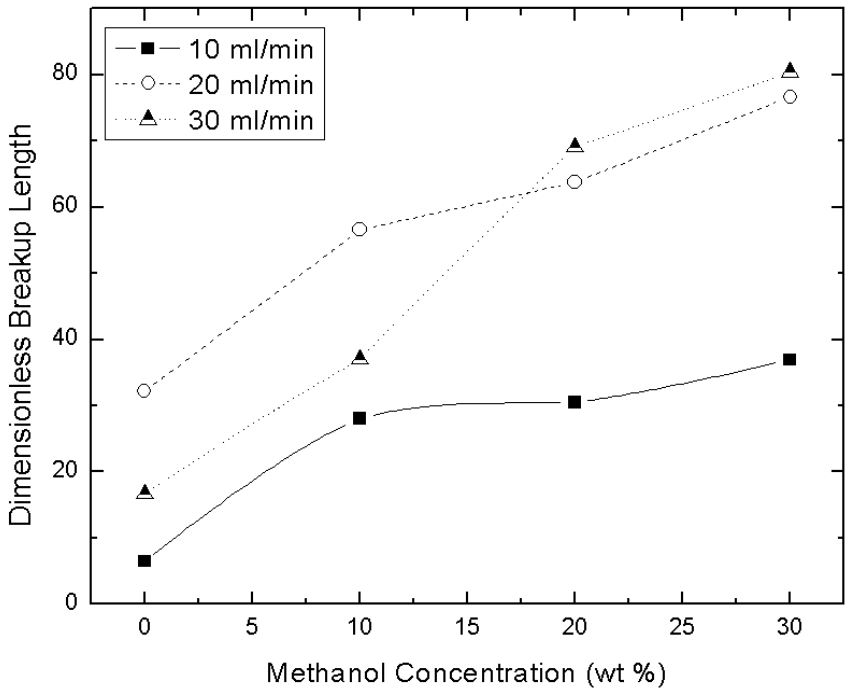

Figure 6.14 – Effect of methanol concentration on jet breakup length for jets of 10 cSt silicone oil into aqueous methanol solutions. Capillary diameter was 0.6 mm

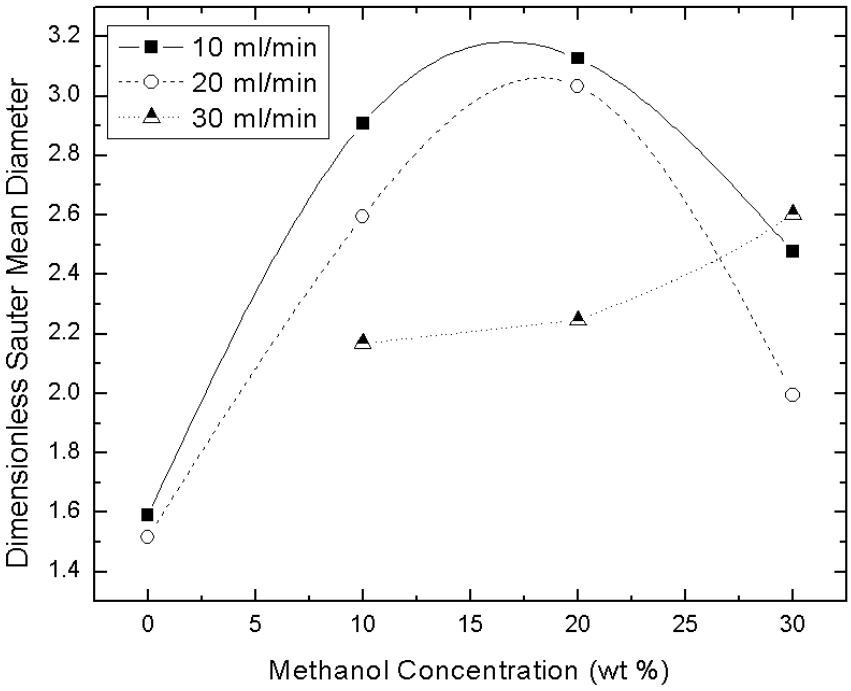

Figure 6.15 – Effect of methanol concentration on the size of droplets produced by jets of 10 cSt silicone oil into aqueous methanol solutions. Capillary diameter was 0.6 mm

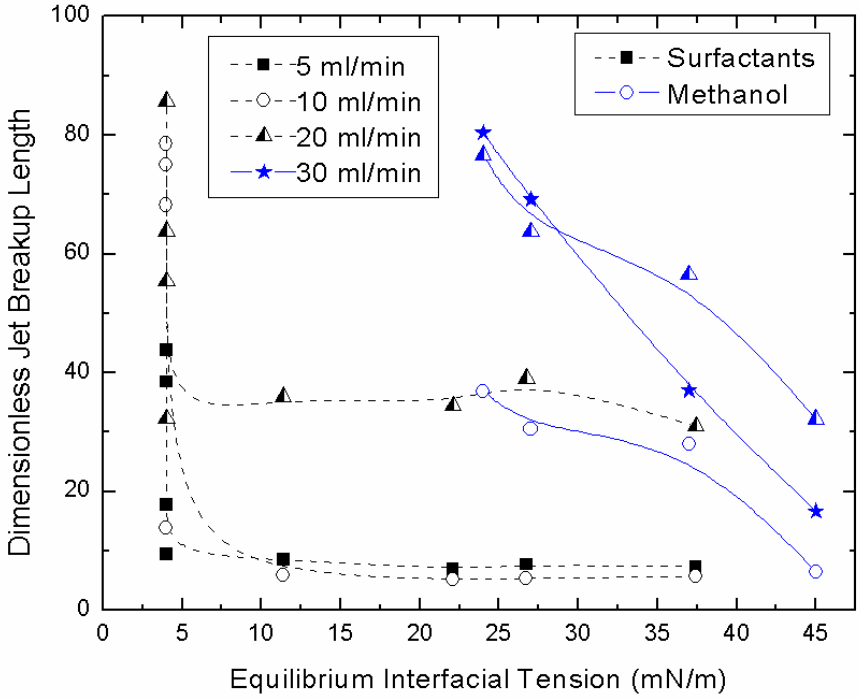

Figure 6.16 – Comparison of dimensionless breakup length for jets with reduced interfacial tension due to methanol or surfactants in the aqueous (continuous) phase. Capillary diameter was 0.6 mm

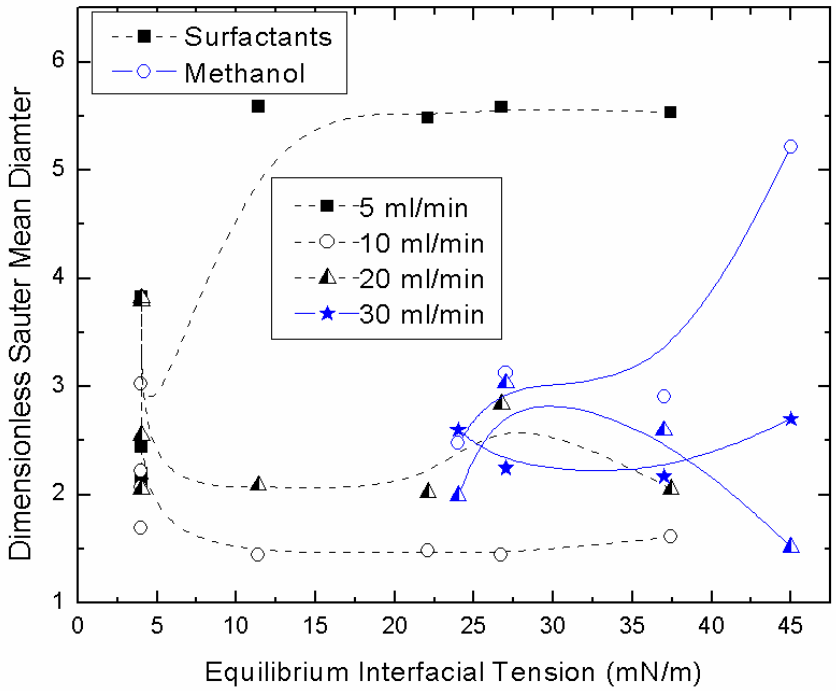

Figure 6.17 – Comparison of dimensionless Sauter mean diameter for jets with reduced interfacial tension due to methanol or surfactants in the aqueous (continuous) phase. Capillary diameter was 0.6 mm

6.1.5 Water-in-Oil Jets

In order to test the effect of the directionality of surfactant transport (eg, from the continuous phase to the interface, or from the jet phase to the interface) and to further expand the range of viscosity ratios tested, a series of experiments were performed where the surfactant-laden aqueous phase was the jet phase, with the viscous oil as the continuous phase. Minor modifications were made to the jet apparatus in order to accommodate a jet phase heavier than the continuous phase. Results for the breakup of a surfactant laden water jet into 10 cSt silicone oil are presented below. Figure 6.18 shows the dimensionless breakup length and Figure 6.19 shows the dimensionless Sauter mean diameter.

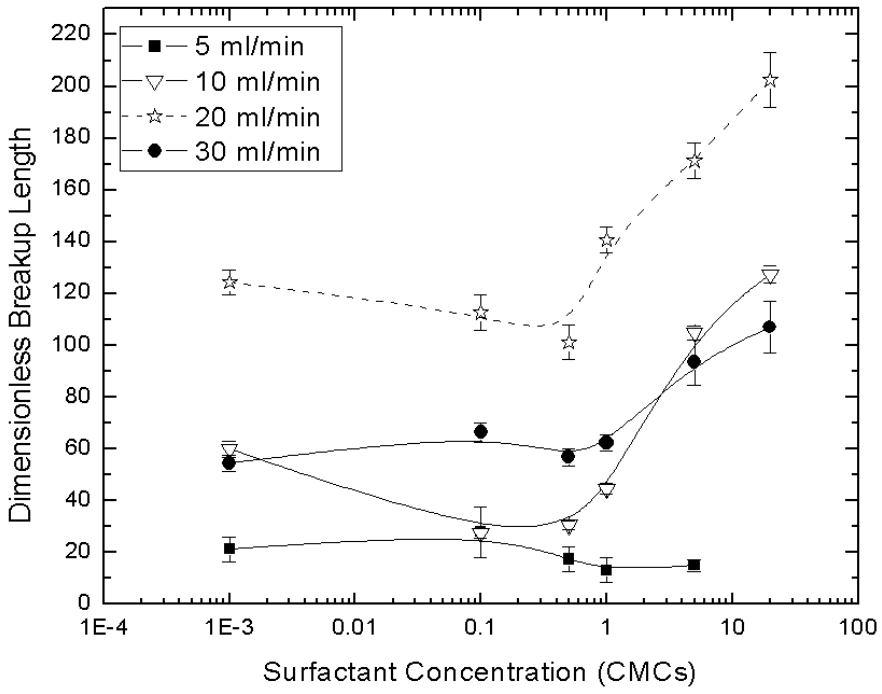

Figure 6.18 – Effect of Triton X-100 surfactant concentration on dimensionless breakup length for a jet of an aqueous surfactant solution into 10 cSt Silicone Oil. Capillary diameter was 0.6 mm

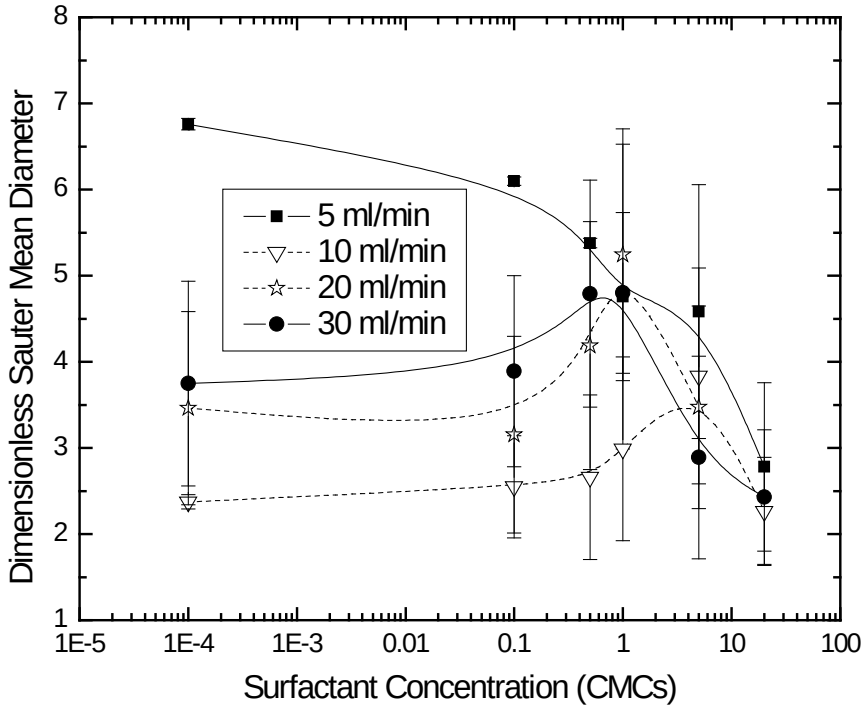

Figure 6.19 – Effect of Triton X-100 surfactant concentration on dimensionless Sauter mean diameter for a jet of an aqueous surfactant solution into 10 cSt Silicone Oil. Capillary diameter was 0.6 mm

6.2: Discussion of Results

Laminar Axisymmetric Jets of one viscous liquid into another are a difficult system to study and model, as it is a coupled system where perturbations in the jet phase (due to capillary instabilities for instance) cause perturbations in the continuous phase and vice versa. As such, simplified models like linear stability, slender jet and even higher order stability theory cannot accurately resolve the physics of the flow, even before the situation is confounded by the addition of surface active agents. In order to predict jet breakup behavior, the complete Navier-Stokes equations (or approximations thereof) must be solved for both the inner and outer fluid. Since this is a laminar flow, these equations can be solved analytically – however, the simulation is still computationally very intensive due to the large range of temporal

and special variation in the instabilities. Homma et al (2006) performed a detailed DNS simulation on a liquid-liquid jet similar to the ones used in this study requiring months of computational time to achieve accurate results. Consequently, mechanistic modeling of this system is not practical. A semi-empirical model is proposed in Section 6.3.

6.2.1 Oil-in-Water Jets

An extensive series of experiments involving jets of one viscous liquid into another was performed. Due to the significant viscosity of the continuous phase, jets do not break up exclusively due to capillary instabilities, but also due to shear layer instabilities. Under most experimental conditions, the shear instabilities were found to be negligible, as they were of insufficient magnitude to cause breakup, and were viscously dissipated quickly. However, under certain circumstances, the frequencies of the shear instabilities were able to interfere constructively with the capillary instabilities and cause the jet to break up pre-emptively. This is seen clearly in Figure 6.2 – At Reynolds numbers between 25 and 50, we see a decrease in Dimensionless Jet Breakup Length with increasing Re in the axisymmetric jetting regime, where we expect a significant increase, as predicted by Figure 2.6. While difficult to describe in text, this constructive interference is clearly evident from the high speed video. Figure 6.20 shows a series of images from the high speed video to attempt to illustrate the phenomenon. Further increases in the Reynolds number (resulting in higher jet velocity) causes the wavelength of the capillary and shear layer instabilities to shift sufficiently to no longer interfere constructively and the jet length increases significantly, resulting in a very sharp transition between jets of a

very short length and jets of a very long length. This phenomenon was only observed in surfactant-free jets, as Marangoni stresses, even of small magnitudes, appear to be sufficient to suppress these shear layer instabilities.

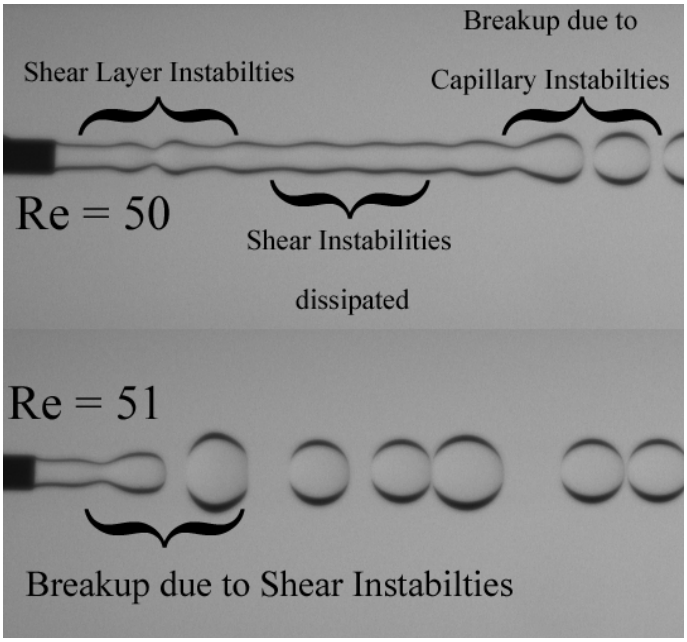

Figure 6.20 – Breakup of jets due to shear instabilities under rare circumstances

The behaviour of oil-in-water jets is quite different that that observed in water-in-air jets. While with water-in-air jets we observed decreasing droplet diameters with increasing Reynolds number, the results for oil-in-water jets are much more regime dependent. As before, the largest droplets were produced during dripping flow. However, in axisymmetric jetting flow, very small droplets are produced, which increase in size to the asymmetric jetting transition, and then decrease in size again. This can be attributed to the viscous drag on the droplets exerted by the continuous fluid. As a droplet starts to form on the end of the jet, it experiences additional drag due to its increasing size. This causes the droplet to slow, resulting in additional fluid being 'pumped' into the droplet, further enlarging it. When the droplet does

eventually detach, it has been enlarged significantly. Once the jet velocity is sufficiently high (in asymmetric jetting), the surrounding fluid is entrained at sufficiently high velocity to reduce this drag phenomena. In fact, at very high jet velocity, this entrained fluid flow is sufficient to remove the enlarging droplet from the tip of the jet due to drag in the opposite direction. Again, these effects are clearly visible from the high speed video. Figure 6.21 shows a series of images from an 8000 fps recording of the breakup of a 0.84 mm jet of 10 cSt silicone oil into deionized water at 20 ml/min, which corresponds to the longest observed axisymmetric jet, which illustrates this phenomena. In Figure 6.21 a total of 3 fluid nodes are observed entering the droplet before final breakup is achieved.

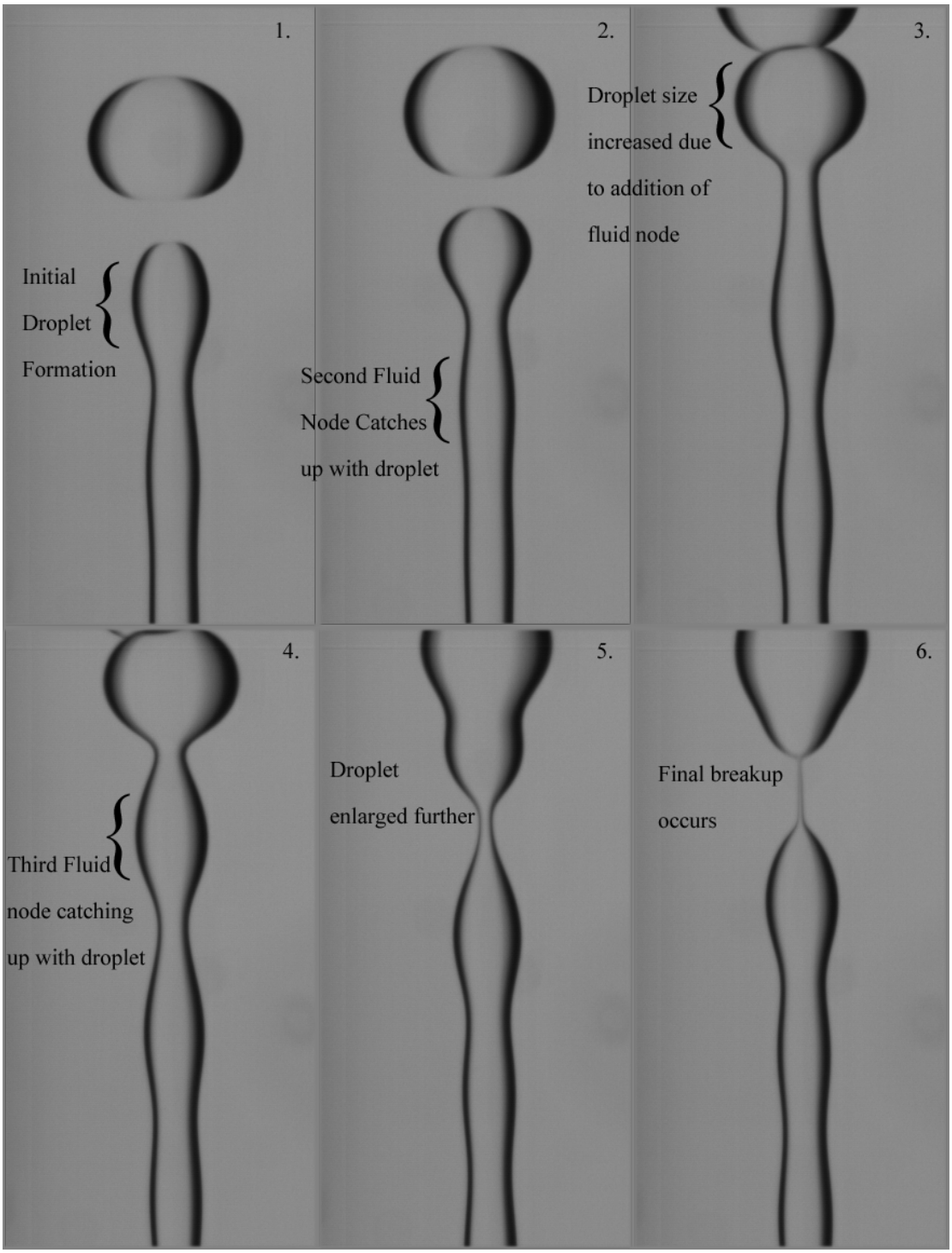

Figure 6.21 – Droplet enlargement due to viscous drag allowing multiple fluid nodes to enter a forming droplet head. Breakup of a 0.84 mm 10 cSt silicone oil into deionized water jet at 20 ml/min. Recorded at 8000 fps

6.2.2 Surfactant-laden Oil-in-Water Jets

A parametric study of surfactant-laden oil jets into water was performed, using two different surfactants – Triton X-100 and Tergitol TMN-6. The parameter space explored was a range of capillary diameters between 0.41 and 0.84 mm, volumetric flow rates between 5 and 30 ml/min, and surfactant concentrations between 0 and 20 times the critical micelle concentration (CMC) of the surfactant.

Figures 6.3 and 6.4 show the effect of surfactant concentration on the dimensionless Sauter mean diameter of droplets resulting from the breakup of a 10 cSt silicone oil jet into aqueous solutions of Triton X-100. The surfactant concentration of 1E-4 represents the deionized water case. Since the Reynolds number poorly correlates the experiments performed with different capillary diameters, the figures are separated by flow rate (Figure 6.3) and capillary diameter (Figure 6.4). Results using the smallest flow rate are presented in Figure 6.3A, the moderate flow rate in Figure 6.3B, and the largest flow rate in Figure 6.3C. Similarly, Results using the smallest, moderate, and largest capillary are presented in Figures 6.4A, B, and C respectively.

Figure 6.3A clearly shows the transition from dripping flow to jetting flow. The open symbols indicate dripping flow, as also evidenced by the large droplet sizes. As surfactant concentration increases, droplet size for both the largest and moderate diameter jets are observed to decrease in size significantly when the surfactant concentration exceeds 1 CMC. In the case of the largest (0.84mm) capillary, the dimensionless Sauter mean diameter decreases from around 7 to around 2.5,

comparable to the droplets produced by the other size capillaries at high surfactant concentration.

Figure 6.3B shows a different phenomenon. In this case, all jets exist in the axisymmetric jetting regime. With increasing surfactant concentration, droplet size is essentially constant until a surfactant concentration of around 1 CMC, then increases with increasing surfactant concentration. Increasing surfactant concentration increases the magnitude of the Marangoni stress and decreases the Weber number, both of which have the effect of reducing the growth rate of the instabilities and increasing the dominant wavelengths of breakup by suppressing high frequency oscillations, resulting in larger droplets being produced (longer wavelengths of breakup result in larger fluid nodes, which ultimately result in larger droplets).

Figure 6.3C shows the final of the 3 flow regimes. At the highest flow rates, these jets are operating in the asymmetric jetting regime. Very little change in droplet size is observed with increasing surfactant concentration in this case. We have attributed this to the fundamentally different breakup mechanism at play under asymmetric jetting. Unlike axisymmetric jetting where the continuous phase is relatively quiescent, in asymmetric jetting there is significant movement of the continuous fluid. The three-dimensional movement of the jet fluid causes large scale recirculation zones in the continuous fluid, which tends to 'tear' large chunks of fluid from the tip of the jet, and then further break these chunks down into smaller droplets. While the flow is fully laminar, these large scale recirculation zones resemble turbulence, albeit

only at very large scales. Since these bulk fluid motions are responsible for the breakup of the jet, the momentum of these large sections of fluid are sufficient to overwhelm the surface forces and as such are insensitive to the magnitude of the Marangoni stress and therefore the surfactant concentration. Secondary breakup events are also commonly observed under asymmetric jetting conditions (the free droplets are observed to break up again in the recirculation zone downstream of the primary breakup location). This results in a very broad droplet size distribution and much larger populations of very small satellite droplets, as observed in Figure 2.7.

In order to better quantify the effect of surfactants on the nature of the jetting regime transitions, a series of 'phase diagrams' were constructed. Figures 6.22 through 6.24 show the approximate locations of the zones of the three phase regimes (dripping flow, axisymmetric flow, and asymmetric flow) at several surfactant concentrations on the jet velocity-capillary diameter plane. Figure 6.25 is reproduced from Clanet and Lasheras (1999) and shows a similar phase diagram for the transition between dripping and (axisymmetric) jetting flow. They include a transitional form labeled as 'Dripping Faucet' between these two which was not observed in our study.

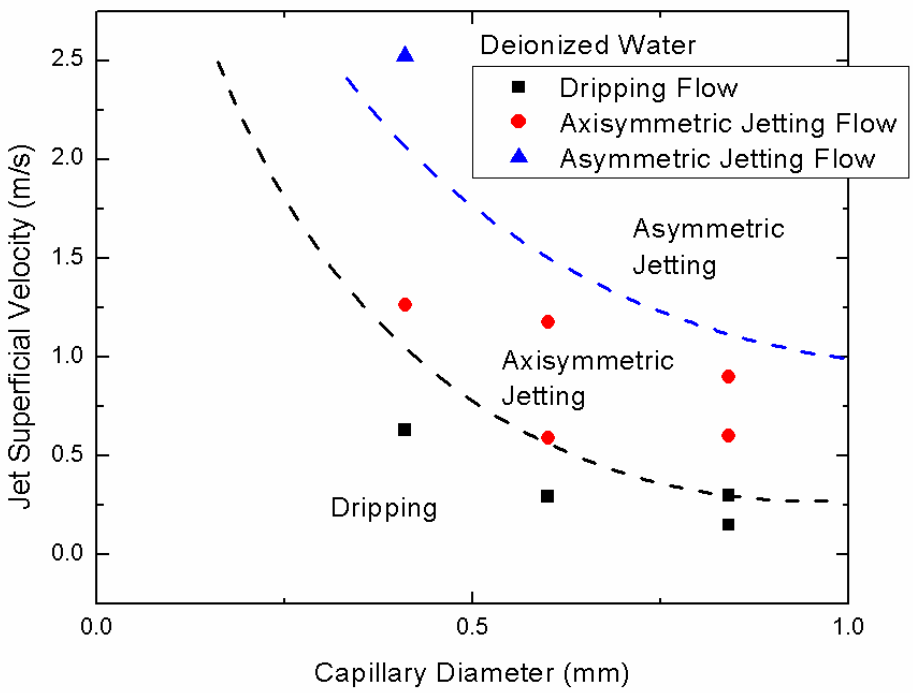

Figure 6.22 – Phase diagram showing the approximate location of transitions between jetting, axisymmetric, and asymmetric jetting regimes for jets of 10 cSt silicone oil in deionized water

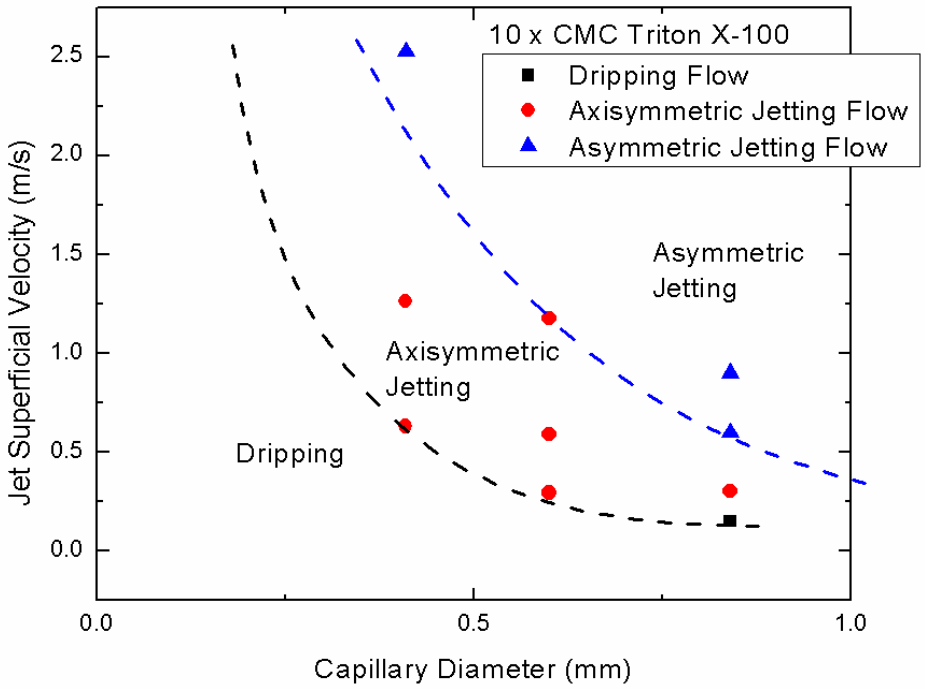

Figure 6.23 – Phase diagram showing the approximate location of transitions between jetting, axisymmetric, and asymmetric jetting regimes for jets of 10 cSt silicone oil in a 10 x CMC solution of Triton X-100 surfactant in water

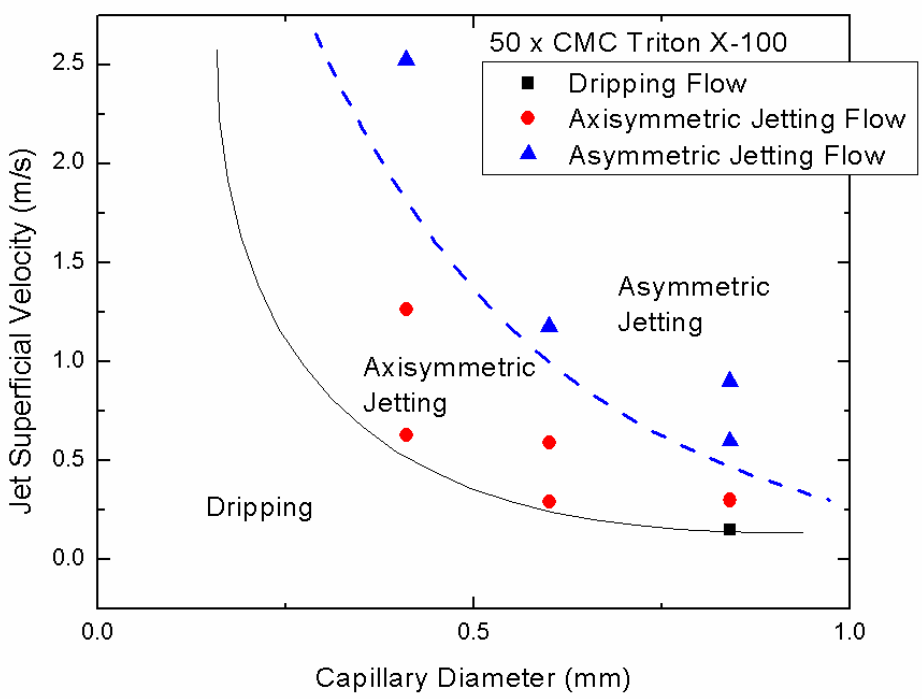

Figure 6.24 – Phase diagram showing the approximate location of transitions between jetting, axisymmetric, and asymmetric jetting regimes for jets of 10 cSt silicone oil in a 50 x CMC solution of Triton X-100 surfactant in water

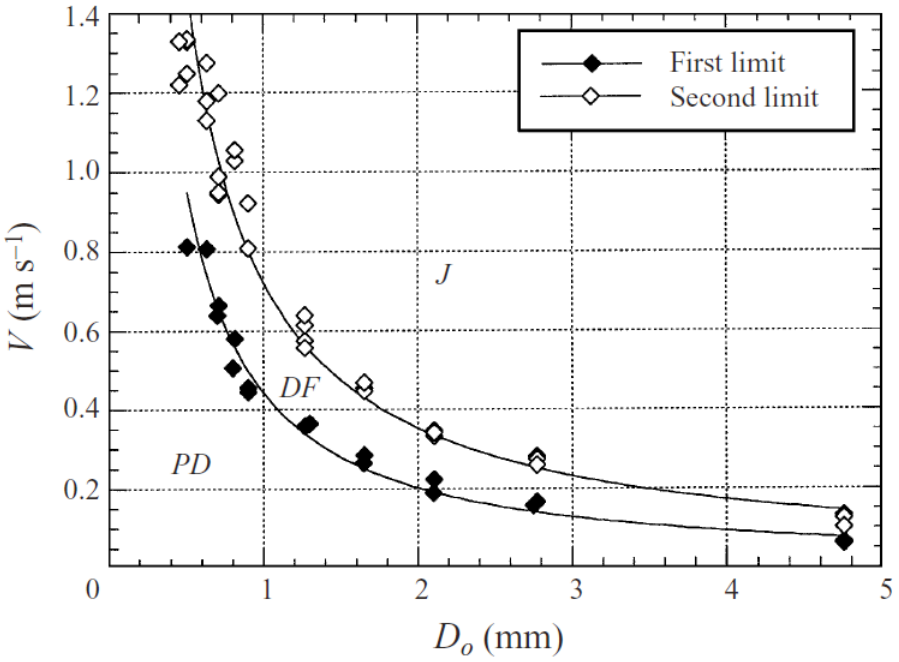

Figure 6.25 – Phase diagram showing the transitions between (axisymmetric) Jetting (J), 'Dripping Faucet' (DF), and 'Periodic Dripping' (PD) regimes for jets of deionized water into air – Reproduced from Clanet & Lasheras (1999)

As shown in these figures, the addition of surfactants causes the transitional boundaries between dripping/jetting regimes to be shifted. The lines shift toward both smaller jet diameters and smaller jet velocities, resulting in experimental conditions at the same diameter and velocity to occur within different flow regimes based on the changes in surfactant concentration. From Figure 6.25 we see qualitatively similar behavior between the dripping-jetting transition in the literature air-water jets and our oil-water jets, although the precise location of the transition varies due to the different experimental conditions. Significantly more data collection around the transition points would be necessary to identify if the intermediate 'Dripping Faucet' regime proposed by Clanet & Lasheras (1999) occurs in the liquid-liquid system or if the viscous continuous phase suppresses the unstable dripping phenomena.

Figures 6.5 and 6.6 show the effect of surfactant concentration on the breakup length of a 10 cSt silicone oil jet into aqueous solutions of Triton X-100. The surfactant concentration of 1E-4 represents the deionized water case. As with the droplet size figures, results are separated by flow rate (Figure 6.5) and capillary diameter (Figure 6.6). Results using the smallest flow rate are presented in Figure 6.5A, the moderate flow rate in Figure 6.5B, and the largest flow rate in Figure 6.5C. Results using the smallest, moderate, and largest capillary are presented in Figures 6.6A, B, and C respectively.

Figure 6.6A shows the effect of surfactant concentration on breakup length for the experiments with the largest Re. As predicted by Figure 2.6, the intermediate flow rate (circular symbols) produces the longest jet due to the presence of asymmetric waves on the higher velocity jet (triangles).

In all cases, a pronounced increase in jet breakup length is noted with increasing surfactant concentration. Jet length is constant at concentrations below the CMC, and then increases strongly at concentrations above the CMC. The primary reason for this is that increasing surfactant concentration gradients on the jet surface increases the magnitude of the Marangoni stresses, which act to oppose any change in the surface area. Marangoni stresses arise when new interfacial area is created (in this case due to the formation of a surface instability). These new interfaces contain no surfactant, causing gradients in interfacial tension between regions of 'old' surface area (which has a certain amount of surfactant adsorbed) and this 'new' surface area. The Marangoni stress can either be relieved by this 'new' surface area being removed (that is, the surface returning to its previous shape) or by the new surface becoming populated with an equal concentration of surfactant from the bulk. Thus, when a capillary wave attempts to cause the jet to break, the Marangoni stress resists the capillary forces and maintains the jet's diameter. That opportunity for the jet to break is missed, and the jet is able to grow at least one wavelength longer. As the capillary wave grows in magnitude further downstream it is eventually able to overcome the Marangoni stress, but this results in a jet which is significantly longer than one which does not have sufficient surfactant coverage. Additionally, increasing surfactant concentration downstream on the jet's surface causes a decrease in interfacial tension,

which increases the Weber number. As seen in Equation 2.9 increasing Weber number results in increased jet breakup lengths.

Since surfactant must diffuse from the surrounding aqueous phase to the jet surface, the effect of the bulk surfactant concentration strongly influences the jet breakup phenomena even at concentrations exceeding the CMC where the static interfacial tension will not change. This shows that the jet surfaces are not fully surfactant coated (eg, a complete monolayer has not yet formed). Since the surface can accept more surfactant, the rate of mass transfer from the bulk to the interface is determined by the gradient in surfactant concentration. With higher bulk surfactant concentration, the mass transfer gradient is high, and as such the rate of surfactant transfer is higher. This also indicates that the rate-limiting step for surfactant transport is the diffusion step, rather than the adsorption of the surfactant from the boundary layer onto the surface (which is not dependent on concentration – (Moorkanikkara & Blankschtein, (2006))). The effect is synergistic in the sense that increasing surfactant concentration allows more surfactant to reach the jet's surface in the short breakup time. This, in turn, stabilizes the jet, increasing the breakup time, which allows for yet more surfactant to diffuse to the surface, which further increases the breakup time, and so on. This is the reason for the very rapid increase in breakup length with increasing surfactant concentration. Clearly, at some point a plateau should be reached when the jet surface becomes saturated with surfactant so rapidly (or the surfactant adsorption becomes the rate-limiting step) that further increases in surfactant concentration no longer have any beneficial effect on the jet breakup length. It appears as though that plateau concentration has nearly been reached in

certain conditions (for example Figure 6.6C), as the dimensionless breakup length did not increase as much between the 20 CMC and 50 CMC values as for the 1 CMC to 10 CMC and 10 CMC to 20 CMC ranges. Testing at higher concentrations is not possible with the current experimental setup as at higher concentrations the continuous phase starts to become opaque as the concentration approaches the cloud point of the surfactant (the cloud point is the condition such that micelles are so populous that they scatter light).

Figures 6.7 and 6.8 show that the effects of Triton X-100 and Tergitol TMN-6 on the breakup of a silicone oil jet into water are extremely comparable when normalized by the critical micelle concentration. The primary differences are that the transition from dripping flow to jetting flow for low velocity jets is observed to occur more gradually with increasing surfactant concentration, as opposed to the sharp transition observed with the Triton X-100. This is attributed to the fact that the CMC for Tergitol TMN-6 is more than an order of magnitude higher than for Triton X-100 (see Table 3.1). This means there is a larger absolute concentration of surfactant molecules in solution, allowing there to be more diffusion to the surface for slowly developing jets (however, since the CMC is much higher, the effect of the surfactant remains small until large concentrations are achieved since this surfactant is not as 'effective' – it's branched structure does not allow for it to pack as tightly onto the interface). There is also some slight differences at very high surfactant concentrations, but at these high concentrations the volumetric fraction of the Tergitol TMN-6 solution may be high enough to be altering the bulk fluid properties due to its large CMC value (at a

concentration of 50 CMC, the volumetric fraction of Tergitol TMN-6 is approximately 1%). To avoid the possibility of the surfactant fluid potentially changing bulk phase properties (density, viscosity, etc.), Triton X-100 surfactant was used exclusively for the remaining experiments.

6.2.3 Modified Viscosity Ratio Oil-in-Water Jets

In order to determine the role variations in viscosity have on the breakup of a jet, several experiments were performed in which silicone oils of higher viscosities were utilized. Surfactant effects have been proposed to act by increasing the 'surface viscosity' as the action of the Marangoni stress is similar to the action of viscosity, by reducing the ability of the free surface to be deformed by shear.

In Figure 6.9 it is observed that as the jet phase viscosity increases from 10 to 50 cSt, jets at low velocity (eg, in the dripping regime) increase in diameter. These silicone oils were found by Padron (2005) to have the same density and interfacial tension with water regardless of their viscosity grade, therefore the difference can only be attributed to the increased resistance of the fluid to flow around the droplet, allowing it to grow slightly larger before detaching. In the axisymmetric jetting regime (10 ml/min), droplet size was also observed to increase. This fits with our theoretical predictions, as when viscosity increases, that increases the value of the Ohnesorge number, which as seen in Figure 2.4, reduces the rate at which instabilities can propagate in the jet, resulting in longer jet breakup lengths and larger droplets (due to larger fluid nodes). Interestingly, at the highest flow rate, we see a transition from the

asymmetric jetting regime at low viscosity back to the axisymmetric regime at high viscosity. Consequently we see a decrease in droplet diameter between the data point at 10 cSt and the data point at 20 cSt. Between 20 and 50 cSt we see an increase in droplet size consistent with our understanding of the behaviour of axisymmetric jets. This transition is attributed to the fact that the more viscous oils are able to damp out the 3-dimensional instabilities responsible for the onset of asymmetric flow, resulting in the axisymmetric-asymmetric transition occurring at higher flow rates relative to the lower viscosity oil.

Figure 6.10 shows the effect of jet phase viscosity of breakup length. For the lowest flow rate, undergoing dripping flow, we observe little change with increasing viscosity, as no stable jet is formed in any of the 3 cases. For the largest flow rate, increasing jet length is observed with increasing viscosity, consistent with the transition back to axisymmetric jetting noted previously. For the moderate flow rate, droplet size is observed to go through a maximum at 20 cSt. For the 10 ml/min data set, it was observed that at the highest viscosity, the jet was breaking up in a 'pseudo-dripping' type regime. A droplet would form at the capillary tip, similar to dripping flow, but after it detached from the capillary rim, it remained supported by a fluid thread, resembling dripping flow. Once the single large droplet would detach, the fluid thread would retract back toward the capillary tip and add its volume to form a new droplet. A series of photographs from this experiment is included in Figure 6.26. It appears that the higher viscosity grades of this silicone oil experience some non-

Newtonian behaviour – the apparent elasticity of this fluid is even more pronounced when surfactants are introduced.

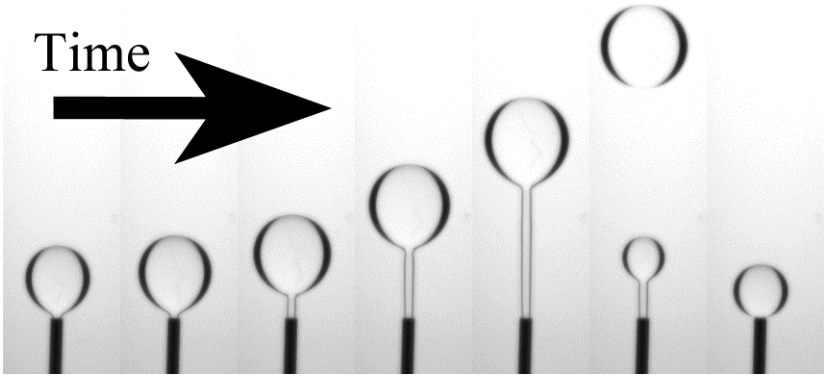

Figure 6.26 – Breakup of a viscous liquid jet at moderate flow rate – 'pseudo-dripping' phenomena. Capillary diameter was 0.6 mm, flow rate was 5 ml/min, oil viscosity was 20 cSt

Experiments were also performed where Triton X-100 surfactant was added to the aqueous phase combined with the increased viscosity continuous phase. Figures 6.11 and 6.12 show the effect of these combined effects of surfactants and viscosity on droplet diameter and jet breakup length, respectively. In Figure 6.12, we see that at high fluid velocity and high surfactant concentration, we observe a very significant increase in breakup length with increasing viscosity – to a value beyond our ability to measure due to the physical dimensions of our equipment. Even at moderate flow rate we saw a significant monotonic increase in breakup length with increasing viscosity. This is attributed to the fact that (as seen in the previous two figures, 6.9 and 6.10) higher viscosity jets are able to develop longer breakup lengths due to their inherent resistance to flow. This results in a longer breakup time, allowing more surfactant to diffuse to the interface. This reduces the interfacial tension, further stabilizing and elongating the jet. The fluid's viscosity also works synergistically

with the Marangoni stress, as both act to oppose deformations of the fluid surface. From Figure 6.11, it was found that the addition of surfactants did not strongly effect the droplet sizes measured for the jetting flow conditions (10 and 20 ml/min, respectively), but did reduce the size of droplets produced by the 5 ml/min condition by causing a transition from the dripping flow regime to the jetting flow regime at high surfactant concentration. In the case of jet breakup, it has been found that droplet size is determined more strongly by the continuous fluid properties than the surface properties at high viscosity ratios.

The most interesting phenomena for high viscosity surfactant laden systems occur under dripping flow. The combination of high viscosity ratio and low fluid velocity allow significant surfactant diffusion, giving rise to a strong surface elasticity. Figure 6.27 shows example images for surfactant laden viscous continuous phase conditions under dripping flow. This phenomenon is observed to be similar to the clean interface case (Figure 6.26), but significantly exaggerated, as the inherent surface elasticity of the viscous oil is enhanced by the presence of the surfactant. Due to the rapid contraction of the 'jet' component of the fluid after the large droplet detaches, the surfactant which has diffused onto that exposed fluid cylinder will be transferred onto the surface of the newly formed droplet, resulting in a much higher surfactant concentration than it would otherwise have achieved (since the droplet has a much smaller surface area to volume ratio than the cylinder that created it – effectively 'concentrating' the surface area). At higher surfactant concentration, this phenomena is suppressed and the jet breaks up in the axisymmetric mode.

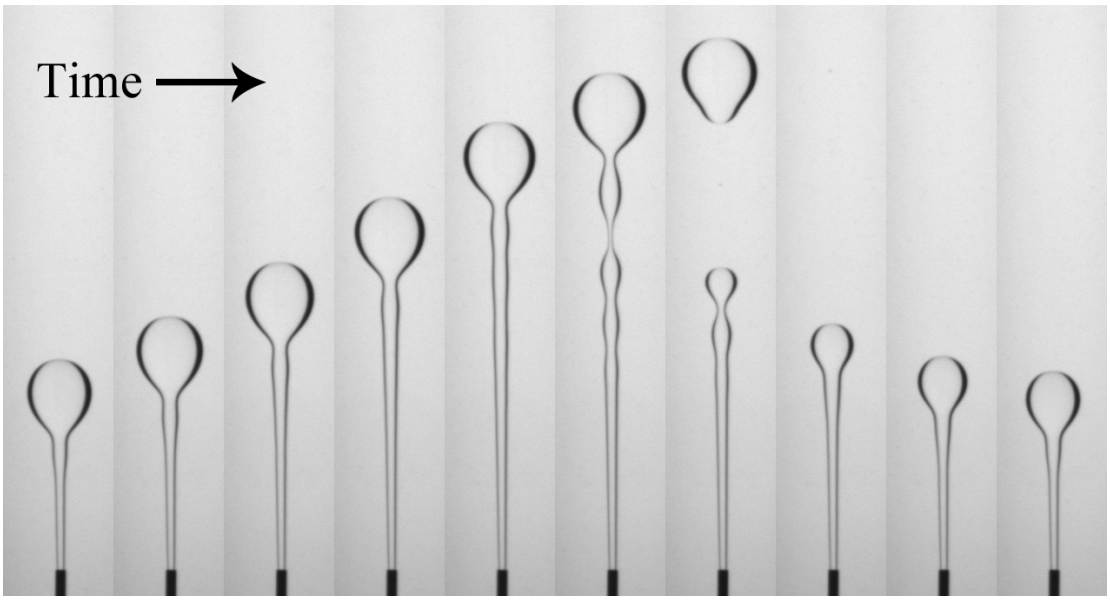

Figure 6.27 – Dripping-type flow for a jet of high viscosity silicone oil (50 cSt) into a 1 CMC solution of Triton X-100 surfactant at 5 ml/min

Due to the additional complexity of the elastic behaviour of the higher viscosity silicone oils, the data from these experiments was excluded from our model.

6.2.4 Modified Interfacial Tension Oil-in-Water Jets

If the primary action of surfactants is to simply reduce the interfacial tension of a fluid surface (that is, if the Marangoni stress can be neglected), then results using a surfactant would be reproducible using clean interfaces of fluids with corresponding interfacial tension values. To test this hypothesis, a series of experiments utilizing a methanol-water solution as the continuous phase was performed. As seen in Figure 6.13, the interfacial tension of silicone oil with aqueous methanol solutions is a function of methanol concentration and decreases from around 45 mN/m (pure water) to around 3 mN/m (pure methanol). However, since methanol is less dense than water, only the concentration range from 0-30% methanol (by weight) can be used

without significantly altering the buoyancy of the dispersed phase and adding additional confounds to the problem (eg, the Bond number must be maintained constant to within a few percent before buoyancy effects become noticeable). From Figure 6.13, we see that this corresponds to a lower limit of approximately 25 mN/m.

From Figure 6.14, we can see that breakup length was found to increase with decreasing interfacial tension. This is consistent with the theoretical background which predicts that as σ decreases, the Ohnesorge number increases, resulting in slower propagation of instabilities and longer breakup times. We also see that for a particular combination of capillary diameter and fluid velocity, this increase is roughly linear, as predicted by the linear stability model.

Figure 6.15 shows the effect of methanol concentration on droplet size. Droplet size is seen to increase with increasing methanol concentration (decreasing interfacial tension) in the 0-20 wt% methanol range, and then is observed to decrease between 20-30 wt%. The initial decrease fits well with our current understanding of jet breakup – as interfacial tension decreases, the Ohnesorge number increases, which decreases the growth rate of instabilities and results in longer dominant wavelengths for breakup. This results in larger fluid nodes forming as the jet destabilizes and therefore, larger droplets are formed. The decrease in droplet size observed between 20 and 30 wt% methanol for the lower flow rates is likely a result of a change in the Bond number, meaning that the buoyancy effect on droplet breakup is having an observable effect on droplet size. This hypothesis is reinforced by the observation

that the highest velocity jet – the 30 ml/min case – continues to grow in size over the entire methanol concentration range. The higher jet velocity will mean that the inertial forces will dominate over the buoyancy forces, meaning the small deviation in the Bond number will play a weaker role and the balance between interfacial and viscous forces will determine the droplet size. It is currently undetermined precisely what impact the Bond number has on droplet breakup, however, since the Bond number was held constant under all other experimental conditions, it was considered outside the scope of this study, although has been suggested as future work.

Figure 6.16 compares the breakup length of a silicone oil jet into a methanol-water solution to the breakup of a jet into aqueous surfactant solutions. The x-axis shows the equilibrium interfacial tension, allowing for the comparison of the two, since both surfactants and methanol will reduce the interfacial tension of the aqueous phase. As clearly observed in the figure, we do not see the data points for the methanol-water solutions collapsing onto the data collected from the surfactant-laden jets. For experimental conditions with comparable equilibrium interfacial tension values, we see that the methanol-water solutions produce jets of much longer length than the surfactant-laden water solutions. Additionally, we observe that the surfactant concentration must meet or exceed the CMC (corresponding to the stacked points at an equilibrium interfacial tension of 3 mN/m) in order to produce jets of length comparable to the methanol-water solutions. Therefore, we can say that the equilibrium interfacial tension of the solution with the oil is not sufficient to fully describe the phenomena. The jet breakup time, especially at low surfactant

concentration, is simply too short relative to the diffusion time for sufficient surfactant to reach the interface in sufficient quantity to effect jet breakup. Therefore, while at a concentration of 10% of the CMC, the equilibrium interfacial tension may be ~22mN/m – comparable to a 30% solution of methanol in water – the actual (dynamic) interfacial tension of the droplets being produced at the top of the jet is much higher – comparable to a jet with no surfactant at all (~45 mN/m). Similarly, a jet with a surfactant concentration well above the CMC, whose equilibrium interfacial tension is around 3 mN/m, is found to have a dynamic interfacial tension at breakup of around 20-30 mN/m, based solely on the corresponding breakup length as compared to the methanol water solution. Therefore, we are able to produce the following plot, Figure 6.28, showing the corresponding relative interfacial tension as a function of breakup time – that is, based on the interfacial age of the jet, indicating how close to the equilibrium value of interfacial tension that jet is. At the long time limit (generally occurring in dripping flow), this value approaches unity, indicating that the interfacial tension is at or near the equilibrium value. At very short breakup time (high velocity jets), the value is quite high, indicating that the effective interfacial tension is much higher than the equilibrium value (eg, is near the clean interface value).

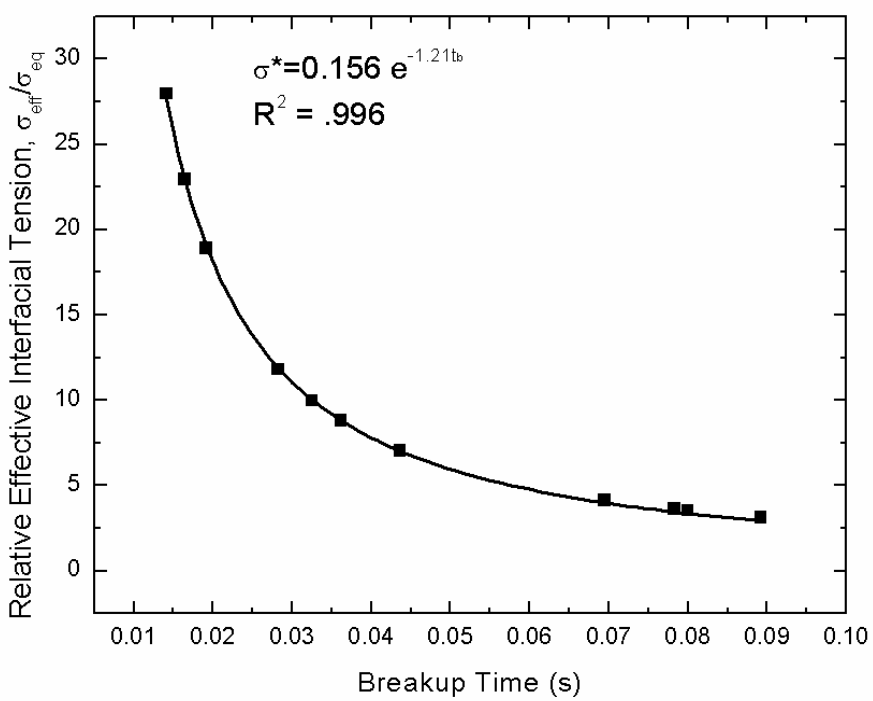

Figure 6.28 – Effective interfacial tension based on breakup time – calculated by matching surfactant laden jet breakup length with jets breaking up in solutions of methanol in water with corresponding constant interfacial tensions

The trend observed in Figure 6.28 is that of an exponential decay, which is consistent with the mechanism of surfactant absorption (see Figure 3.6). By fitting the exponential decay, Equation 6.1 can be calculated. The two parameters in this equation will vary based on the diffusivity of the surfactant, and therefore will vary if the temperature, surfactant type, or viscosity ratio is changed, but does not depend on the surfactant concentration.

$$\sigma^* = C_1 e^{-C_2 t_b}$$
$$C_1 = 0.156 \quad C_2 = 1.21 \tag{6.1}$$

where σ^* is the relative effective interfacial tension as defined in Figure 6.28, t_b is the breakup time (the breakup length divided by the superficial jet velocity), C_1 and C_2 are empirical fitting parameters.

6.2.5 Water-in-Oil Jets

Figure 6.18 shows the effect of surfactant concentration on the breakup length of an aqueous jet into a viscous oil phase. This represents the opposite case to the previous data in that the surfactants are present in the jet phase instead of the continuous phase. Additionally, the viscosity ratio is less than unity, as the continuous oil phase is approximately 100 times more viscous than the jet phase.

Jet breakup lengths were observed to consistently go through a minimum between 0.5-1xCMC concentration of surfactant in the jetting phase. The decrease in jet length between the no surfactant and minimum jet length case is only a difference of approximately 10% in all cases, and the precise mechanism by which this occurs is not well understood. From Figure 6.19 it is seen that there is a corresponding maximum in droplet diameter. The increase in droplet diameter explains the decrease in jet length (since for a fixed volume of fluid, if more fluid is in the droplets, less can be contained in the fluid cylinder), however the underlying cause for the droplet maxima/jet minima is currently unexplained. A similar phenomenon was observed by Padron (2005) in high shear mixers, and is discussed in greater detail in section 6.4.

Beyond the maxima, jet breakup lengths were observed to increase significantly with increasing surfactant concentration, consistent with previous findings in the oil-in-water jets. Asymmetric jets were also found to increase with increasing surfactant concentration. For oil-in-water jets it was found that under asymmetric jetting

conditions, the continuous fluid motion was responsible for jet breakup, and that there was significant continuous fluid motion caused by the 3-dimensional instabilities and high velocity of the jet. However, for the water-in-oil jet the jet phase is unable to impart as much momentum on the continuous fluid, even at high jet velocities, due to the low viscosity ratio. As such, very little continuous fluid motion is observed outside a narrow boundary layer of entrained oil flow. As such the continuous fluid motion (or lack thereof) plays a much smaller role in the jet breakup and the surface forces are not overwhelmed. Thus, the reduction in interfacial tension caused by the increasing surfactant concentration has a significant effect on the jet breakup length, allowing the jet to increase in length even under asymmetric jetting conditions. The behaviour under axisymmetric jetting conditions is consistent with our previous observations. Under the lowest flow rate condition – 5 ml/min – we observed a transition from dripping flow to axisymmetric jetting flow once the surfactant concentration exceeded 0.5 x CMC, comparable to the oil-in-water case. The jet length was not observed to increase as significantly as in the oil-in-water case, however, from Figure 6.19 a strong decrease in the droplet size is observed, indicating that the breakup had indeed transitioned into the jetting mode (confirmed by examining the high speed imagery). Overall, the viscous continuous phase acted to significantly reduce the magnitude of surface instabilities, resulting in longer jets and larger droplets. A more thorough investigation of the effect of low viscosity ratios on jet breakup is needed to separate the effects of surfactants from the effects of continuous phase viscosity, and has been proposed in the Future Work section.

Testing using oil-phase surfactants to determine if directionality of surfactant diffusion is significant is also recommended.

6.3: Model Validation

In Chapter 4 a semi-empirical model to determine the breakup length of a surfactant laden jet was proposed (Equation 4.6). Figure 6.29 shows the results for the model with utilizing the long-time solution of the Ward-Tordai equation (Equation 3.20) to estimate the instantaneous interfacial tension.

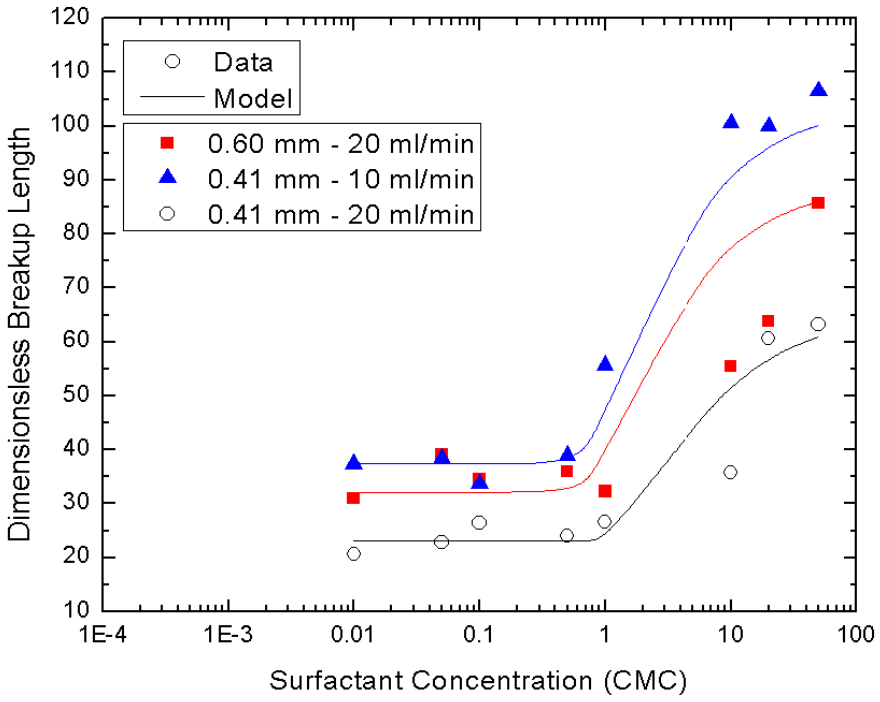

Figure 6.29 – Comparison of measured dimensionless breakup lengths with those calculated using equation 6.6, with instantaneous interfacial tension values predicted using equation 3.20 for a jet of 10 cSt silicone oil into aqueous surfactant solutions

The agreement between the model and the measured values is quite good. The model succeeds in accurately predicting what concentration of surfactant is sufficient to cause the jet length to diverge from the no-surfactant case (experimentally determined

to be at ~1 CMC surfactant concentration), and also predicts the rate of increase of the jet breakup length with increasing surfactant concentration with reasonable accuracy.

The weakness of this model is that it is only able to accurately predict the transition point and elongation for jets within the axisymmetric jetting regime. For jets starting in, or transitioning to, the asymmetric jetting regime, a similar increase in jet length is predicted (since the interfacial tension is calculated to decrease) although experimentally no increase is observed since the breakup of the jet is not due to the same capillary instabilities. Similarly, the model is unable to predict the transition from dripping flow to jetting flow, and so significantly under-predicts jet breakup lengths for cases starting in dripping flow and transitioning to axisymmetric jetting at moderate surfactant concentration. Higher concentration data points can be fitted by estimating an 'equivalent jet length' – that is, using the model 'backwards' to predict what the zero-surfactant jet length would be assuming the jet remained in axisymmetric flow as surfactant concentration is reduced - however this is largely a thought exercise with limited usefulness.

We have demonstrated a powerful model to determine the effect of surfactant concentration on the breakup of a laminar liquid jet, utilizing the physicochemical properties of the surfactant, as well as the properties of the fluids in use and the geometry of the jet. While previous knowledge of the clean interface jet length is needed for prediction of the surfactant-laden length, in the absence of reliable

experimental results there are several computational fluid dynamics techniques for estimating this quantity with reasonable accuracy, as discussed in Chapter 2.

6.4: Applications to High Shear Mixing

This study was conducted under the auspices of the High Shear Mixing Research Group at the University of Maryland, and as such it was hoped that this work would be useful in the field of High Shear Mixing. To that end, the data from laminar axisymmetric jets is compared to the data collected from a Silverson L4R Batch Rotor-Stator Mixer. The system in question is identical in both cases, with 10 cSt silicone oil as the dispersed phase and aqueous solutions of Triton X-100 as the continuous phase. While the mixer operates in turbulent flow and the jet in laminar flow, there are qualitative similarities between the data. Figure 6.30 shows the effect of surfactant concentration on the dimensionless Sauter mean diameter for droplets produced by a laminar jet at the high and low end of the Reynolds number range studied. Figure 6.31 shows a similar plot for the size of droplets produced by a high shear mixer (Data from Padron, (2005)). There is no corresponding quantity to the breakup length for a high shear mixer, and so those values are not compared.

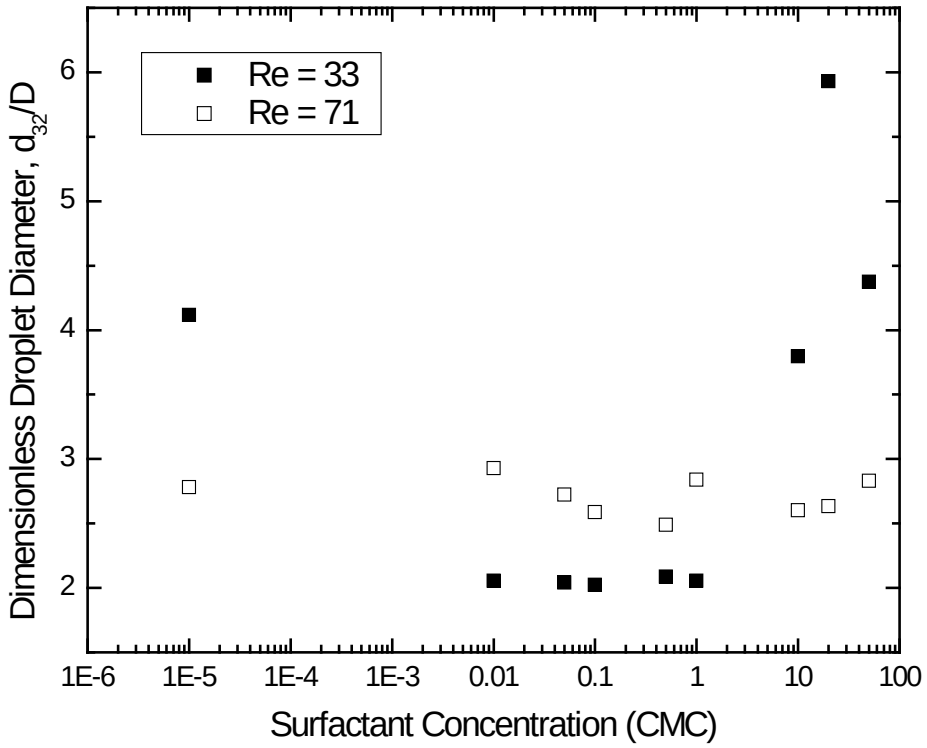

Figure 6.30 – Effect of Triton X-100 surfactant on the size of droplets produced by a laminar axisymmetric jet of 10 cSt oil into water at high and low Reynolds number

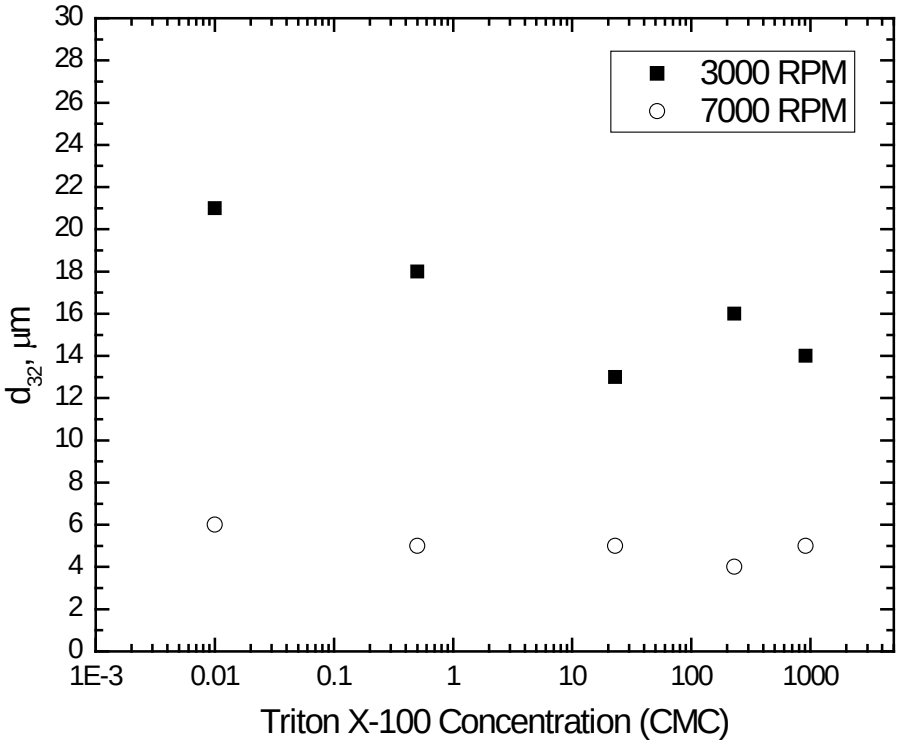

Figure 6.31 – Effect of Triton X-100 surfactant on the size of droplets produced by a high shear mixer dispersing 10 cSt silicone oil into water at high and low mixer rotor speed (mixer speed is proportional to Re)

As seen in Figure 6.30, at low Re, the droplet size goes through a minimum around the CMC of Triton X-100, due to the transition from an unstable jetting/dripping flow regime at very low surfactant concentration to a stable jetting flow regime, and then subsequent increase in droplet size due to increasing surfactant concentration attributed to reduction in interfacial tension and increasing viscosity allowing longer wavelength instabilities to dominate. At high Reynolds numbers, very little change is observed with increasing surfactant concentration, as the jet is operating in the asymmetric jetting regime where the breakup is dominated by 3-dimensional interactions between the continuous and jet phase, and not the capillary instability. As such, the interfacial phenomena are less relevant as the breakup is dictated primarily by bulk phase phenomena (as observed in section 6.1.2).

Figure 6.31 shows the effect of surfactant concentration on droplet diameters produced by a high shear mixer. Similar to the jet breakup experiment, at low Rotor speed (corresponding to low Re), droplet diameter is observed to go through a minimum at around a 1 CMC surfactant concentration. While the same breakup regime transitions are not present in the high shear mixer, the mechanism by which droplets break up is still altered based on the surfactant concentration. At low or zero surfactant concentration, droplets stretch and break into two large primary droplets (accompanied by 1 or more tiny satellite droplets) due to the system's high interfacial tension. At high surfactant loading, the Marangoni stress strongly opposes droplet deformation, meaning that the size threshold of droplets that are able to be broken is much larger, resulting in a larger mean droplet size. At moderate surfactant

concentration, droplets are able to be easily stretched by the shearing field in the high shear mixer, but when the shear is removed, the ends of the stretched drop cannot expand and reabsorb the fluid from the connecting fluid thread as easily due to the Marangoni stress, and so more fluid ends up in satellite droplets formed from that liquid bridge (resulting in smaller primary droplets). This results in an overall reduction in Sauter mean diameter at these moderate concentrations.

At high rotor speed, very little change is observed with changes in surfactant concentration, similar to the jet breakup case. In the case of the high shear mixer, this is attributed to the extremely rapid convective mass transport of surfactant to the fluid interfaces at high rotor speed, which is able to quickly resolve the Marangoni stress. There are also likely more droplet bursting-type events at these high Reynolds numbers (as opposed to droplet-stretching type breakup events) which are more sensitive to the bulk fluid properties than the interfacial properties.

While no direct correlations between high shear mixing and laminar jet breakup can be made at this time, these qualitative similarities in the data suggest that there is much to be learned about the more hydrodynamically complex systems using the laminar jet as an experimental analogue.

Chapter 7: Summary and Conclusions

In this chapter, the major results and conclusions of this study will be summarized. Given the breadth of the study, and the many different variables investigated, there are many different results to summarize. These results have been broken down by topic for the ease of the reader.

The general conclusions of the study are as follows. First; the axisymmetric laminar jet is a powerful investigative tool for analyzing the behaviour of liquid droplets and dispersions. The experimental apparatus constructed for this study allows for a large variety of different systems to be investigated, and allows for precise control of the relevant variables. The system is modular and would allow for installation of different measurement devices or changes in geometry, orientation, etc.

Secondly, we have proven that surface active agents have a significant impact on the decay of a laminar axisymmetric jet. These effects are not simply due to the reduction in interfacial tension caused by the surfactant, as the kinetics of surfactant transport on the time scale of the jet breakup phenomena have been shown to be of critical importance. Additionally, phenomena such as droplet size and breakup lengths going through minima/maxima at intermediate concentrations of surfactants cannot be explained by interfacial tension alone.

7.1: Air-Water Jets

In Chapter 5, a parametric study of surfactant laden jets of water into air was presented. Two different surfactants – Triton X-100 and Tergitol TMN-6 – were utilized. Jet flow rate, capillary diameter, surfactant concentration, and surfactant type were the primary variables investigated. The following conclusions were drawn from the data:

- Dimensionless Jet Breakup Length (L_b^*) and Dimensionless Sauter Mean Diameter (d_{32}^*) were found to increase with increasing Reynolds number (jet velocity). These changes are consistent with Rayleigh-Tomotika Linear jet theory, and are well modeled using existing ($We^{1/2}$) correlations for clean (non-surfactant laden) jets.
- Laminar jets are stabilized by the presence of surfactants. Large surfactant concentrations (relative to the CMC) are required to cause significant effects due to the long time required for surfactant to diffuse to the interface compared to the rapid breakup time. Increased surfactant concentration increases diffusive flux and allows more surfactant to reach the interface in that short time span.
- Equilibrium surface tension values are not sufficient to collapse the data based on dimensionless analysis. Therefore, the kinetics of surfactant transport are significant and are necessary for correlation of the data. The model proposed in Chapter 4 accurately predicts jet breakup length for surfactant laden jet by accounting for the rate of change of interfacial tension due to surfactant diffusion.

- The mechanism of droplet production is extremely complex for water jets into air. Surfactants have been shown to increase the size of fluid nodes by causing a shift in the dominant wavelength responsible for breakup, but also reduce the number of nodes of fluid entering the final droplets. Satellite droplet production was found to decrease with increasing surfactant concentration, however, the survival rate of produced satellite drops increased as they were less likely to be re-absorbed into a primary droplet. These competing mechanisms generally resulted in a slight reduction in the Sauter mean diameter of droplets produced with increasing surfactant concentration, but no clear trends are observed.

7.2: Oil-Water Jets

In chapter 6, viscous liquid jets into other viscous media with and without surfactants were investigated. Substantial results were reported, and are summarized below.

7.2.1 Oil Jets into Clean Water

- Three distinct regimes were identified, which depend on the flow rate, diameter, and interfacial properties of the jet. These regimes are Dripping flow, Axisymmetric Jetting flow, and Asymmetric Jetting flow. This is consistent with numerical simulation results reported in the literature.
- At constant capillary diameter and surface properties, jets transition from dripping to axisymmetric jetting and then to asymmetric jetting with increasing jet velocity (flow rate).

- For jets without surfactants, the influence of shear layer instabilities was pronounced in the axisymmetric jetting regime, causing jets to destabilize 'prematurely', resulting in jet lengths much shorter than predicted. This is because the theoretical predictions only account for capillary instabilities.

7.2.2 Oil Jets into Aqueous Surfactant Solutions

- The two surfactants tested, Triton X-100 and Tergitol TMN-6, were found to have extremely similar effectiveness on jet breakup when their concentrations were normalized by the CMC (Critical Micelle Concentration).
- At constant capillary diameter and jet velocity, jets were found to transition from the dripping mode to the axisymmetric jetting mode and from the axisymmetric jetting mode to the asymmetric jetting mode with increasing surfactant concentration.
- A critical minimum concentration of surfactant to affect jet breakup was identified, and is roughly equivalent to the critical micelle concentration for the conditions tested.
- Above the critical surfactant concentration, jet length is observed to increase significantly in the axisymmetric jetting regime. This includes situations where an experiment transitions from dripping flow, resulting in a jet of significant length.
- Droplet size is observed to decrease in the dripping flow regime with increasing surfactant concentration. A sudden decrease in droplet size is

accompanied by the transition to jetting flow. Droplet size in the axisymmetric regime is found to moderately increase, as predicted theoretically.

- Droplet size and breakup length are insensitive to surfactant concentration in the asymmetric jetting regime, as the jet breakup is dominated by continuous-fluid flow patterns, rather than interfacial effects.

7.2.3 Oil Jets of Increased Viscosity into Aqueous Surfactant Solutions

- Jet breakup length was found to increase with increasing viscosity ratio.
- In the axisymmetric jetting regime, droplet size was observed to decrease with increasing viscosity.
- Increasing surfactant concentration caused a significant increase in breakup length when combined with high viscosity oils under all conditions.

7.2.4 Oil Jets into Methanol-Water solutions

- Increasing methanol concentration (decreasing interfacial tension) resulted in increased jet lengths and droplet sizes. This agrees with theoretical predictions.
- Results did not agree with surfactant solutions with corresponding equilibrium interfacial tensions. This indicates that the surfactant solutions are not at equilibrium.
- By fitting the breakup length to the interfacial tension of a corresponding methanol solution, an expression for surfactant diffusion with time was constructed for utilization in the model proposed in Chapter 4.

7.2.5 Water Jets into Oil

- Increasing surfactant concentration was found to increase breakup length under all conditions for water-in-oil jets (including asymmetric jetting).
- Droplet size was observed to go through a maximum at moderate surfactant concentration. Visco-elastic behaviour of the fluid was also observed at moderate surfactant concentration, resulting in a 'pseudo-dripping' type breakup phenomenon. These effects are related and further investigation is recommended in the Future Work section.

7.3: Model Validation

A general expression for the prediction of breakup length for surfactant laden jets was presented in Chapter 4. In order to utilize this expression, a (sub) model is needed to determine the interfacial tension as a function of interfacial age. Utilizing the measured physicochemical properties of the surfactant at the silicone oil-water interface (the diffusivity and surface excess concentration) and a long-time approximation of the Ward-Tordai equation, a value of interfacial tension as a function of time can be calculated. This approach resulted in good agreement over a wide variety of surfactant concentrations and jet conditions. Since the interfacial age and the jet breakup length are related, the solution scheme is iterative. However, it was found to converge rapidly and as such is a powerful and useful model for determining jet breakup length in the presence of surfactants.

This model was shown to be useful for both the oil-water and water-air systems, within the axisymmetric jetting regime.

7.4: Future Work & Recommendations

This study's primary goal was to identify the effect of surfactants on the breakup length and droplet size resulting from the breakup of laminar liquid jets. Therefore, the primary variable tested was the surfactant concentration and type. The remaining variables were tested parametrically, as they were too numerous to test thoroughly. This has allowed us to identify the important variables for future study.

It is recommended that additional study be performed in order to separate the effect of the viscosity ratio from the effect of surfactants, and more importantly the directionality of surfactant transport. In our experiments it was difficult to discern whether the phenomena observed for water-in-oil jets (for instance, the droplet size experiencing a maxima at the critical minimum surfactant concentration) was due to the directionality of surfactant transport (from the jet phase outward), or due to differences in the interaction of the phases due to the very low value of the viscosity ratio. Additional experiments at a variety of low viscosity ratios should be performed in order to determine this. Additionally, experiments involving oil-phase surfactants would also be recommended, if a suitable surfactant (eg, one with similar diffusivity and effectiveness as the aqueous surfactants tested) can be located.

Secondly, a more thorough investigation of the nature of the transitions between the various breakup modes is recommended. While the transition between dripping and jetting is relatively well explored in the literature, the transition between 2-

dimensional (axisymmetric) and 3-dimensional (asymmetric) jetting is not, in particular the effect of surface active agents on these transitions has been given minimal attention. In order to quantify the boundaries between these regimes, a much more extensive set of jet velocities and jet diameters need to be tested. As jet diameters are somewhat limited by the size of available capillary tubes, the primary variable will be velocity. To that end, modifications in the experimental procedure are proposed. The current experimental setup allows for very constant pulseless flow of the jet fluid, but does not have very good resolution for jet velocities – that is – it is very difficult to make small changes in the flow rate, due to the large pressure drop in the piping and range of the micrometer valve. It is recommended that a high-precision syringe pump be used instead, allowing for more precise control of the flow rate and better ability to make small changes. The downside of this approach is that the total experimental run time will be limited by the volume of the syringe utilized, but considering the transitions in question generally occur at flow rates of under 20 ml/min, this should not pose a serious problem.

Finally, it is suggested that the effect of the jet phase buoyancy (The Bond number) be investigated. In general, the Bond number was held constant throughout this study, however a departure from expected trends was observed at the highest methanol concentration in the experiments involving oil jets into methanol-water solutions. In that case, the Bond number differed from the no-methanol case by approximately 5%. A systematic way to test variations in the Bond number without modifying the interfacial tension is recommended to determine if the reduction in

droplet size observed at high methanol concentration is attributed to buoyancy, as hypothesized, or if there is another phenomena at play as non-dynamic interfacial tension values tend to low values. Selection of a fluid system with constant interfacial tension but variable density may prove challenging.

One additional course of study not considered in this work, but common in the literature, is to impose 'forced' frequencies onto the jet (via mechanical, acoustic, or pneumatic means). This will create instabilities with specific wavelengths, rather than allowing the dominant wavelength to be selected organically. By forcing a particular instability wavelength onto a jet, it may be possible to better quantify the effect of the surfactants on the interfacial phenomena, by removing the surfactant's ability to effect the selection of dominant wavelengths for breakup (allowing only the instability propagation rate to be effected). By forcing a particular wavelength onto the jet, the droplet size should be independent of interfacial effects; however, breakup lengths may still be affected significantly by altering the interfacial conditions.

Additionally, a computational study could be undertaken by integrating the model proposed in Chapter 6 with one of the numerical simulation methods proposed in the literature to attempt to simulate the breakup of a surfactant-laden jet.

Appendices

Appendix 1: Computer codes

A1.1 - Determination of Jet Breakup Length

Part 1 – ImageJ Macro

```
macro "Batch Breakup Length" {
    dir = getDirectory("Choose a Directory ");
    list = getFileList(dir);

    tvalue=getNumber("Enter Upper Threshold", 175)
    setBatchMode(true);
    for (i=0; i<list.length; i++) {
        path = dir+list[i];
        showProgress(i, list.length);
        if (!endsWith(path,"/")) open(path);
        if (nImages>=1) {
          //run("8-bit");
          //run("Deinterlace ");
          setThreshold(0, tvalue);
          run("Convert to Mask");
            txtPath = path+".txt";
            run("Save XY Coordinates...", "background=0 suppress
save=["+txtPath+"]");
            close();
        }
    }
}
```

Part 2 – Matlab code

```
function [breakup]=jetlength(datafile_n,scale_fac,batch)

%%%%%%%%%%%%%%%%%%%%%%%%%%%%%%%%%%%%%%%%%%%%%%%%%%%%
%
%   MATLAB function to Calculate the Breakup
%   Length of a liquid Jet.  Reads datafiles
%   From ImageJ macro or can be called as a
%   function for batch analysis (such as the
%   function BUL_batch.m)
%
%   Inputs:
%     datafile - This should be an array of X,Y
%        values, measured in pixels
%     Scale_fac - The is the scale factor to
%        convert pixels to mm.  Typically 40-200
%     batch - asks if this is a batch calculation
%        0 for yes, 1 for no.
```

```
%
%   Copyright (c) Justin Walker 2008
%
%%%%%%%%%%%%%%%%%%%%%%%%%%%%%%%%%%%%%%%%%%%%%%%%%%%%

% Import Data
if batch==1;
    datafile=load(datafile_n);
else
    datafile=datafile_n;
end
%X_px=datafile(:,1); %read X & Y values from data file
Y_px=datafile(:,2);
Y_max=max(Y_px);
Y_px_sc_us=Y_max-Y_px;  %invert order of Y
Y_px_sc=sort(Y_px_sc_us);    %sort
Y_px=Y_px_sc;
%Y_sc=max(Y_px_sc); %find range of Y
BUL_test = 0;
i=0;
b = 0;

while BUL_test ~= 1
    i=i+1;
    if i>=(size(Y_px)-2)
        b = 1;
        BUL_test=1;
    end
    if Y_px(i+1)-Y_px(i)>1
       BUL_test=1;
       BUL_px = Y_px(i);
    end

end
if b == 1
    breakup = Y_max/scale_fac; %condition for when no droplets exist
else
    breakup = BUL_px/scale_fac;
end
```

A1.2 - Determination of Droplet Diameter

ImageJ Macro

```
macro "Batch Particle Size" {
    dir = getDirectory("Choose a Directory ");
    list = getFileList(dir);
    tvalue=getNumber("Enter Upper Threshold", 175)
    setBatchMode(true);
    for (i=0; i<list.length; i++) {
        path = dir+list[i];
        showProgress(i, list.length);
        if (!endsWith(path,"/")) open(path);
        if (nImages>=1) {
          //run("8-bit");
```

```
          //run("Deinterlace ");
          setThreshold(0, tvalue);
          run("Convert to Mask");
                run("Close-");
//                run("Dilate");
          run("Fill Holes");
//                run("Erode");
//                run("Erode");
//                run("Erode");
//                run("Dilate");
          run("Watershed");
          run("Analyze Particles...", "size=0.25-Infinity
circularity=0.5-1.00 show=Nothing display exclude");
            close();
        }
    }
}
```

A1.3 – Jet Breakup Length Model

Matlab code

```
function
[lb_fit]=surflb2(lb_clean,sigma_clean,sigma_eq,d_cap,v_flow,
surf_conc, Temp, dens, visc)

vflow=v_flow*1.666666667*10^(-8);   %Convert ml/min to m³/s
dcap=d_cap*.001;                    %Convert mm to m
sigmaclean=sigma_clean/1000;        %Convert mN/m to N/m
sigmaeq=sigma_eq/1000;              %Convert mN/m to N/m

We_clean= 16*dens*vflow^2/(pi^2*sigma_clean*dcap^3);
Oh_clean=visc/sqrt(dens*sigma_clean*(dcap/2));
w_clean=fminsearch(@(n) -linjet(n,Oh_clean), .5);
tb_clean=(lb_clean/1000)*pi()*(dcap/2)^2/vflow;
tb=1.5*tb_clean;
check=1;
count=1;
lb_t(count,1)=count;
lb_t(count,2)=lb_clean;
% for so/water G_inf=3.09E-6; % mol / m^2
G_inf=2.87E-6; % mol / m^2
% for so/water a_L=1.5E-6; % mol / l
a_L=5.91E-6; % mol / l
D_AB=5.02E-10; % m^2/s
CMC=2.19E-4; % mol/l
Surf_conc = surf_conc*CMC*1000; % mol/m^3
R=8.31451; % J/mol K
T=Temp+273.15; % °K

while (abs(check)>0.0001) && (count<100)
    count=count+1;
    %sigma_eff=0.156*sigma_eq*exp(-1.21*tb);
    sigma_WT=(R*T*G_inf^2)/(2*Surf_conc)*sqrt(pi/(D_AB*tb));
    sigma_eff=sigmaeq + sigma_WT;
```

```
    if sigma_eff>sigmaclean
        sigma_eff=sigmaclean;
    end
    We_eff=We_clean*(sigmaclean/sigma_eff);
    Oh=Oh_clean*sqrt(sigmaclean/sigma_eff);
    w_eff=fminsearch(@(n) -linjet(n,Oh), .5);
    lb_fit=lb_clean*w_clean/w_eff*(We_eff/We_clean)^0.5;
    lb_t(count,1)=count;
    lb_t(count,2)=lb_fit;
    tb_fit=(lb_fit)/1000*pi()*(dcap/2)^2/vflow;
    check = tb_fit-tb;
    tb=tb_fit;
end
if count>99
    disp('Maximum iterations exceeded');
    sprintf('Calculated tb is %d, the previous iteration yielded
%d',tb,tb+check);
end
```

A1.4 – Calculation of equivalent spherical diameter for droplets imaged in orthogonal planes

```
function [results]=stereodrop(datafile_front,datafile_side)

% Import Data

numfront=size(datafile_front,1);
numside=size(datafile_side,1);

if numfront==0 || numside==0
    results=[0,0,0,0];
    return
end

if datafile_front(1)==0 && datafile_side(1)==0
    results=[0,0,0,0];
    return
end


if numfront > numside
    totalnum = numside;
else
    totalnum = numfront;
end

front_BY=datafile_front(1:totalnum,5);
side_BY=datafile_side(1:totalnum,5);

front_width=datafile_front(1:totalnum,6);
side_width=datafile_side(1:totalnum,6);
```

```
front_height=datafile_front(1:totalnum,7);
%side_height=datafile_side(1:totalnum,7);

%front_major=datafile_front(1:numfront,8);
%side_major=datafile_side(1:numside,8);

%front_minor=datafile_front(1:numfront,9);
%side_minor=datafile_side(1:numside,9);

dropx=zeros(1,totalnum);
dropy=zeros(1,totalnum);
dropz=zeros(1,totalnum);

% droplet fitting routine
if totalnum==1
    if (front_BY(1) < side_BY(1)*1.10) && (front_BY(1) >
side_BY(1)*.9)
            dropx(1)=front_width(1);
            dropy(1)=front_height(1);
            dropz(1)=side_width(1);
    else
            dropx(1)=0;
            dropy(1)=0;
            dropz(1)=0;
    end
end
for i=1:totalnum-1
    %write droplet matching code here
        if (front_BY(i) < side_BY(i)*1.10) && (front_BY(i) >
side_BY(i)*.9)
            dropx(i)=front_width(i);
            dropy(i)=front_height(i);
            dropz(i)=side_width(i);
        elseif (front_BY(i) < side_BY(i+1)*1.10) && (front_BY(i) >
side_BY(i+1)*.9)
            dropx(i)=front_width(i);
            dropy(i)=front_height(i);
            dropz(i)=side_width(i+1);
        elseif (front_BY(i+1) < side_BY(i)*1.1) && (front_BY(i+1) >
side_BY(i)*.9)
            dropx(i)=front_width(i+1);
            dropy(i)=front_height(i+1);
            dropz(i)=side_width(i);
        else
            dropx(i)=0;
            dropy(i)=0;
            dropz(i)=0;
        end
end



%calculate droplet volume
volume_drop=4/3.*pi().*dropx/2.*dropy/2.*dropz/2;
results=[dropx',dropy',dropz',volume_drop'];
```

A1.5 – Determination of Interfacial Tension from Pendant Drop experiments

```
function [sigma]=pdrop4a(datafile,scale_fac)

% Assumed Values - edit as nessescary
rhoL = 935; % droplet phase density - kg/m^3
rhoG = 996.7;  % continuous phase density - kg/m^3
accg = 9.81;  % Acceleration due to gravity - m/s^2

% Import Data

Y_px=datafile(:,2);
Y_min=min(Y_px); %scale Y values
Y_px_sc=Y_px-Y_min;
Y_sc=max(Y_px_sc); %find number of discrete Y values

width=zeros(Y_sc,2); %initialize array for drop widths
row=0; % row counter
i=1; % dummy loop variable
while i<(length(datafile)-1)
    pcon=0; % dummy loop variable
    widthi=0; % width increment
    while pcon==0
        widthi=widthi+1; %increment width
        if datafile(i,1)>datafile(i+1,1) %search for end of row
(when x value decreases)
            row=row+1; %increment row number and save values
            width(row,1)=row;
            width(row,2)=widthi;
            pcon=1; %Throw dummy variable to exit loop
        end
        i=i+1; % go to next datapoint
        if i>=(length(datafile)-1)
                pcon=1; %Exit loop if end of file is reached
        end
    end
end

widthrow=(width(:,2));
D_max=max(widthrow);

Ds_px=width(D_max,2);

De=D_max/scale_fac;  % Divide by scale factor to convert pixels to
mm
Ds=Ds_px/scale_fac;
S = Ds/De;  % Calculate Shape Factor
H = 1/(0.315*S^(-2.608));  % From Pedron, 2005

% Calculate Interfacial Tension

sigma = 1000*abs(rhoL-rhoG)*accg*(De/1000)^2/H;  % Calculated in
mN/m
```

Appendix 2: Tabulated Data for Jet Breakup Experiments

A2.1 – Collected Breakup Length Data for Air-Water Jets

Flow Rate	Needle ID (mm)		0.41	Std Dev	0.6	Std Dev	0.84	Std Dev
30 ml/min	None		67.79	3.1242	54.7941	2.7938	47.2339	3.9024
	Tergitol TMN-6	0.01 x CMC	68.3597	4.7109	48.4705	3.6263	47.7062	4.2675
		0.1 x CMC	41.6265	4.9851	49.9585	2.8743	38.6394	2.719
		0.5 x CMC	45.261	3.287	51.7875	51.7875	50.5807	3.6902
		1 x CMC	47.4334	6.3142	54.8664	4.316	58.3668	3.4183
		10 x CMC	50.8248	9.4597	71.8565	5.6568	78.7344	6.8602
	Triton X-100	0.1 x CMC	47.5899	5.996	52.6622	3.305	42.1786	3.8818
		0.5 x CMC	55.6521	1.1878	50.4738	3.1702	40.2183	3.4262
		1 x CMC	47.8487	4.4369	49.0996	3.5201	44.3911	3.8486
		10 x CMC	62.0258	7.929	70.7758	4.5073	74.2607	5.7355
20 ml/min	None		42.3572	2.3925	32.6321	1.5291	6.8441	1.6227
	Tergitol TMN-6	0.01 x CMC	45.8747	3.1749	31.1526	2.5747	8.1598	1.6197
		0.1 x CMC	32.2137	2.2839	31.1985	2.1127	10.4661	1.9149
		0.5 x CMC	28.3097	1.9458	31.8119	2.2756	32.3965	3.1601
		1 x CMC	36.6342	2.7497	35.0811	2.3436	38.7719	3.5084
		10 x CMC	54.5946	6.285	50.8113	3.0342	50.584	3.7649
	Triton X-100	0.1 x CMC	33.3721	2.3581	31.8653	2.2989	6.1011	1.5611
		0.5 x CMC	38.518	2.7617	31.0281	2.3964	12.923	1.5655
		1 x CMC	31.9693	2.0315	29.064	2.4743	28.8452	2.9684
		10 x CMC	47.9824	3.7435	46.3393	3.3433	49.6954	3.9846
10 ml/min	None		20.4104	1.4195	4.8592	1.3169	Dripping	n/a
	Tergitol TMN-6	0.01 x CMC	20.9936	1.5776	4.5003	1.1505	Dripping	n/a
		0.1 x CMC	17.6503	1.3638	4.3798	1.1846	Dripping	n/a
		0.5 x CMC	16.3918	1.1795	8.3313	1.1486	2.9164	1.0377
		1 x CMC	24.8672	1.9759	20.7976	1.7197	2.873	0.93657
		10 x CMC	27.9686	1.957	26.3023	1.9294	3.287	0.75619
	Triton X-100	0.1 x CMC	16.2122	1.221	4.5489	1.2043	4.2711	1.0115
		0.5 x CMC	21.0134	2.1119	4.2959	1.1412	3.1793	0.99344
		1 x CMC	19.894	1.2256	4.2413	0.83508	3.0646	1.0031
		10 x CMC	17.9468	1.6566	23.9896	2.0274	3.0668	1.0324

A2.2 – Collected Equivalent Spherical Diameter Data for Air-Water Jets

Flow Rate	Needle ID		.41 mm	Std Dev	.60 mm	Std Dev	.84 mm	Std Dev
30 ml/min	None		0.8527	0.2569	1.1379	0.2664	1.2301	0.3999
	Tergitol TMN-6	0.01 x CMC	0.8783	0.2414	1.1348	0.2647	1.6855	0.5508
		0.1 x CMC	1.0363	0.29746	1.0759	0.25646	1.2956	0.42479
		0.5 x CMC	0.94095	0.17601	1.2637	1.5306	1.3957	0.38438
		1 x CMC	1.153	0.24598	1.122	0.2888	1.2613	0.34742
		10 x CMC	0.978	0.1868	1.1934	0.27084	1.3552	0.3748
	Triton X-100	0.01 x CMC	n/a	n/a	n/a	n/a	n/a	n/a
		0.1 x CMC	1.0063	0.25259	1.2514	0.27282	1.5911	0.45739
		0.5 x CMC	0.82241	0.18384	1.3023	0.36618	1.6186	0.46672
		1 x CMC	0.86518	0.17164	1.1856	0.30055	1.4842	0.3884
		10 x CMC	0.88489	0.15834	1.2835	0.25516	1.4513	0.36913
20 ml/min	None		1.1429	0.2328	1.1939	0.3448	1.8357	0.3473
	Tergitol TMN-6	0.01 x CMC	0.7879	0.1898	1.1771	0.2614	2.2151	0.4208
		0.1 x CMC	0.75265	0.19279	1.1655	0.24913	1.7146	0.36318
		0.5 x CMC	0.91053	0.19141	1.37	0.34404	1.1981	0.35871
		1 x CMC	1.1781	0.30374	1.2673	0.33376	1.2471	0.31754
		10 x CMC	0.9377	0.1839	1.1047	0.33385	1.424	0.37023
	Triton X-100	0.01 x CMC	n/a	n/a	n/a	n/a	n/a	n/a
		0.1 x CMC	0.77242	0.1577	1.2046	0.26307	1.7776	0.45238
		0.5 x CMC	0.83846	0.18393	1.2597	0.36612	1.6789	0.3841
		1 x CMC	0.78579	0.14564	1.1823	0.29038	1.0451	0.40748
		10 x CMC	0.93447	0.19275	1.0781	0.26905	1.4794	0.35528
10 ml/min	None		1.0451	0.2271	1.4805	0.3908	3.1993	0.3668
	Tergitol TMN-6	0.01 x CMC	0.8062	0.1872	1.5115	0.3359	3.9184	0.5699
		0.1 x CMC	0.80001	0.19044	1.4632	0.2443	2.995	0.3883
		0.5 x CMC	0.91332	0.1905	1.7201	0.27095	3.008	0.33
		1 x CMC	1.0916	0.23888	1.3777	0.29242	2.1363	0.28896
		10 x CMC	0.99417	0.22218	1.1871	0.29631	1.2782	0.2911
	Triton X-100	0.01 x CMC	n/a	n/a	n/a	n/a	n/a	n/a
		0.1 x CMC	0.93368	0.21457	1.6623	0.32319	2.9691	0.56986
		0.5 x CMC	0.94636	0.19222	1.7169	0.27616	3.1918	0.33381
		1 x CMC	0.91177	0.19438	1.7299	0.15029	3.0759	0.3032
		10 x CMC	0.91552	0.18183	1.0588	0.21636	2.688	0.22132

A2.3 – Collected Breakup Length Data for Surfactant-Laden Water-Oil Jets

Flow Rate	Needle ID		.41 mm		.60 mm		.84 mm	
			Raw (mm)	SD	Raw (mm)	SD	Raw (mm)	SD
5 ml/min	None	1.00E-05	2.99	1.9267	4.7443	1.3479	n/a	n/a
	Tergitol TMN-6	0.01	n/a	n/a	3.3551	0.95633	n/a	n/a
		0.05	n/a	n/a	3.0916	1.0138	n/a	n/a
		0.1	n/a	n/a	3.1942	0.89732	n/a	n/a
		0.5	n/a	n/a	4.2016	1.6939	n/a	n/a
		1	n/a	n/a	7.6968	2.0066	n/a	n/a
		10	n/a	n/a	21.4605	2.8707	n/a	n/a
		50	n/a	n/a	28.1349	2.595	n/a	n/a
	Triton X-100	0.01	2.7031	1.2778	4.4226	1.2638	n/a	n/a
		0.05	2.4686	0.51359	4.6197	1.3589	n/a	n/a
		0.1	3.8866	1.2839	4.1203	1.5487	n/a	n/a
		0.5	3.2381	1.0465	5.126	1.8343	n/a	n/a
		1	2.9613	0.74763	5.648446	2.853861	n/a	n/a
		10	19.7862	2.6971	10.66849	1.329485	n/a	n/a
		20	33.9628	2.4616	23.0649	2.0082	n/a	n/a
		50	39.5121	2.7719	26.2928	1.8171	n/a	n/a
10 ml/min	None	1.00E-05	17.3097	2.5209	3.8801	0.62947	5.7677	1.6738
	Tergitol TMN-6	0.01	n/a	n/a	2.5646	0.80341	n/a	n/a
		0.05	n/a	n/a	3.0573	0.62898	n/a	n/a
		0.1	n/a	n/a	2.4626	0.68397	n/a	n/a
		0.5	n/a	n/a	15.1961	3.055	n/a	n/a
		1	n/a	n/a	18.1402	1.7596	n/a	n/a
		10	n/a	n/a	46.104	3.0997	n/a	n/a
		50	n/a	n/a	63.6636	4.376	n/a	n/a
	Triton X-100	0.01	15.3386	1.6431	3.3957	1.0025	5.8194	1.7202
		0.05	15.7443	2.1057	3.2451	1.0122	5.974	1.7523
		0.1	13.8508	2.4908	3.1113	1.1483	5.7781	1.4503
		0.5	15.9934	1.4647	3.5845	1.1193	6.0524	1.8733
		1	22.8589	3.1623	8.338128	0.042491	6.4621	2.0042
		10	41.2596	7.2061	40.94103	2.455989	41.0175	3.2845
		20	41.0226	5.2009	44.9569	3.4094	43.0017	2.8076
		50	43.6787	5.7511	47.137	3.4222	36.1799	2.6997

Flow Rate	Needle ID		.41 mm		.60 mm		.84 mm	
			Raw (mm)	SD	Raw (mm)	SD	Raw (mm)	SD
20 ml/min	None	1.00E-05	9.5135	1.9063	19.3017	3.7148	5.519	1.6479
	Tergitol TMN-6	0.01	n/a	n/a	10.4165	1.0984	n/a	n/a
		0.05	n/a	n/a	17.2058	2.6683	n/a	n/a
		0.1	n/a	n/a	13.0332	1.8563	n/a	n/a
		0.5	n/a	n/a	16.5624	2.806	n/a	n/a
		1	n/a	n/a	15.9905	2.126	n/a	n/a
		10	n/a	n/a	21.2308	4.6842	n/a	n/a
		50	n/a	n/a	31.2127	5.6308	n/a	n/a
	Triton X-100	0.01	8.4494	1.7222	18.6253	4.2012	5.8406	1.633
		0.05	9.3443	1.5116	23.4512	3.4244	5.4861	1.4781
		0.1	10.8443	2.036	20.6904	4.856	6.335	1.3252
		0.5	9.8456	1.3817	21.5919	5.6344	10.3698	1.9032
		1	10.9185	1.6559	19.36429	2.938921	12.2895	1.8206
		10	14.6602	4.5203	33.26821	5.369758	40.2496	12.0488
		20	24.8622	7.779	38.2928	7.9685	51.1102	11.5295
		50	25.947	8.43	51.4492	7.3215	42.6174	4.6409
30 ml/min	None	1.00E-05	n/a	n/a	n/a	n/a	23.0015	2.7434
	Tergitol TMN-6	0.01	n/a	n/a	n/a	n/a	n/a	n/a
		0.05	n/a	n/a	n/a	n/a	n/a	n/a
		0.1	n/a	n/a	n/a	n/a	n/a	n/a
		0.5	n/a	n/a	n/a	n/a	n/a	n/a
		1	n/a	n/a	n/a	n/a	n/a	n/a
		10	n/a	n/a	n/a	n/a	n/a	n/a
		50	n/a	n/a	n/a	n/a	n/a	n/a
	Triton X-100	0.01	n/a	n/a	n/a	n/a	23.0331	3.1475
		0.05	n/a	n/a	n/a	n/a	23.8335	3.1641
		0.1	n/a	n/a	n/a	n/a	19.8746	2.5964
		0.5	n/a	n/a	n/a	n/a	21.5625	2.7716
		1	n/a	n/a	n/a	n/a	30.938	4.355
		10	n/a	n/a	n/a	n/a	24.2143	5.0153
		20	n/a	n/a	n/a	n/a	33.1798	7.2289
		50	n/a	n/a	n/a	n/a	24.4061	5.1874

A2.4 – Collected Mean Droplet Size Data for Surfactant-Laden Water-Oil Jets

Flow Rate	Needle ID		.41 mm		.60 mm		.84 mm	
			D32	Std. Dev	D32	Std. Dev	D32	Std. Dev
5 ml/min	None	1.00E-05	1.5678	0.0312	5.2155	0.0162	n/a	n/a
	Tergitol TMN-6	0.01	n/a	n/a	3.9942	0.019	n/a	n/a
		0.05	n/a	n/a	3.5696	0.0129	n/a	n/a
		0.1	n/a	n/a	2.8053	0.0075	n/a	n/a
		0.5	n/a	n/a	2.8872	0.0219	n/a	n/a
		1	n/a	n/a	3.028	0.1387	n/a	n/a
		10	n/a	n/a	1.7746	0.1918	n/a	n/a
		50	n/a	n/a	1.3688	0.0954	n/a	n/a
	Triton X-100	0.01	1.4995	0.0239	5.5355	0.0038	n/a	n/a
		0.05	1.2548	0.0014	5.5842	0.7346	n/a	n/a
		0.1	1.3644	0.0497	5.4853	0.1779	n/a	n/a
		0.5	2.4834	0.0597	5.5871	0.0131	n/a	n/a
		1	1.247	0.0031	2.139578	0.107346	n/a	n/a
		10	2.3818	0.0184	3.829164	0.633056	n/a	n/a
		20	2.0553	0.1939	2.4674	0.0281	n/a	n/a
		50	1.9658	0.3379	2.233	0.047	n/a	n/a
10 ml/min	None	1.00E-05	1.5133	0.2467	1.5909	0.0779	6.9855	0.03
	Tergitol TMN-6	0.01	n/a	n/a	0.9979	0.0433	n/a	n/a
		0.05	n/a	n/a	0.9539	0.0039	n/a	n/a
		0.1	n/a	n/a	0.9582	0.0031	n/a	n/a
		0.5	n/a	n/a	1.9989	0.2639	n/a	n/a
		1	n/a	n/a	1.6571	0.4122	n/a	n/a
		10	n/a	n/a	1.4931	0.2175	n/a	n/a
		50	n/a	n/a	1.5721	0.2133	n/a	n/a
	Triton X-100	0.01	1.323	0.2558	1.61	0.04	6.5942	0.3049
		0.05	1.2507	0.0149	1.4489	0.0115	6.803	0.0066
		0.1	1.998	0.0598	1.4815	0.0094	5.0736	0.0134
		0.5	1.5155	0.0355	1.44	0.02	4.9074	0.1779
		1	2.1169	0.5541	1.692853	0.084933	4.7127	0.0597
		10	2.3087	0.5495	3.029668	0.500879	2.648	0.1838
		20	4.0423	0.4662	4.0033	0.3002	2.4159	0.1518
		50	2.4741	0.3731	2.7682	0.1612	2.4088	0.2323

Flow Rate	Needle ID		.41 mm		.60 mm		.84 mm	
			D32	Std. Dev	D32	Std. Dev	D32	Std. Dev
20 ml/min	None	1.00E-05	1.4349	0.3149	4.1172	0.5	2.701	0.0233
	Tergitol TMN-6	0.01	n/a	n/a	1.0918	0.3523	n/a	n/a
		0.05	n/a	n/a	1.447	0.4003	n/a	n/a
		0.1	n/a	n/a	1.9165	0.5657	n/a	n/a
		0.5	n/a	n/a	1.4024	0.3961	n/a	n/a
		1	n/a	n/a	1.8274	0.3288	n/a	n/a
		10	n/a	n/a	1.8628	0.281	n/a	n/a
		50	n/a	n/a	2.5351	0.3342	n/a	n/a
	Triton X-100	0.01	1.2502	0.159	2.055	0.6619	2.192	0.0194
		0.05	1.1736	0.1987	2.8407	0.5332	2.3199	0.0038
		0.1	1.2502	0.159	2.0247	0.3304	2.2443	0.1816
		0.5	1.4238	0.2297	2.0878	0.5178	2.6551	0.1231
		1	2.5387	0.6379	2.056474	0.634978	3.0111	0.6679
		10	2.05	0.4721	3.795711	1.179335	2.7133	0.401
		20	1.1787	0.1435	5.93	0.6498	3.01	0.7365
		50	n/a	n/a	4.3735	0.6732	3.6387	0.6036
30 ml/min	None	1.00E-05	n/a	n/a	n/a	n/a	2.7815	0.7544
	Tergitol TMN-6	0.01	n/a	n/a	n/a	n/a	n/a	n/a
		0.05	n/a	n/a	n/a	n/a	n/a	n/a
		0.1	n/a	n/a	n/a	n/a	n/a	n/a
		0.5	n/a	n/a	n/a	n/a	n/a	n/a
		1	n/a	n/a	n/a	n/a	n/a	n/a
		10	n/a	n/a	n/a	n/a	n/a	n/a
		50	n/a	n/a	n/a	n/a	n/a	n/a
	Triton X-100	0.01	n/a	n/a	n/a	n/a	2.928	0.584
		0.05	n/a	n/a	n/a	n/a	2.7246	0.6014
		0.1	n/a	n/a	n/a	n/a	2.5863	0.6695
		0.5	n/a	n/a	n/a	n/a	2.4885	0.5803
		1	n/a	n/a	n/a	n/a	2.8379	0.7366
		10	n/a	n/a	n/a	n/a	2.6004	0.6818
		20	n/a	n/a	n/a	n/a	2.6324	0.6196
		50	n/a	n/a	n/a	n/a	2.8309	0.7985

A2.5 – Collected Breakup Length Data for Methanol Solution Water-Oil Jets

Flow Rate	Methanol wt%	10 cSt	
		Raw (mm)	Std. Dev
10 ml/min	0	3.8801	0.62947
	10	16.8275	1.4346
	20	18.269	2.4931
	30	22.1318	2.0406
	38	12.7572	2.3184
20 ml/min	0	19.3017	3.7148
	10	33.9334	3.5233
	20	38.2536	6.4326
	30	45.9964	4.9712
	38	28.7283	3.4666
30 ml/min	0	10.001	2.020
	10	22.2065	2.8507
	20	41.485	7.529
	30	48.2324	10.2288
	38	31.4725	6.8439

A2.6 – Collected Mean Droplet Size Data for Methanol Solution Water-Oil Jets

Flow Rate	Methanol wt%	10 cSt	
		D32	Std Dev
10 ml/min	0	1.5909	0.0779
	10	2.9084	0.8778
	20	3.1257	0.0276
	30	2.4763	0.2235
	38	1.9856	0.3945
20 ml/min	0	1.5173	0.5
	10	2.5958	0.8334
	20	3.0335	0.8924
	30	1.9957	0.525
	38	1.6478	0.2762
30 ml/min	0	n/a	n/a
	10	2.1686	0.8082
	20	2.2466	0.8354
	30	2.6032	0.6377
	38	n/a	n/a

A2.7 – Collected Breakup Length Data for Water Jets into High Viscosity Oils

Flow Rate	Triton X-100 Conc.	10 cSt		20 cSt		50 cSt	
		Raw (mm)	SD	Raw (mm)	SD	Raw (mm)	SD
5 ml/min	0	4.7443	1.3479	6.0172	2.9421	5.6421	1.6484
	1	5.6484458	2.853861	5.5352	2.332	22.8793	9.275
	20	23.0649	2.0082	26.1536	3.0982	54.6143	3.7094
10 ml/min	0	3.8801	0.62947	17.1805	1.6014	9.3435	3.2674
	1	8.3381278	0.042491	6.472	1.4608	43.7871	7.7192
	20	44.9569	3.4094	56.8918	5.321	106.8866	6.8917
20 ml/min	0	19.3017	3.7148	30.9129	2.9441	41.7072	2.3121
	1	19.364294	2.938921	33.5886	3.8817	60.3068	7.4771
	20	38.2928	7.9685	71.2391	14.0532	170*	n/a*

A2.8 – Collected Mean Droplet Size Data for Water Jets into High Viscosity Oils

Flow Rate	Triton X-100 Conc.	10 cSt		20 cSt		50 cSt	
		D32	Std. Dev	D32	Std. Dev	D32	Std. Dev
5 ml/min	0	5.2155	0.0162	6.1779	0.0187	5.7805	0.1998
	1	2.1395778	0.107346	4.8293	0.2306	5.9634	0.22
	20	2.4384	0.0281	2.6745	0.3812	2.9974	0.4844
10 ml/min	0	1.5909	0.0779	2.7445	0.2019	3.6895	0.3175
	1	1.6928528	0.084933	3.3859	0.5125	4.2719	0.3512
	20	2.2243	0.3002	2.5788	0.5768	3.0566	0.0749
20 ml/min	0	4.1172	0.5	2.3007	0.4752	2.5345	0.6565
	1	2.0564736	0.634978	3.1374	0.8863	3.0255	1.1323
	20	3.8219	0.6498	3.01	0.8728	n/a*	n/a*

* The jet was observed to impinge on the top of the cell; consequently, no droplets were formed. Reported jet breakup length is the distance to the top of the cell, actual breakup length in an infinite container would exceed this value.

A2.7 – Collected Dimensionless Breakup Length Data for Jets of Viscous Oils into Aqueous Surfactant Solutions (Capillary Size was 0.6mm for all cases)

Surfactant Concentration	Flow Rate:	5 ml/min	Std. Dev	10 ml/min	Std. Dev	20 ml/min	Std. Dev	30 ml/min	Std. Dev
1.00E-03		21.25517	4.7814	59.8925	2.9704	124.3937	4.776	54.51417	3.2486
0.1		27.95633	9.6946	27.382167	1.8477	112.6333	6.9901	66.44967	3.8164
0.5		17.44767	4.8855	30.672167	1.677	101.1638	6.6167	56.80067	3.4191
1		13.24833	4.8554	44.647167	2.1535	140.7792	5.062	62.36667	3.1333
5		14.98383	2.3539	104.89183	2.691	171.3247	6.751	93.48667	8.6906
20		n/a	n/a	127.44467	3.4454	202.4642	10.4958	107.0817	9.8953

A2.8 – Collected Mean Droplet Size Data for Jets of Viscous Oils into Aqueous Surfactant Solutions (Capillary Size was 0.6mm for all cases)

Surfactant Concentration	Flow Rate:	5 ml/min	Std. Dev	10 ml/min	Std. Dev	20 ml/min	Std. Dev	30 ml/min	Std. Dev
1.00E-04		6.75824	0.06703	2.37363	0.08242	3.46154	1.12088	3.74725	1.18681
0.1		6.0989	0.04835	2.54945	0.59341	3.15385	1.14286	3.89011	1.10989
0.5		5.37802	0.05495	2.65934	0.95604	4.18681	1.43956	4.79121	1.31868
1		4.75824	1.76923	2.98901	1.06593	5.24176	1.46154	4.8	0.93407
5		4.58242	1.47253	3.83516	1.25275	3.47253	1.17582	2.89	1.17582
20		2.78022	0.97802	2.26374	0.62637	n/a	n/a	2.42857	0.78022

References

Ambravaneswaran, B., Subramani, H.J., Phillips, S.D., and Basaran, O.A. **2004**. Dripping-Jetting Transitions in a Dripping Faucet. *Physical Review Letters* 93(3); 034501-1-4

Anshus, B.E. **1973**. The effect of Surfactants in the Breakup of Cylinders and Jets. *Journal of Colloid and Interface Science* 43(1); 113-121

Arai, M., and Amagai, K. **1999**. Surface wave transition before breakup on a laminar liquid jet. *International Journal of Heat and Fluid Flow* 20; 507-512

Attané, P. **2006**. Response to "'Breakup length of forced liquid jets'". *Physics of Fluids* 18(1); 019102-1-2

Bogy, D.B. **1979**. Drop formation in a circular liquid jet. *Annual Review of Fluid Mechanics* 11; 207-228

Bousfield, D.W., Stockel, I.H, and Nanivadekar, C.K. **1990**. The breakup of viscous jets with large velocity modulations. *Journal of Fluid Mechanics* 218; 601-617

Burkholder, H.C., and Berg, J.C. **1974**. Effect of Mass Transfer on Laminar Jet Breakup: Part 1. Liquid Jets in Gases. *AICHE Journal* 20(5); 863-872

Burkholder, H.C., and Berg, J.C. **1974**. Effect of Mass Transfer on Laminar Jet Breakup: Part 2. Liquid Jets in Liquids. *AICHE Journal* 20(5); 872-880

Chandrasekhar, S., **1961**. Hydrodynamic and hydromagnetic stability. *Clarendon Press, Oxford*, pp. 515-576

Chang, C.-H., and Frances, E.I. **1995**. Adsorption dynamics of surfactants at the air/water interface: a critical review of mathematical models, data, and mechanisms. *Colloids and Surfaces A: Physicochemical and Engineering Aspects* 100; 1-45

Chaudhary, K.C., and Maxworthy, T. **1980**. The nonlinear capillary instability of a liquid jet. Part 2. Experiments on jet behavior before droplet formation. *Journal of Fluid Mechanics* 96(2); 275-286

Chaudhary, K.C., and Redekopp, L.G. **1980**. The nonlinear capillary instability of a liquid jet. Part 1. Theory. *Journal of Fluid Mechanics* 96(2); 257-274

Clanet, C. and Lasheras, J.C. **1999**. Transition from dripping to jetting. *Journal of Fluid Mechanics* 383; 307-326

Cramer, C., Berüter, B., Fischer, P., and Windhab, E.J. **2002**. Liquid Jet Stability in a Laminar Flow Field. *Chemical Engineering Technology* 25(5); 499-506

Cramer, C., Fischer, P., and Windhab, E.J. **2004**. Drop formation in a co-flowing ambient fluid. *Chemical Engineering Science* 59; 3045-3058

Craster, R.V., Matar, O.K., and Papageorgiou, D.T. **2002**. Pinchoff and satellite formation in surfactant covered viscous threads. *Physics of Fluids* 14(4); 1364-1376

Craster, R.V., Matar, O.K., and Papageorgiou, D.T. **2009**. Breakup of surfactant-laden jets above the critical micelle concentration. *Journal of Fluid Mechanics* 629; 195-219

Das, T.K. **1992**. Formation of Monosized Droplets by a Vibrating Liquid-Liquid Jet. *Atomization and Sprays* 2; 37-44

Das, T.K. **1997**. Droplet Formation with single and multiple nodes from a liquid jet in immiscible liquids. *Atomization and Sprays* 7; 407-415

Das, T.K. **1997**. Prediction of Jet Breakup Length in Liquid-Liquid Systems using the Rayleigh-Tomotika Analysis. *Atomization and Sprays* 7; 549-559

Debler, W., and Yu, D. **1988**. The break-up of laminar liquid jets. *Proceedings of the Royal Society of London, Series A* 415; 107-119

Eastoe, J., Dalton, J.S., Rogeuda, P.G.A., Crooks, E.R., Pitt, A.R., and Simister, E.A. **1997**. Dynamics Surface Tensions of Nonionic Surfactant Solutions. *Journal of Colloid and Interface Science* 188; 426-430

Eggers, J. **1997**. Nonlinear dynamics and breakup of free-surface flows. *Reviews of Modern Physics* 69(3); 865-929

Eggers, J., and Villermaux, E. **2008**. Physics of Liquid Jets. *Reports on Progress in Physics* 71; 036601

Eggleton, C.D., and Stebbe, K.J. **1998.** An Adsorption–Desorption-Controlled Surfactant on a Deforming Droplet. *Journal of Colloid and Interface Science* 208(1); 68-80

Fenn, III, R.W., and Middleman, S. **1969**. Newtonian Jet Stability, The Role of Air Resistance. *AICHE Journal* 15(3); 379-383

García, F.J., and González, H. **2008**. Normal-mode linear analysis and initial conditions of capillary jets. *Journal of Fluid Mechanics* 602; 81-117

Gavis, J., and Modan, M. **1967**. Expansion and Contraction of Jets of Newtonian Liquids in Air: Effect of Tube Length. *The Physics of Fluids* 10(3); 487-497

Geer, J.F., and Strikwerda, J.C. **1983**. Vertical slender jets with surface tension. *Journal of Fluid Mechanics* 135; 155-169

Goldin, M, Yerushalmi, J., Pfeffer, R., and Shinnar, R. **1969**. Breakup of a laminar capillary jet of a viscoelastic fluid. *Journal of Fluid Mechanics* 38(4) 689-711

González, H., and García, F.J. **2006**. Comment on "Breakup length of forced liquid jets". *Physics of Fluids* 18(1); 019101-1-2

González, H., and García, F.J. **2009**. The measurement of growth rates in capillary jets. *Journal of Fluid Mechanics* 619; 179-212

Grant, R.P., and Middleman, S. **1966**. Newtonian Jet Stability. *AICHE Journal* 12(4); 669-678

Hiemenz, P.C. and Rajagopalan, R. **1997**. Principles of Colloid and Surface Chemistry. *Marcel Dekker, Inc. New York*, pp. 279-280

Hirt, C.W., and Nichols, B.D. **1981**. Volume of Fluid (VOF) Method for the Dynamics of Free Boundaries. *Journal of Computational Physics* 39; 201-225

Homma, S., Koga, J., Matsumoto, S., Song, M., and Tryggvason, G. **2006**. Breakup mode of an axisymmetric liquid jet injected into another immiscible liquid. *Chemical Engineering Science* 61; 3986-3996

Janssen, J.J.M., Boon, A., and Agterof, W.G.M. **2004**. Influence of dynamic interfacial properties on droplet breakup in simple shear flow. *AICHE Journal* 40(12); 1929-1939

Jin, F., Gupta, N.R., and Stebe, K.J. **2006**. The detachment of a viscous drop in a viscous solution in the presence of a soluble surfactant. *Physics of Fluids* 18(2); 022103-1-10

Kalaaji, A., Lopez, B., Attané, P., and Soucemarianadin, A. **2003**. Breakup length of forced liquid jets. *Physics of Fluids* 15(9); 2469-2479

Keller, J.B. **1983**. Capillary waves on a vertical jet. *Journal of Fluid Mechanics* 135; 171-173

Kitamura, Y., Mishima, H., and Takahashi, T. **1982**. Stability of Jets in Liquid-Liquid Systems. *The Canadian Journal of Chemical Engineering* 60; 723-731

Kroesser, F.W., and Middleman, S. **1969**. Viscoelastic Jet Stability. *AICHE Journal* 15(3); 383-386

Kwak, S. and Pozrikidis, C. **2001**. Effect of surfactants on the instability of a liquid thread or annular layer. *International Journal of Multiphase Flow* 27; 1-37

Lafrance, P. **1975**. Nonlinear breakup of a laminar liquid jet. *The Physics of Fluids* 18(4); 428-432

Liao, Y.-C., Frances, E.I., and Basaran, O.A. **2006**. Deformation and breakup of a stretching liquid bridge covered with an insoluble surfactant monolayer. *Physics of Fluids* 18(2); 022101-1-21

Liao, Y-C., Subramani, H.J., Franses, E.I., and Basaran, O.A. **2004**. Effects of Soluble Surfactants on Deformation and Breakup of Stretching Liquid Bridges. *Langmuir* 20; 9926-9930

Lin, S.P. **2003**. Breakup of liquid sheets and jets. *Cambridge University Press, New York*, pp. 210-220

Lyklema, J. **2000**. Fundamentals of Interface and Colloid Science. Volume III: Liquid-Fluid Interfaces. *Academic Press, San Diego,* pp 1.33-1.36 & A1.42-A1.43

McGough, P.T. and Basaran, O.A. **2006**. Repeaterd Formation of Fluids Threads in Breakup of a Surfactant-Covered Jet. *Physical Review Letters* 96(5); 054502-1-4

Middleman, S. **1995**. Modeling Axisymmetric Flows – Dynamics of Films, Jets, and Drops. *Academic Press, San Diego,* pp 2-38 & 78-122

Milliken, W.J., and Leal, L.G. **1994**. The Influence of Surfactant on the Deformation and Breakup of a Viscous Drop: The Effect of Surfactant Solubility. *Journal of Colloid and Interface Science* 166(2); 275-285

Milliken, W.J., Stone, H.A., and Leal, L.G. **1992**. The effect of surfactant on the transient motion of Newtonian drops. Physics of Fluids A 5(1); 69-79

Moorkanikkara, S.N., and Blankschtein, D. **2006**. New methodology to determine the rate-limiting adsorption kinetics mechanism from experimental dynamic surface tension data. *Journal of Colloid and Interface Science* 302; 1-19

Mun, R.P., Byars, J.A., and Boger, D.V. **1998**. The effects of polymer concentration and molecular weight on the breakup of laminar capillary jets. *Journal of Non-Newtonian Fluid Mechanics* 74; 285-297

Narasinga Rao, E.V.L., Kumar, R., and Kuloor, N.R. **1966**. Drop formation studies in liquid-liquid systems. *Chemical Engineering Science* 21; 867-880

Nayfeh, A.H. **1970**. Nonlinear Stability of a Liquid Jet. *The Physics of Fluids* 13(4); 841-847

Padron, G. A., **2005**. Effect of surfactants on drop size distributions in a batch, rotor-stator mixer. *Chemical and Biomolecular Engineering, University of Maryland. College Park, Maryland*. Ph.D. Dissertation

Rayleigh, L.,**1879**. On the Capillary Phenomena of Jets, *Proceedings of the Royal Society of London* 29(196-199); 71-97

Savart, F. **1833**. Mémoire sur la Consititution des Veines liquids lancées par des orifices circulaires en mince paroi <<On the Formation of liquid Jets issuing from circular orificies in thin plates>>. *Annales des Chimie et des Phsyique* 53; 337-386

Scheele, G.F., and Meister, B.J. **1968**. Drop Formation at Low Velocities in Liquid-Liquid Systems. *AICHE Journal* 14(1); 9-19

Skelland, A.H.P, and Walker, P.G. **1989**. The Effects of Surface Active Agents on Jet Breakup in Liquid-Liquid Systems. *The Canadian Journal of Chemical Engineering* 67; 762-770

Skelland, A.H.P., and Johnson, K.R. **1974**. Jet Break-up in Liquid-Liquid Systems. *The Canadian Journal of Chemical Engineering* 52; 732-738

Song, B, and Springer, J. **1996**. Determination of Interfacial Tension from the profile of a Pendant Drop Using Computer-Aided Image Processing. 1. Theoretical. *Journal of Colloid and Interface Science* 184; 64-76

Song, B, and Springer, J. **1996**. Determination of Interfacial Tension from the profile of a Pendant Drop Using Computer-Aided Image Processing. 2. Experimental. *Journal of Colloid and Interface Science* 184; 77-91

Sterling, A.M., and Sleicher, C.A. **1975**. The instability of capillary jets. *Journal of Fluid Mechanics* 68(3); 477-495

Stone, H.A., Bentley, B.J. & Leal, L.G. **1986**. An experimental study of transient effects in the break-up of viscous drops. *Journal of Fluid Mechanics* 173; 131-158

Stone, H.A., and Leal, L.G. **1990**. The effects of surfactants on drop deformation and breakup. *Journal of Fluid Mechanics* 220; 161-186

Subramani, H.J., Yeoh, H.K., Suryo, R., Xu, Q., Ambravaneswaran, B., and Basaran, O.A. **2006**. Simplicity and complexity in a dripping faucet. *Physics of Fluids* 18(3); 032106-1-13

Taub, H.H. **1976**. Investigation of nonlinear waves on liquid jets. *The Physics of Fluids* 19(8); 1124-1129

Timmermans, M-L. E., and Lister, J.R. **2002**. The effect of surfactant on the stability of a liquid thread. *Journal of Fluid Mechanics* 459; 289-306

Tomotika, S. **1935**. On the Instability of a Cylindrical Thread of a Viscous Liquid surrounded by Another Viscous Fluid. *Proceedings of the Royal Society of London, Series A, Mathematical and Physical* 150(870); 322-337

Vassallo, P., and Ashgriz, N. **1991**. Satellite formation and merging in liquid jet breakup. *Proceedings of the Royal Society of London, Series A* 443; 269-286

Vlahovska, P.M., and Lowenberg, M. 2005. Deformation of a surfactant-covered drop in a linear flow. Physics of Fluids 17(10); 103103-1-18

Ward, A.F.H., and Tordai, L. 1946. Time-Dependence of Boundary Tensions of Solutions. 1. The Role of Diffusion in Time-Effects. *Journal of Chemical Physics* 14(7); 453-461

Webseter, D.R., and Longmire, E.K. 2001. Jet pinch-off and drop formation in immiscible liquid-liquid systems. *Experiments in Fluids* 30; 47-56

Xue, Z., Corvalan, C.M., Dravid, V., and Sojka, P.E. **2008**. Breakup of shear-thinning liquid jets with surfactants. *Chemical Engineering Science* 63; 1842-1849

Yang, H., Park, C.C., Hu, Y.T., and Leal, L.G. **2001**. The coalescence of two equal-sized drops in a two-dimensional linear flow, *Physics of Fluids* 13(5) 1087-1106.

Yuen, M-C. **1968**. Non-linear capillary instability of a liquid jet. *Journal of Fluid Mechanics* 33(1); 151-163

Zeppieri, S. Rodríguez, J., and López de Ramos, A.L. **2001**. Interfacial Tension of Alkane + Water Systems. *Journal of Chemical Engineering Data* 46; 1086-1088